Structural and Spectroscopic Studies of Solvated Metal Ions

Alireza Abbasi

Doctoral Thesis

Structural Chemistry
Stockholm University 2005

Doctoral Dissertation
29 April 2005
Magnéli Hall
Stockholm University

Structural Chemistry
Arrhenius Laboratory
Stockholm University
S-106 91 Stockholm
Sweden

ISBN 91-7155-013-5
Printed in Sweden by Intellecta Docusys

To Elaheh and Pardis

تقدیم به همسر و دختر عزیزم

Experiments are the only means of knowledge at our disposal; the rest is poetry, imagination.

Max Planck

Abstract

Crystallographic and spectroscopic studies have been performed of structures, coordination and chemical bonding for series of trivalent metal ions solvated by two oxygen-coordinating solvents, water and dimethyl sulfoxide (DMSO). The hydrated scandium(III) and lanthanoid(III) ions, La to Lu, are surrounded by tricapped trigonal prisms of aqua ligands in the isomorphous series of trifluoromethanesulfonates, $[M(H_2O)_n](CF_3SO_3)_3$. For the smallest ions, M = Er, Tm, Yb, Lu, Sc, the hydration numbers decrease, n = 8.96(5), 8.8(1), 8.7(1), 8.5(1), 8.0(1), respectively, with decreasing size of the ion. The crystal structures at ambient temperature indicate randomly distributed vacancies of the capping oxygen atoms, and ^2H solid-state NMR of the diamagnetic $[M(H_2O)_n](CF_3SO_3)_3$, M = Sc, Lu, Y and La compounds revealed increasing mobility of the water ligands in the coordination sphere with increasing temperature, also for the fully nonahydrated La^{III} and Y^{III} ions. The stretching force constants of the Ln-O bonds, evaluated from vibrational spectroscopy, increased from 0.81 to 1.16 N cm^{-1} for the Ln-6O trigonal prism in a smooth correlation with the bond distances from La to Lu. For the capping Ln-3O bonds the increase from 0.49 to 0.65 N cm^{-1} reflects the increased ligand-ligand repulsion with decreasing ion size. This is also the reason for the water deficiency of the Er, Tm, Yb, Lu and Sc salts, and for $[Sc(H_2O)_{8.0}](CF_3SO_3)_3$ the repulsion induced a phase transition at about 185 K that, by low temperature crystallography, was found to distort the coordination of water molecules toward a monocapped trigonal prism around the scandium(III) ion.

All crystal structures of the octakis(dimethyl sulfoxide)lanthanoid(III) iodides comprise discrete $[Ln(dmso)_8]^{3+}$ complexes surrounded by iodide ions. The lanthanum(III) and praseodymium(III) compounds crystallize in the orthorhombic space group *Pbca* with more efficient packing than for the heavier and smaller ions in the lanthanoid series, which crystallize in the monoclinic space group $P2_1/n$. The group 13 metal ions, aluminium(III), gallium(III), indium(III), thallium(III), and also scandium(III) of group 3, form crystalline hexakis(dimethyl sulfoxide) solvates in the space group $R\bar{3}$, with octahedral MO_6 coordination entities, which are increasingly compressed along one threefold axis for increasing ionic size. EXAFS measurements on the solvated ions display similar M-O bond distances in dimethyl sulfoxide solution as in the solid solvates. For all the solid dimethyl sulfoxide solvates the strength and nature of the metal-oxygen bond has been evaluated by normal coordinate analysis of vibrational spectra, and correlated with the S-O stretching vibrational mode.

Distortions from regular octahedral six coordination are discussed for the hydrated isoelectronic soft mercury(II) and thallium(III) ions in the solid bisaquamercury(II) and trisaquatallium(III) trifluoromethanesulfonates, in terms of pseudo Jahn-Teller effects (PJTE). Mercury(II), generally more strongly influenced by PJTE distortions, displays a 2 + 4 Hg-O coordination forming chains that are held together in sheets by hydrogen bonds and in layers by van der Waals interactions, which explain the fragile structure of the crystals.

Abbreviations

DMSO	Dimethyl Sulfoxide, $(CH_3)_2SO$
DSC	Differential Scanning Calorimetry
EXAFS	Extended X-ray Absorption Fine Structure
FT	Fourier Transform
IR	Infrared Absorption
JTE	Jahn-Teller effect
PJTE	Pseudo Jahn-Teller effect
TGA	Thermogravimetric Analysis
Triflate	Trifluoromethanesulfonate, $CF_3SO_3^-$
TTP	Tricapped Trigonal Prism
XRD	X-Ray Diffraction
YAG	Yttrium Aluminum Garnet

List of Papers

This thesis is based on the following papers, which are referred to in the text by their Roman numerals (reproduced by permission from Inorganic Chemistry, American Chemical Society; the Royal Society of Chemistry, Dalton Transactions; Spectrochimica Acta Part A, Elsevier, and Chemistry, a European Journal):

I. Dimethyl sulfoxide solvates of the aluminium(III), gallium(III) and indium(III) ions. A crystallographic, EXAFS and vibrational spectroscopic study
A. Molla-Abbassi, M. Skripkin, M. Kritikos, I. Persson, J. Mink and M. Sandström
J. Chem. Soc., Dalton Trans. **2003**, *9*, 1746

II. Structure of the dimethyl sulfoxide solvated thallium(III) ion in solution and in the solid state
G. Ma, A. Molla-Abbassi, M. Kritikos, A. Ilyukhin, F. Jalilehvand, V. Kessler, M. Skripkin, M. Sandström, J. Glaser, J. Näslund and I. Persson
Inorg. Chem. **2001**, *40*, 6432

III. Vibrational spectroscopic force field studies of dimethyl sulfoxide and hexakis(dimethyl sulfoxide)scandium(III) iodide, and crystal and solution structure of the hexakis(dimethyl sulfoxide)scandium(III) ion
M. Skripkin, P. Lindqvist-Reis, A. Abbasi, J. Mink, I. Persson and M. Sandström
Dalton Trans. **2004**, 4038

IV. Crystallographic, vibrational spectroscopic and force field studies of oktakis(dimethyl sulfoxide) lanthanide(III) solvates
A. Abbasi, M. Skripkin, E. Damian, J. Mink, A. -S. Ullström, I. Persson, Y. Sidorov and M. Sandström, in manuscript

V. Highly hydrated cations: deficiency, mobility and coordination of water in crystalline nonahydrated scandium(III), yttrium(III) and lanthanoid(III) trifluoromethanesulfonates

A. Abbasi, P. Lindqvist-Reis, L. Eriksson, D. Sandström, S. Lidin, I. Persson, and M. Sandström

Chem. Eur. J. **2005,** in press

VI. Infrared and Raman spectroscopic and theoretical studies of nonaaqua complexes of trivalent rare earth metal ions

J. Mink, M. Skripkin, L. Hajba, C. Németh, A. Abbasi and M. Sandström

Spectrochim. Acta A **2005**, in press

VII. Structure and bonding of bisaquamercury(II) and trisaquathallium(III) trifluoromethanesulfonate

A. Molla-Abbassi, L. Eriksson, J. Mink, I. Persson, M. Sandström, M. Skripkin, A.-S. Ullström and P. Lindqvist-Reis,

J. Chem. Soc., Dalton Trans. **2002**, *23*, 4357

Table of Contents

1. INTRODUCTION

The current thesis is part of a study of the structure and bonding in metal-ligand complexes and coordination compounds with focus on the properties of solvated metal ions. The type of complex formation that occurs when dissolving an electrolyte and solvent molecules attach to the ions is called solvation. When an electrolyte solution crystallizes, the metal ions often appear in the solid compounds surrounded by solvent molecules, i.e. as charged complexes in coordination compounds called solvates.[1]

For understanding the properties and reactions of solvated metal ions, structural investigations to reveal the coordination geometry and the characteristics of the metal-ligand bonding are essential. For example, the lanthanoid(III) and scandium(III) trifluoromethanesulfonate compounds have found increasing use as selective catalysts in organic synthesis as water-tolerant Lewis acids,[2,3] and structural studies are needed for elucidating the mechanisms and improving the processes.

When studying the coordination properties of metal ions, the characteristic structural effects can be brought out, in particular in solution, by using monodentate ligands in excess, and by comparing trends in similar complexes within a group of elements or for isoelectronic ions. In this study the structures, coordination numbers and bonding, have been compared for series of metal ions solvated by two important oxygen-coordinating solvents, water and dimethyl sulfoxide. Single-crystal x-ray diffraction, x-ray absorption fine structure (EXAFS) and vibrational spectroscopy, have been used to study the dimethyl sulfoxide solvated aluminium(III), gallium(III), indium(III), thallium(III), scandium(III) ions, and several lanthanoid(III) ions, both in solution and in coordination compounds,[I-IV] followed by aqua complexes of scandium(III) and lanthanoid(III) ions,[V,VI] and also the isoelectronic mercury(II) and thallium(III) ions in bisaquamercury(II) and trisaquathallium(III) trifluoromethanesulfonate.[VII] The coordination and bond character have been discussed in terms of increasing size of the metal ions, the effect of ligand-ligand repulsion, the electronic character of the bonds to the metal ions, and the hydrogen bonding to the surrounding. For the soft mercury(II) and thallium(III) ions, with d^{10} electronic configuration in the valence shell, possible effects of covalency and *d*-orbital participation in the bonding have been investigated, and compared to the more electrostatic bonding character for the scandium(III) and lanthanoid(III) ions.

1.1 Acid-base and complex formation concepts

A complex forms when ligands L_1, L_2 … L_n attach to a central atom, e.g. a metal ion M^{n+}. Each ligating atom is regarded as bringing one lone-pair of electrons to the central atom in the complex. The general Lewis acid-base concept describes a substance that acts as an **electron pair acceptor** as a **Lewis acid**, and conversely the ligand that acts as **electron pair donor** is a **Lewis base**.

It is useful to describe the behavior of the Lewis acids and bases in complex formation as belonging to two main classes, **hard** and **soft** acids and bases. Soft acids can form strong bonds when accepting electron pairs from polarizable 'soft' ligands, whereas metal ions classified as hard acids prefer less polarizable 'hard' ligand atoms.[4] Thus, a hard metal ion would prefer to coordinate oxygen atoms, instead of sulfur or iodide. Metal ions classified as intermediate show no strong preferences. According to this principle, thallium(III) and mercury(II) belong to the group of soft metal ions, while aluminium(III), gallium(III), indium(III), scandium(III) and the lanthanoid(III) ions are classified as hard.[5]

For solvent molecules as ligands (L), Gutmann's donor number, D_N, scale, describes the coordination ability (Lewis basicity) of the solvent relative to medium-hard acceptors. It is defined as the negative enthalpy value of the formation of the 1:1 adducts between the ligand L and the standard Lewis acid $SbCl_5$ in a diluting 1,2-dichloroethane medium.[6]

$$L{:}(\text{solvent}) + SbCl_5 \longleftrightarrow L{:}SbCl_5 \quad D_N = -\Delta H_r^{o}\,(\text{kcal/mol}) \qquad (1)$$

For soft-soft interactions, the bonding between the metal ion and the donor atom of a neutral solvent molecule is generally of more covalent character. A donor strength scale, D_S, classifying the donor strength of solvent molecules toward soft acceptors, has been derived based on the change in the Hg-Br stretching vibration frequency of the $HgBr_2$ molecule in the gas phase and in the solvated molecules in solution.[6]

$$D_S = \nu_{HgBr_2}\,(\text{gas}) - \nu_{HgBr_2}\,(\text{solv}) \qquad (2)$$

1.2 High coordination numbers and coordination polyhedra

The **coordination number** is defined as the number of σ-bonds between the ligands and the central atom. The ligating atom in the Lewis base that forms the bond to the central atom is called the **donor** atom. It is standard practice to regard the donor atoms directly attached to the central atom as defining a **coordination polyhedron**.

For six coordinated oxygen atoms the ligand-ligand repulsion favors an octahedral configuration of the six ligands around the central metal ion. In the model of a regular octahedral complex used in crystal field (CF) theory with the Cartesian axes along the bond directions, the d_{z^2} and $d_{x^2-y^2}$ metal atom orbitals are strongly repelled by the ligands (by Pauli repulsion) in comparison to the other *d*-orbitals (d_{xy}, d_{xz} and d_{yz}), which have their lobes between the axes. Thus, the five *d* orbitals split into two sets of degenerate orbitals, belonging to the e_g and t_{2g} symmetry species in the $\mathbf{O}_h$ point group, respectively (Fig. 1),[7] with the d_{z^2} and $d_{x^2-y^2}$ orbitals having higher energy.

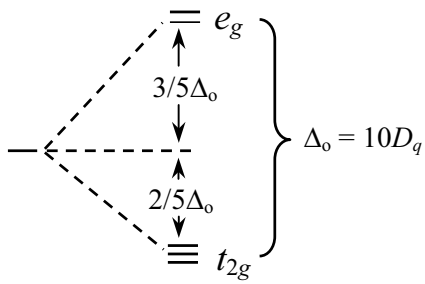

Figure 1. *The five d orbitals of the central atom M splits into two sets with two and three degenerate orbitals of e_g and t_{2g} symmetry, respectively, in an octahedral crystal field.*

For octahedral coordination polyhedra there are three common types of distortion. Firstly, tetragonal elongation or contraction along a $\mathbf{C}_4$ axis, reducing the symmetry from $\mathbf{O}_h$ to $\mathbf{D}_{4h}$ (see section 1.3), secondly different lengths of two $\mathbf{C}_4$ axes, further reducing the symmetry to $\mathbf{D}_{2h}$, and finally trigonal distortion with elongation or contraction along one of the $\mathbf{C}_3$ axes, resulting in $\mathbf{D}_{3h}$ symmetry.

Coordination number seven is rather unusual. The additional energy gain of forming the seventh bond is counteracted by increasing ligand-ligand interactions and weaker bond strength; and for transition metal ions the non-octahedral geometry reduces the ligand field stabilization energy. The coordination polyhedron for seven coordinated ligand atoms can be described as a pentagonal bipyramid, a capped octahedron, or a monocapped trigonal prism. The coordination polyhedron of the scandium(III) ion in the hydrated trifluoromethanesulfonate salt at low temperature can be regarded as a monocapped trigonal prism (see section 3.2.4.1).

To obtain eight-coordination with monodentate ligands two factors are important. Firstly, the metal ion should be large enough to accommodate eight ligands without too severe ligand-ligand repulsion. Secondly, eight-coordination is favored by a high formal oxidation state, because eight dative

bonds to a metal ion in a low oxidation state would result in excess electron density around the central metal. Common oxidation state is +3 or greater, although e.g. aqua ions of Ba^{2+}, Sr^{2+} and Ca^{2+} are known with coordination number eight.[8,9] However, a high oxidation state reduces the ionic radius of the metal ion; therefore the coordination number eight is much less common than six-coordination.

The coordination polyhedron can be viewed as a cube, a square antiprism, $\mathbf{D}_{4d}$, or a dodecahedron, $\mathbf{D}_{2d}$. The latter two polyhedra can be obtained by distorting the cube (Figure 2). The cubic conformation, which has higher ligand-ligand repulsion energy, rarely occurs in discrete complexes.[10] The eight-coordinated complexes of the solvated dimethyl sulfoxide lanthanoid(III) ions are found to be distorted square antiprisms.

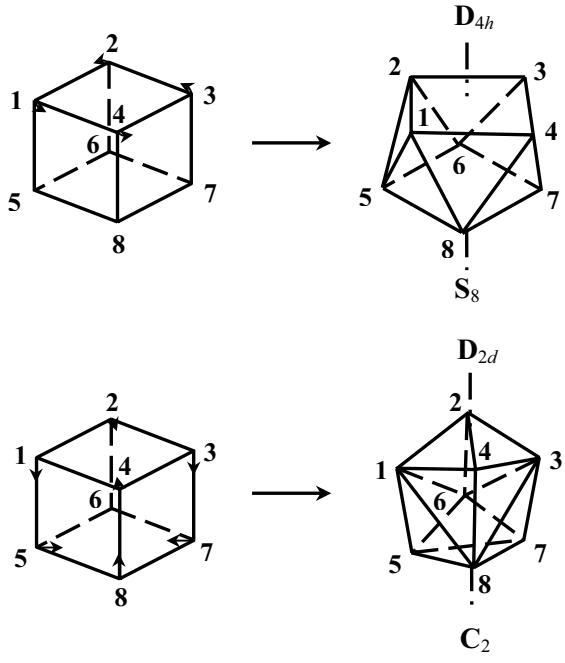

Figure 2. *Coordination number 8: Distortion of a cube to: (top) square antiprism and (bottom) dodecahedron (Ref. 10).*

Higher coordination numbers than 8 are not very common with monodentate ligands. Discrete nine-coordinate structures are found for complexes such as $[Ln(H_2O)_9]^{3+}$ with two groups of metal-oxygen distances in a tricapped trigonal prism (TTP).[10] The capped square antiprism is a configuration with slightly higher energy of nine ligand atoms.

1.3 Jahn-Teller effects

Distortion of an octahedral configuration may take place even when all six ligands of the complex are equivalent, if induced by the electronic configuration of the central atom. For some transition metal ions, e.g. Cu^{2+}, Cr^{2+} and Mn^{3+}, two *trans* donor atoms ('axial' in the distorted octahedron) are generally found farther from (or occasionally closer to) the central atom than the four equivalent 'equatorial' ones. A well known example is the hydrated Cu^{2+} ion, $Cu(OH_2)_6^{2+}$, with four Cu-O distances at 1.95 Å and two longer at about 2.29 Å.[11]

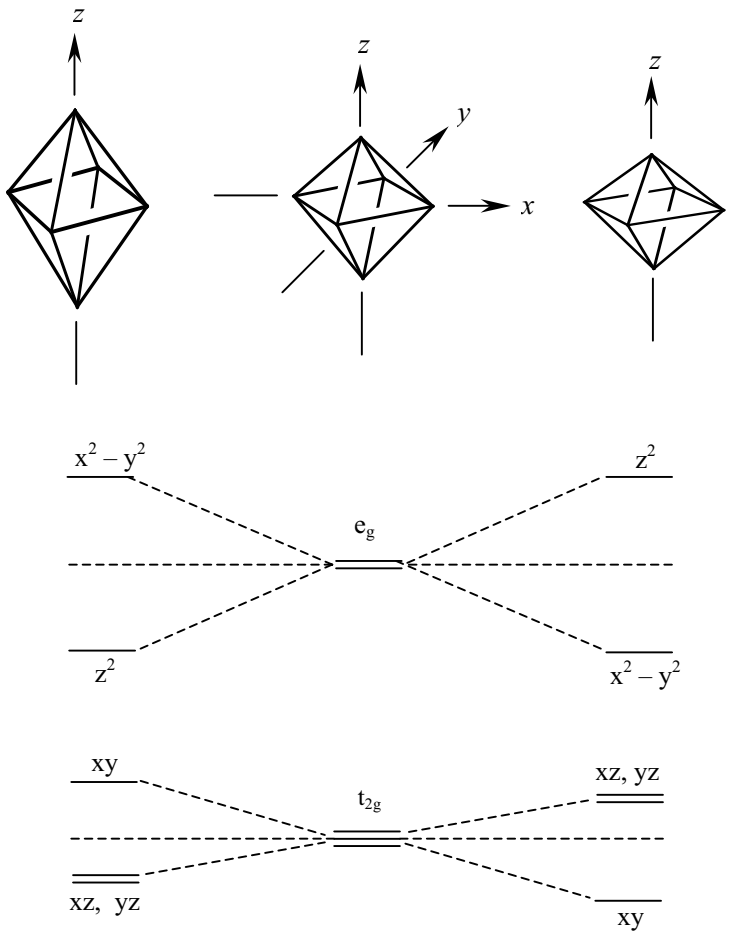

Figure 3. *Jahn-Teller effect. Tetragonal distortion of octahedral (O_h) symmetry further splits the energy levels of the two groups of degenerate atomic d- orbitals: (Z-out (left) and Z-in (right)).*

The reason is that for certain degenerate electronic states a coupling between the electronic and nuclear motions, called Jahn-Teller vibronic coupling, can reduce degeneracy and lead to instability of the regular nuclear configuration and reduce its symmetry. In the case of the $Cu(OH_2)_6^{2+}$ ion a two-fold degenerate electronic ground state of symmetry species '*e*' (Figure 1) interacts with a two-fold degenerate (E_g) vibrational mode, leading to a tetragonal elongation of the octahedral configuration, where the direction of the elongation may alternate.[12]

For the Cu^{2+} ion with a d^9-electronic configuration, in the simplified scheme based on the crystal field model, the splitting of the ground electronic state due to this vibronic coupling can be regarded as a separation of the energy levels of the e_g atomic orbitals by ligand repulsion, as shown in Fig. 3. Thus, one of the two e-symmetry orbitals, $d_{x^2-y^2}$ or d_{z^2} will be singly occupied and the complex will distort to an energy minimum along a normal coordinate belonging to the E_g symmetry species of the $\mathbf{O}_h$ point group.

1.3.1 Pseudo Jahn-Teller effect (PJTE)

The Jahn-Teller effect described above deals with molecular distortions due to vibronic coupling that splits an electronically degenerate ground state. In a more general description of Jahn-Teller effects the vibronic mixing of two (or several) nondegenerate electronic states, induced by nuclear displacements, is called the pseudo Jahn-Teller effect (PJTE).[12] For the current study, the vibronic coupling between a non-degenerate ground state, as for the mercury(II) and thallium(III) complexes, and an excited state, is of special interest.

A strong PJT vibronic coupling may lead to instability of the ground state, with nuclear displacements and symmetry lowering similar to the Jahn-Teller instability for degenerate electronic states. If the vibronic mixing with the excited state is small, this may only give rise to a shallow potential surface of the ground state along the active normal coordinate (Fig. 4). This plasticity effect may appear as an increase in the vibrational amplitude, or the disorder parameter, σ, in a structural determination.[12]

Mercury(II) and the trivalent metal ions in group 13 (except Al^{3+}) possess a non-degenerate ground state with a d^{10} electron configuration. The tendency of mercury(II) to coordinate two strongly bonded ligands in digonal or linear configuration is well known. For the hexahydrated $Hg(OH_2)_6^{2+}$ ion theoretical *ab initio* calculations reveal a weak PJTE, which is consistent with the large, experimentally observed, disorder parameter σ in the hexaaqua-complexes formed (see section 2.1.2).[13]

One aim of the present study, especially for the heavy mercury(II) and thallium(III) ions with small energy differences between the 5*d* and 6*s*

valence electron levels, was to seek for a possible influence of PJTE distortion on the structure of their solvates.[VII]

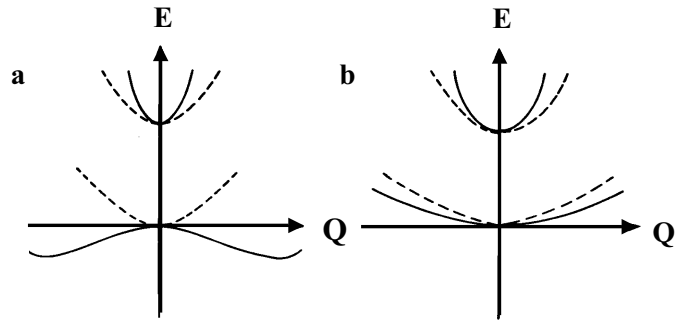

Figure 4. *Potential energy of electronic states of a molecular system with (a) strong and (b) weak PJTE, where E is the potential energy for nuclear displacement along a normal coordinate Q. Dashed lines represent ground and excited states without vibronic mixing (ref 12).*

1.4 Force constants and potential surfaces

The chemical bonds in a molecule can perform vibrational motions, stretching, bending, etc. Fortunately, the intricate composite vibrational motion of all the atoms in a molecular complex can be described by a set of independent motions called normal modes. For a polyatomic molecule there are 3N-6 normal modes of vibrational motion (3N-5 for linear molecules), each with its characteristic frequency.[14] For the simple case of a diatomic vibrating molecule, the restoring force F can be assumed to obey Hooke's Law $F = -K(R - R_o)$, where the force is proportional to the deviation from the equilibrium bond distance R_o (Figure 5). The frequency of the vibration is then, in the so-called harmonic approximation, proportional to the square root of K/μ:

$$\bar{\nu} = \frac{1}{2\pi c}\sqrt{\frac{K}{\mu}} \qquad (3)$$

where $\bar{\nu}$ is the wave number in cm^{-1}, c the speed of light $3.00 \cdot 10^{10}$ cm/s, K the force constant in N/m, and μ the reduced mass in kg.

Extending this concept developed for diatomic molecules to polyatomic molecules is not straightforward. The internal motion can be characterized by a set of force constants that, in the general harmonic approximation, would contain one force constant for each pair-wise interaction in the molecule. We are then faced with the problem of selecting normal

coordinates that will allow the use of a consistent set of force constants, which directly relate to the stretching and bending of chemical bonds.

Werner Kutzelnigg has stated: "The chemical bond is a highly complex phenomenon, which eludes all attempts at simple description". In fact, there is no simple relation between bond energy and force constant, and it is not even easy to judge which bond is stronger when comparing two force constants. The force constant is a measure of the curvature of the potential surface near the equilibrium position, while the depth of the potential energy curve gives the dissociation energy (Figure 5).[14] Therefore, the larger force constant has the sharper curvature of the potential well near the bottom, but that does not necessarily mean that the potential well is deeper.

However, in a series of molecules of similar type, satisfactory correlations between force constants and bond distances can be found. If the metal-ligand bond can be approximately described as an ion-dipole coulombic interaction, then the energy dependence versus distance is:[15]

$$W(r) \approx 1 / r^2 \qquad (4)$$

If the interaction energy, $W(r)$, can be considered to be proportional to the force constant, e.g. in a series of metal solvates coordinating an oxygen atom, then 'r' relates to the bond length between the metal ions and the oxygen donor atom of the ligand. Inherent assumptions are that the shape of the potential well of the metal-ligand bond, and the effect of ligand-ligand repulsion, are similar in the series of complexes. In the harmonic approximation, the frequency is proportional to the square root of the force constant (Eqn. 3), so then follows:

$$\overline{\nu} \approx 1 / r \qquad (5)$$

Based on these approximate relations, correlations between force constants and metal-oxygen bond distances, K against $1/r^2$ (Eq. 4), and the frequency ν against $1/r$ (Eq. 5), are discussed in section 3.2.3 (where r denotes the bond distance).

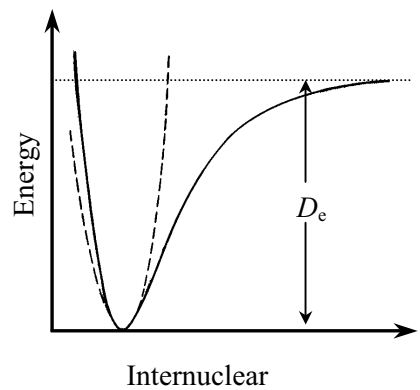

Figure 5. *Potential energy curve of a diatomic molecule versus inter-nuclear distance; the dotted line is the harmonic oscillator potential function (ref 14).*

2. EXPERIMENTAL METHODS

2.1 Structural techniques

2.1.1 Crystallography

Radiation with a wavelength in the vicinity of interatomic distances (100-300 pm or 1-3 Å) is scattered by crystals. Diffraction is a consequence of interference of scattered x-rays, which for a crystal leads to a large number of observable 'reflections' with characteristic directions. The position of the diffracted beams is related to the unit cell parameters, and the intensity is related to the type of atoms and their arrangement within the unit cell. The square root of the total intensity of a reflection (after attenuation corrections) is proportional to the structure factor, $|F_{hkl}|$. The structure factor corresponds to sums of wave motions, considering both amplitude and phase. Since the experimental measurements provide intensities, which can be related to the amplitudes, the problem is to deduce the phases. This is what in crystallography is called the phase problem.

In the present studies, relationships between the intensities of various reflections were used to propose solutions to the phase problem directly. In these direct methods plausible structural models are derived, and used for calculating structure factors, F_c. When a structural model comprising all atoms has been achieved, structural parameters are refined to minimize the difference between the observed and calculated structure factors. Residuals or *R-values* indicate how well the structural model fits to the experimental data.[16] The conventional (unweighted) R-value is defined as:

$$R = \frac{\sum_{hkl} \| F_o | - | F_c \|}{\sum_{hkl} | F_o |} \qquad (6)$$

The diffraction experiment consists of a source, a sample and a detector. The source used was Mo-target x-ray tubes, and a graphite monochromator was used to select MoKα radiation, 0.7107 Å. The monochromatized beam passes through a narrow collimator tube. The crystal was mounted on a goniometer and its position centered in the x-ray beam.

Single crystal x-ray diffraction studies can be performed if it is possible to crystallize and obtain suitable single crystals of the sample. In the present study, the samples were, if needed, recrystallized several times to obtain

single crystals with sufficient quality (generally, the cleaner and more well-defined surfaces the better crystals).

The data collections were made on small crystals enclosed in thin-walled glass capillaries at room temperature, by means of STOE imaging-plate, Bruker SMART or Oxford Instruments Xcalibur, equipped with a CCD detector (crystal to detector distance 5.00 cm). The STOE IPDS, Bruker and CrysAlis program packages, respectively, were used for indexing and integrating the single crystal reflections. Low temperature measurements were made for crystals of $[Tl(dmso)_6](ClO_4)_3$ (at 150 K) and $[Sc(H_2O)_{8.0}](CF_3SO_3)_3$ (at 250, 200, 150 and 100 K).

Absorption corrections were performed with the programs X-RED and X-Shape.[17] In X-shape symmetry-equivalent reflections were used to optimize the crystal shape and size. Such corrections become important when the crystal shape is very anisotropic (e.g. a thin plate). For the thin crystal of the bisaqamercury(II) trifluoromethanesulfonate compound the estimated standard deviation (esd) was reduced 50% by the absorption correction, and the value obtained for the Hg-O distances to water molecules changed by about 0.016 Å.

The structures were solved by direct methods using SHELXS-97,[18] and refined using full-matrix least-squares method on F^2, SHELXL-97.[19] All non-hydrogen atoms were refined anisotropically. Hydrogen atoms belonging to the methyl group of a dimethyl sulfoxide molecule were introduced at calculated positions, allowing riding motion on the C atom and rotation about the C-S bond with fixed C-H distance and SCH and HCH angles.[I-IV] For the water molecules in the hydrated compounds the hydrogen atoms were located from the residual electron density map and refined with a tight restraint of the O-H bond length allowed to vary within 0.01 Å, while keeping the H···H distance at a value corresponding to the H-O-H angle 104.5°.[V] In addition, in the bisaquamercury(II) and trisaquathallium(III) trifluoromethanesulfonate compounds the hydrogen bond H···O distances to the acceptor oxygen atoms were restrained much more loosely, within 0.05 Å.[VII] This way of modeling was used to allow almost rigid water molecules to reorient, as no riding atom model is available for water molecules in SHELXL97.

2.1.2 Extended X-ray Absorption Fine-Structure (EXAFS) spectroscopy

When the energy of the incident x-rays ($E_{h\nu}$) is greater than the threshold energy (E_o, the binding energy of an inner-core electron), photoelectrons are ejected with kinetic energy, $E_{kin} = E_{h\nu} - E_o$. The outgoing photoelectron wave of the absorber will be backscattered by surrounding neighboring atoms, producing an incident photoelectron wave. Constructive and destructive

interference between the outgoing and backscattered photoelectron waves give rise to the EXAFS oscillations (Fig. 6). Because the oscillation is a direct consequence of the interactions between the absorber atom and its surrounding, EXAFS provides information of the photo-absorber and its local environment, especially the distance from the absorber to its near neighbors.[20-22]

Single backscattering (SS), corresponding to the scattering pathway from the absorber atom to its nearest neighbours, is used to determine the near neighbor distance. However, the ejected electron wave can be scattered by more than one atom before returning to the central atom, giving rise to multiple scattering (MS). Multiple back-scattering pathways are always longer than the single backscattering and their EXAFS oscillations then become most prominent in the low-*k* region.

This technique can be used for any aggregation state (solid, liquid or gas), in all kinds of environment such as crystalline solids, glasses, amorphous phases, liquids and solutions. For elements lighter than calcium, EXAFS oscillations suitable for structure studies are difficult to obtain because of the high x-ray absorption. In favorable cases, EXAFS of good quality can be collected with fluorescence techniques on metal ions in dilute samples that are hard to obtain at high concentrations.

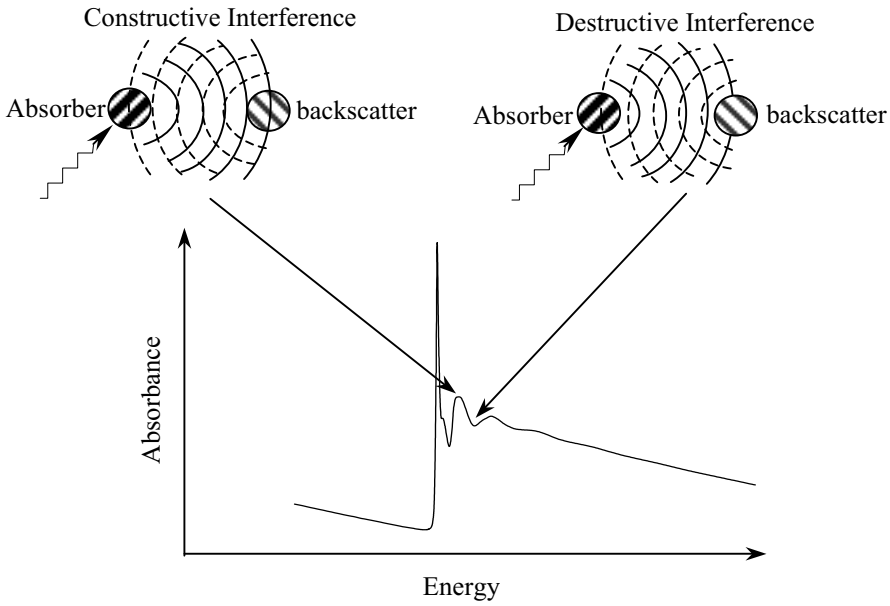

Figure 6. *Constructive and destructive interference between the outgoing and backscattered photoelectron waves give rise to the EXAFS oscillation.*

The usefulness of EXAFS as a technique for structural analysis depends on accurate knowledge of the phase shifts and scattering amplitudes in the EXAFS formula:

$$\chi_i(k) = \sum_j \frac{N_j S_o^2(k)}{kR_j^2} \left| f_{eff}(k) \right|_j exp(-2k^2\sigma_j^2) exp\left[-2R_j / \Lambda(k)\right] sin\left[2kR_j + \phi_{ij}(k)\right] \quad (7)$$

in which:

N_j = Number of backscatterers in the *j*th shell

R_j = Distance between the central atom *i* and the backscatterers in the *j*th shell in single backscattering

$S_o^2(k)$ = Amplitude reduction factor

$f_{eff}(k)$ = Effective amplitude function for each scattering path

$exp(-2\sigma_j^2 k^2)$ = Debye-Waller factor in the harmonic approximation

σ_j = Debye-Waller parameter accounting for thermal and configurational disorder

$\Lambda(k)$ = Photoelectron mean free path

$exp\left[-2R_j / \Lambda(k)\right]$ = Mean free path factor

$\left[2kR_j + \phi_{ij}(k)\right]$ = Total phase = $\Psi_{ij}(k)$

$\phi_{ij}(k)$ = Phase shift due to the coulombic potential of the central atom *i* and of the backscattering atom *j*

2.1.2.1 EXAFS data collection

x-ray absorption data, for mercury and thallium L_3 edge, and for gallium, indium and scandium *K* edge, were collected in transmission mode at the Stanford Synchrotron Radiation Laboratory (SSRL). The experimental conditions were similar to those described previously.[I-III,VII] The solutions were kept in cells with a 1-5 mm Teflon spacer and Mylar foil windows. The solids was finely ground and diluted with boron nitride (BN) to reduce self-absorption and pin-hole effects, and to achieve an absorption change over the edge of about one logarithmic unit. The mixture was sealed between Kapton tape or Mylar tape windows. Energy calibration of the x-ray absorption spectra was achieved by simultaneously recording the absorption edge of the corresponding metal foils (for mercury an amalgamated tin foil), and assigning their first inflection point.[23] After energy calibration, typically 3-4 scans were averaged for each sample.

2.2.2.2 EXAFS data reduction

In order to extract the experimental EXAFS function, the data must be processed with the following steps:[24]

- A pre-edge subtraction to remove the background absorption. A linear function is fitted by least-squares methods to the pre-edge region of the spectrum and then subtracted from the raw data.
- Normalization in order to obtain a proper amplitude scale and spline subtraction to remove the background absorption.
- Conversion of the energy scale to *k*-space (from eV to the photoelectron wave number or wave vector, k /Å^{-1}) and k^3-weighting of EXAFS oscillations.
- Fourier transformation of the EXAFS functions to the corresponding peaks in *r*-space, to evaluate the main interatomic distances between the absorber and the backscatterers.

The EXAFSPAK program package was used for the energy calibration and averaging procedures, which were followed by pre-edge subtraction, data normalization and spline removal.[21,22,25] Fig. 7 outlines the steps in the data reduction and extraction of the EXAFS oscillation.

2.1.2.3 EXAFS curve fitting

Curve fitting involves comparison of the experimental EXAFS data with a model function calculated as a sum of separate oscillations obtained for atomic pair interactions, together describing an assumed coordination polyhedron or molecular structure.[26] The k^3-weighted experimental EXAFS function were used for curve fitting with the oscillating function of the model by least-squares refinements of the parameters of the atomic pair interactions. Phase and amplitude functions for single and multiple scattering pathways within the assumed molecular model were calculated by means of theoretical *ab initio* methods, using the FEFF7 program.[27] The input files to FEFF7 were normally compiled from appropriate crystal structure data, to contain the Cartesian coordinates of all atoms within a radius of 5 Å from the absorbing metal in the center.

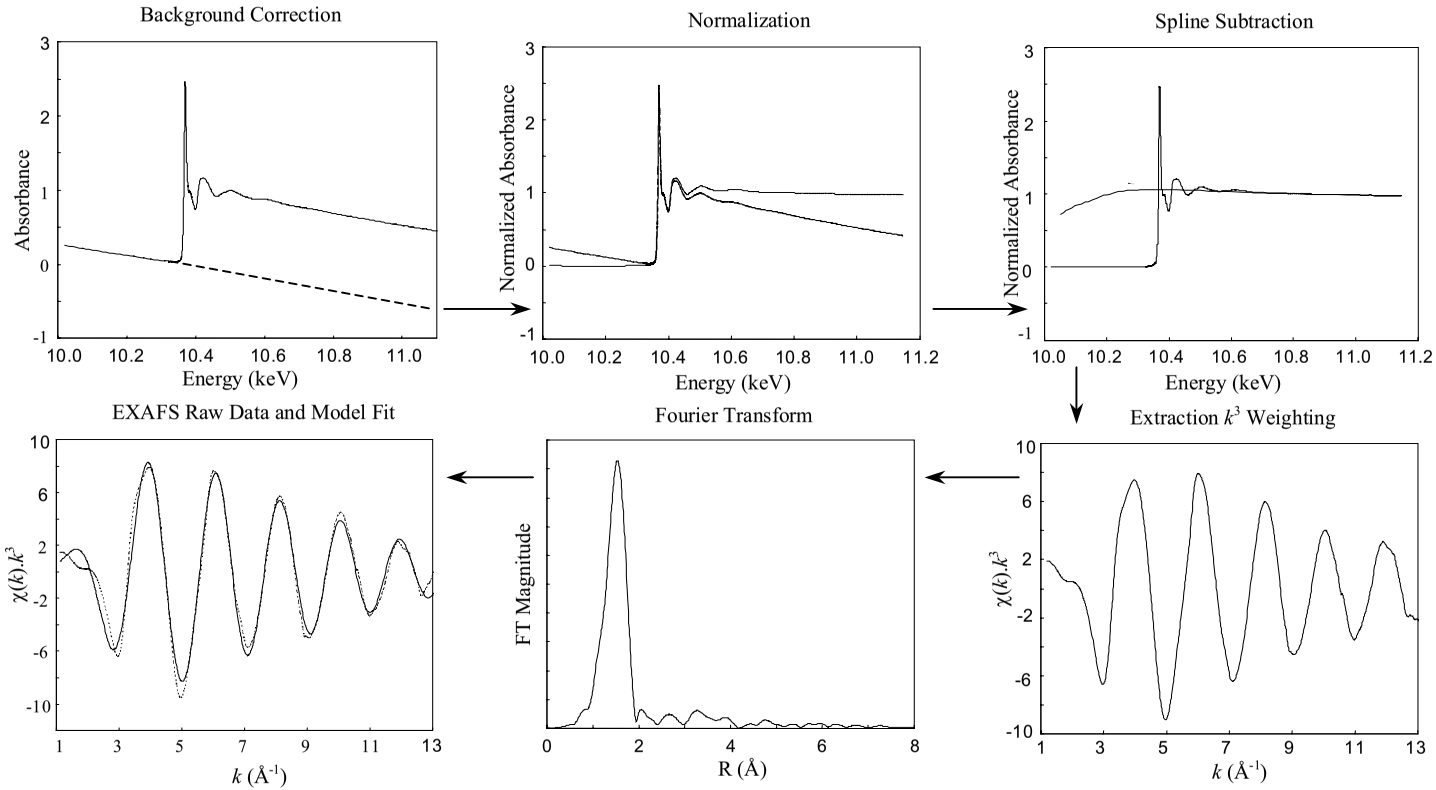

***Figure 7**. Different steps in the EXAFS data treatment procedure.*

2.2 Vibrational Spectroscopy

Vibrational spectroscopy is a useful tool to characterize complexes and study bond formation. The principal techniques for measuring vibrational spectra are infrared absorption and Raman scattering. Because of the different principles for the Raman or IR activity of a vibrational mode the techniques provide complementary information, often with opposite intensity dependence, especially for highly symmetric species. For centrosymmetric species the selection rules exclude Raman active vibrational frequencies in the IR-spectrum, and vice versa.

2.2.1 Infrared (IR) absorption

When photons of various energies ($h\nu_1$, $h\nu_{vib}$, $h\nu_2$, etc.) interact with molecular species in the sample, only photons with energies corresponding to the energy needed to excite a normal mode can be absorbed, provided this molecular vibration gives rise to a fluctuating change in the dipole moment (Fig. 8). IR spectra are recorded by measuring the transmittance of photons through the sample.[28]

The far- and mid-infrared absorption spectra of the solid compounds were obtained by means of a Bio-RAD FTS 6000 FT-IR spectrometer. The far-infrared spectrum was recorded with the sample enclosed in polyethylene disks. The mid-infrared spectra were measured using KBr pellets for the aluminium(III), gallium(III) and indium(III) samples, but for the thallium(III) and mercury(II) solvates Nujol mull between BaF_2 windows was used to avoid complex formation with bromide.

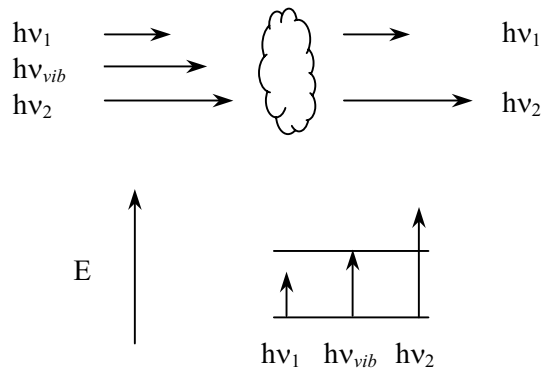

Figure 8. *IR absorption: Only photons with energy equal to vibrational transitions within a molecule can be absorbed.*

For the dimethyl sulfoxide solvent and hexakis(dimethyl sulfoxide)-scandium(III) iodide, mid-IR (200–4000 cm^{-1}) absorption spectra were recorded in purged atmosphere using a Bio-Rad (Digilab) FTS 175 spectrometer with a CsI beamsplitter. Far-infrared spectra (50 – 700 cm^{-1}) were recorded with a Bio-Rad (Digilab) FTS-40 spectrometer with a wire-mesh beamsplitter. Sample cells with silicon windows were used for the liquids. Pellets were prepared of solid samples, diluted with cesium iodide for mid-IR and polyethylene for far-IR.

2.2.2 Raman scattering

Raman scattering is excited with a different mechanism than infrared spectroscopy. When incident light (usually visible or near infrared) of energy $h\nu_o$ interacts with a molecule, an elastic scattering process called Rayleigh scattering with photons of the same energy $h\nu_o$ has the highest probability. In an inelastic scattering process, which has much lower probability, the photon energy changes to a higher or lower value ($h\nu_o \pm h\nu_{vib}$). This is called Raman scattering, and the change in frequency corresponds to the energy difference between two vibrational states of the molecule when exciting a normal mode (Fig. 9). The molecular vibration must induce a change in the polarizability for the vibrational transition to become Raman active.[28]

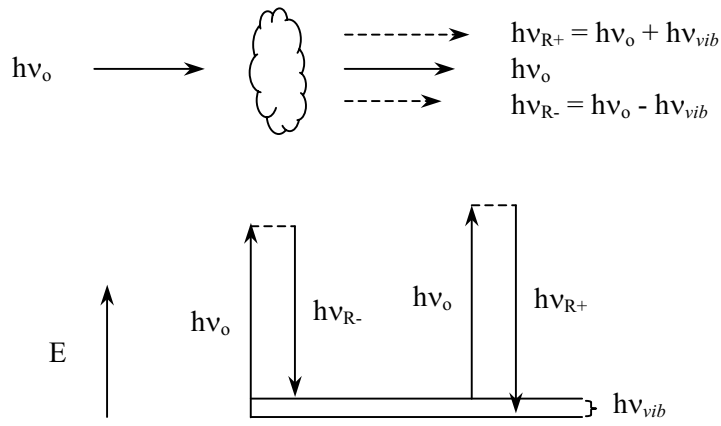

Figure 9. *Raman scattering: Inelastically scattered quanta obtain smaller or larger energies by the amount of vibrational energy transitions, $h\nu_{vib}$.*

Raman spectra of the solid compounds were obtained using a Renishaw System 1000 spectrometer, equipped with a Leica DMLM microscope, a 25 mW diode laser (782 nm) and a Peltier-cooled CCD detector, whereas Raman spectra of liquids were recorded on a dedicated Bio-Rad FT-Raman spectrometer with an Adlas DTY-321 Nd-YAG laser (1024 nm, 150 mW).

2.2.3 Normal coordinate analysis

The frequency of the normal vibration is determined by the kinetic and potential energies of the atoms in the molecule. The potential energy (V) depends on the interaction between the atoms and can be described in terms of force constants, F,[14] according to

$$V = 1/2 \sum_{i,j=1}^{3N-6} F_{ij} S_i S_j \qquad (10)$$

where S is an internal coordinate and N is the number of atoms.

The kinetic energy (T), which can be easily expressed using Cartesian displacement coordinates, becomes more complex when internal coordinates are used and can be written as:

$$T = 1/2 \sum_{i,j=1}^{3N-6} (G^{-1})_{ij} \dot{S}_i \dot{S}_j \qquad (11)$$

where $\dot{S}$ is dS/dt, and G is the matrix that describes kinetic energies in terms of mass-weighted Cartesian displacements.

The sum of the changes in the energies during a fundamental vibration is zero, which can be expressed by Newton's equation in the Lagrange form:

$$\frac{d}{dt}\left(\frac{\partial T}{\partial \dot{S}_i}\right) + \frac{\partial V}{\partial S_i} = 0 \qquad (12)$$

By combining equations 10, 11 and 12:

$$\sum_{j=1}^{3N-6} (G^{-1})_{ij} \ddot{S}_j + \sum_{j=1}^{3N-6} F_{ij} S_j = 0 \qquad (13)$$

These 3N-6 equations have the general solution

$$S_i = A_j \sin\left(\sqrt{\lambda} t + \alpha\right) \qquad (14)$$

Substituting values of 14 in equation 13 we get

$$\sum_{j=1}^{3N-6} \left(F_{ij} - (G^{-1})_{ij} \lambda\right) A_j = 0 \qquad (15)$$

These are called the secular equations and in these types of equations, the determinant of the coefficients of the *A* values must equal zero.

$$\begin{vmatrix} F_{11}-(G^{-1})_{11}\lambda & F_{12}-(G^{-1})_{12}\lambda & \dots & F_{1,3N-6}-(G^{-1})_{1,3N-6}\lambda \\ F_{21}-(G^{-1})_{21}\lambda & F_{22}-(G^{-1})_{22}\lambda & \dots & F_{2,3N-6}-(G^{-1})_{2,3N-6}\lambda \\ \dots & \dots & \dots & \dots \\ F_{3N-6,1}-(G^{-1})_{3N-6,1}\lambda & F_{3N-6,2}-(G^{-1})_{3N-6,2}\lambda & \dots & F_{3N-6,3N-6}-(G^{-1})_{3N-6,3N-6}\lambda \end{vmatrix} = 0 \quad (16)$$

Equation 16 is called the secular determinant and can be written as

$$\left|F - G^{-1}\Lambda\right| = 0 \quad (17)$$

where Λ is the matrix of eigenvalues (eigenvalues λ_i are related to vibrational frequencies, ν as $\nu_i = \frac{1}{2\pi c}\sqrt{\lambda_i}$). A more convenient expression is obtained by multiplying by $|\mathbf{G}|$:

$$\left|G\right|\left|F - G^{-1}\Lambda\right| = 0 \text{ to get } \left|GF - GG^{-1}\Lambda\right| = 0 \text{ or}$$

$$\left|GF - E\Lambda\right| = 0 \quad (18)$$

The theoretical calculation of vibrational frequencies is based on the solution of the secular equation 18 by determination of the **F** and **G** matrices. When modeling the system, very often the number of unknown force constants exceeds the number of experimental frequencies and a system of equations results where the number of parameters is larger than the number of experimental data. For a meaningful normal coordinate analysis of the bonds and interactions in a molecular species, it is necessary to cover all accessible molecular vibrational frequencies. This requires the use of both Raman and IR spectroscopy and a careful procedure for assignments of the bands.

Additional experimental frequencies can be obtained by isotopic substitution, especially deuteration where the mass of the system increases but the force constants are assumed to be constant. Also, based on previous experience, correlations between the parameters can be introduced, or in some cases estimated force constants can be introduced as fixed values, or an interaction can be neglected.

Normal coordinate analyses of the spectra and force field calculations were performed by means of Wilson's **GF** matrix method. A PC-based program package developed by J. and L. Mink,[29] was used to compute force constants and to fit calculated vibrational frequencies, using a symmetrized valence force-field.

3. SOLVATION OF METAL IONS

3.1 Solvents and anions

The preparation and purification of solvated metal salts, solvents and solutions, have been described in papers I-VII. The solvents in the present study, water and dimethyl sulfoxide, are both hard Lewis bases, coordinating via their oxygen atoms to the investigated metal ions. Both are excellent solvents for electrolytes, but otherwise with very different properties. The coordinated water molecule can also act as a weak Lewis acid, and serve as a proton donor in combination with strong bases. Therefore, the structural properties of aqueous solutions and hydrated solids are mainly controlled by hydrogen bonding. For hydration studies of highly charged ions in aqueous solution the pH should be kept low due to the risk of hydrolysis reactions.

Dimethyl sulfoxide is an aprotic solvent, highly structured because of strong intermolecular dipole-dipole interactions, but only capable of very weak interactions via the methyl protons. Solid DMSO solvates can be useful in syntheses as a source of anhydrous metal ions.[30]

3.1.1 Water

Water is a ubiquitous solvent with unique properties, and the physical characteristics of the water molecule have been thoroughly studied. The high permittivity and dipole moment (Table 1), makes water an excellent solvent for electrolytes. Even though the water molecule consists of only two elements, the structure of liquid water is very complex because of the intermolecular hydrogen bonding.[♣] Water molecules in liquid and solid phases are involved in two different types of O-H interactions; covalent O-H bonds within the water molecule, and relatively weak hydrogen bonds (O-H···O) between the water molecules. Thus, a water molecule can accept two and donate two hydrogen bonds, and is in the ice structure tetrahedrally surrounded by four other molecules. These hydrogen bonds can be broken due to the dynamical motion of atoms in liquid water. This results in a statistical distribution of water molecules with different coordination numbers. Recently, oxygen-edge x-ray absorption studies indicated a much larger number of broken hydrogen bonds than reported previously; the mean number of hydrogen bonds for water molecules in liquid water was found to be close to 3.[31] Some properties of liquid water are summarized in Table 1.

[♣] A hydrogen bond is a (nearly) linear interaction mediated by a hydrogen atom between two strongly electronegative atoms, X-H···X.

3.1.2 Dimethyl sulfoxide (DMSO)

Dimethyl sulfoxide is a hygroscopic colorless, highly structured liquid (see paper III), with high dipole moment (μ) and permittivity (ε), *cf.* Table 1. Even though the toxicity of pure DMSO is low, it penetrates easily through the skin, probably because of its polar nature, its ability to accept hydrogen bonds and its compact molecular structure. It has been tested as a carrier through the skin of active substances for medical purposes. This ability makes adequate skin protection necessary when handling DMSO solutions containing toxic compounds.[32]

The dimethyl sulfoxide molecule is an ambidentate ligand. However, coordination *via* the sulfur atom takes place only for very soft metal ions, e.g. palladium(II), platinum(II) and rhodium(III), and the relatively hard group 13 metal ions are strongly solvated *via* the oxygen atom, as also the soft mercury(II) and thallium(III) ions.[II,33,34] The anions are solvated via weak interactions with the methyl hydrogen atoms. This, together with the high permittivity, makes DMSO an efficient solvent for electrolyte solutions, even for highly charged metal ions. Some properties of liquid DMSO are presented in Table 1.

Table 1. *Physical properties of water and DMSO.*[a]

Solvent	Formula	Mp/°C	Bp/ °C	μ / D	ε	D_N	Ds
Water	H_2O	0.0	100.0	1.85	78.5	18.0	17
DMSO	$(CH_3)_2SO$	18.5	189.0	3.96	46.4	29.8	27.5

[a] Melting point (Mp), boiling point (Bp), dipole moment (μ), permittivity (ε), D_N number (eqn. 1) and Ds (eqn. 2).

As a preliminary to the study of dimethyl sulfoxide as a ligand to metal ions, we performed a normal coordinate analysis of the vibrational spectra of liquid dimethyl sulfoxide.[III] We remeasured the vibrational spectra of normal and deuterated liquid dimethyl sulfoxide, including the far-infrared region, and performed calculations to obtain a force field that was suitable to adapt to coordinated dimethyl sulfoxide in solvates,[III] in order to evaluate the changes induced in the solvated dimethyl sulfoxide compounds. For coordination studies the S-O stretching mode is the most significant dimethyl sulfoxide band, with decreasing frequency when the oxygen atom is coordinated, and increasing for sulfur coordination, and the shifts of S-O stretching frequencies have been discussed extensively in the literature.[35]

The dimethyl sulfoxide molecule was described in the $\mathbf{C}_s$ point group. Of the totally 24 fundamental normal modes 13 belong to the *A'* symmetry species, while the remaining 11 of *A''* symmetry do not preserve the mirror plane.

3.1.3 Anions

Three counter ions, which are used in the current study, are perchlorate, iodide or trifluoromethanesulfonate. Because of potential risk of explosions with perchlorates in organic solvents, as well as crystallographic disorder with different orientations for the perchlorate ion, as observed e.g. in the compounds $[M(dmso)_6](ClO_4)_3$, M = Tl and In, [II,36] other non-coordinating anions than perchlorate were of interest.

Compounds with the mono-atomic anion iodide are not explosive or suffer from orientational disorder. Another reason to use iodide is to avoid vibrational bands from the anion when studying the solvated metal ions. Because iodide is a soft donor, it does not bind to the hard acceptor metal ions in the presence of solvent molecules. However, iodide ions form strong complexes with the soft acceptor mercury(II), and could not be used for the solvated thallium(III) compounds because of formation of e.g. the $Tl(dmso)_2I_3$ complex.[37]

Trifluoromethanesulfonate has been used as a non-coordinating counter ion to form stable salts e.g. with nonahydrated lanthanoid(III) ions. However, when investigating trifluoromethanesulfonate in this study as anion instead of perchlorate for the mercury(II) and thallium(III) hydrates, trifluoromethanesulfonate ions were found to replace water ligands in the hexaaqua ions of mercury(II) and thallium(III), when the hydrated salts crystallize from an aqueous solution. Thus, the effect on the trifluoromethanesulfonate ion itself of the bond to the metal ion became a subject of interest. Firstly, a suitable force field was derived for the non-coordinated trifluoromethanesulfonate anion and the force constants were calculated using experimental data from the literature.[VII]

The free trifluoromethanesulfonate ion can be described in $\mathbf{C}_{3v}$ point group symmetry with normal vibrations belonging to $5A_1 + A_2 + 6E$ symmetry species. All normal vibrations, except the A_2 torsional mode, are infrared and Raman active. We proposed a slightly modified assignment of vibrational frequencies for the trifluoromethanesulfonate ion, in general agreement with that based on *ab initio* calculations by Lindgren et al.[38] The frequencies reported (from the literature) and those calculated for the normal vibrations of the free $CF_3SO_3^-$ anion, are summarized in Table 2, and force constants are presented in Table 4, paper VII.

Table 2. *Observed and calculated frequencies (cm^{-1}) and potential energy distribution (PED) for the free $O_3SCF_3^-$ anion.*

Species	Obs.[a]	Calc.	PED[b] (%)	Assignment
A_1	1230	1230	42 $\nu_s(CF_3)$, 29 $\delta_s(CF_3)$, 25 $\nu(CS)$	CF_3 sym str
	1038	1038	81 $\nu_s(SO_3)$, 8 $\delta_s(SO_3)$, 8 $\nu_s(CF_3)$	SO_3 sym str
	766	766	40 $\nu_s(CF_3)$, 34 $\delta_s(CF_3)$, 20 $\nu(CS)$	CF_3 umbrella
	637	637	65 $\delta_s(SO_3)$, 18 $\delta_s(CF_3)$, 11 $\nu_s(SO_3)$	SO_3 umbrella
	321	320	51 $\nu(CS)$, 28 $\delta_s(SO_3)$, 19 $\delta_s(CF_3)$	CS str
A_2	-	50	97 $\tau(CF_3)$	CF_3 torsion
E	1285	1285	79 $\nu_a(SO_3)$	SO_3 asym str
	1188	1188	50 $\nu_a(CF_3)$, 32 $\delta_a(CF_3)$, 10 $\nu_a(SO_3)$	CF_3 asym str
	580	580	93 $\delta_a(SO_3)$	SO_3 asym def
	520	516	60 $\delta_a(CF_3)$, 39 $\nu_a(CF_3)$	CF_3 asym def
	353	350	69 $\rho(SO_3)$, 19 $\rho(CF_3)$, 6 $\nu_a(CF_3)$	SO_3 rocking
	208	213	73 $\rho(CF_3)$, 24 $\rho(SO_3)$,	CF_3 rocking

[a] Symmetry coordinates and experimental data adopted from Ref. 38.

[b] Notation of vibrational modes: ν- stretching; δ- bending; ρ- rocking; s- symmetric; a- asymmetric

3.2 Solvated metal ions

All the hydrated trivalent metal ions in group 13, (M = Al, Ga, In, and Tl) form hexaaqua species,[39-44] while in group 3 the hydration number of the trivalent metal ions increases with increasing atomic number, both in solution and in the solid state. In aqueous solution scandium(III) probably coordinates seven water molecules in a monocapped trigonal prism.[45] Yttrium(III) is found to coordinate eight water molecules in a square antiprism in aqueous solution, and nine in a tricapped trigonal prism in the solid triflluoromethanesulfonate salt.[46,47] Lanthanum(III) forms nonaaqua TTP complexes both in aqueous solution and in the solid state.[48]

From dimethyl sulfoxide solution the trivalent group 13 metal ions crystallize in octahedral hexakis(dimethyl sulfoxide) solvates, [I,II] as also scandium(III) iodide.[III] However, the other group 3 ions, yttrium(III) and lanthanum(III), coordinate eight dimethyl sulfoxide molecules in their solvates.[IV,49] In papers I-IV the structures of the dimethyl sulfoxide solvates of aluminum(III), gallium(III), indium(III), scandium(III) and some lanthanoid(III) iodides, and of hexakis(dimethyl sulfoxide)-thallium(III) perchlorate, are described in solution and in the solid state. Paper V treats deficiency and mobility of coordinated water in the crystalline nonahydrates of scandium(III) and lanthanoid(III) trifluoromethane-sulfonates. In paper VI, infrared and Raman spectroscopic and theoretical studies of nonaaqua lanthanoid(III) trifluoromethanesulfonate have been discussed. Finally, the bonding and PJTE on the d^{10} ions mercury(II) and thallium(III), by studying their crystalline trifluoromethanesulfonate hydrates is examined in VII.

3.2.1 Coordination number six:

3.2.1.1 Hexakis(dimethyl sulfoxide)aluminium(III) (**1**), gallium(III) (**2**), indium(III) (**3**) iodide, hexakis(dimethyl sulfoxide)thallium(III) perchlorate (**4**), and scandium(III) iodide (**5**)

Crystal structures

All trivalent group 13 metal ions coordinate six dimethyl sulfoxide ligands in the compounds **1**, **2**, **3** and **4,** as also scandium(III) in **5** (Fig. 10), while the other group 3 metal ions show a different trend. Yttrium(III) and lanthanum(III) coordinate eight dimethyl sulfoxide molecules in a square antiprismatic fashion.[IV,49] When comparing the solvates of yttrium(III) and thallium(III), which have similar ionic radii in six-coordination, 0.900 and 0.885 Å,[50] respectively, the higher degree of covalent bonding character for the thallium(III) ion of group 13 is evident from its lower solvation number. The crystal structures of the compounds **1-5** could all be satisfactorily described in the space group $R\bar{3}$. The trivalent metal ions are located in a site of $\bar{3}$ symmetry surrounded by six equidistant oxygen-bonded dimethyl sulfoxide ligands, Figs. 10 and 11.

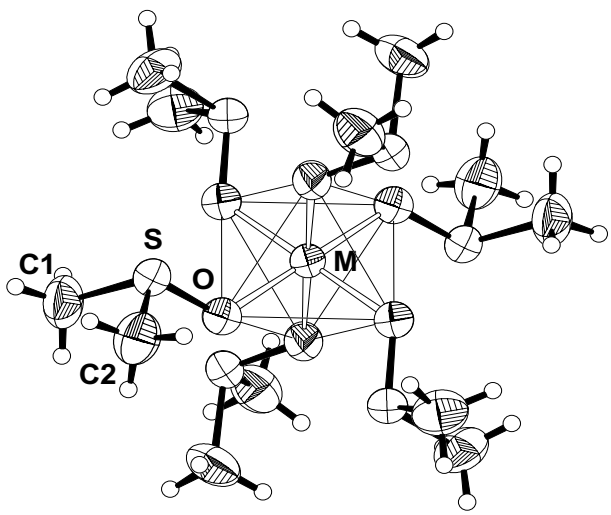

Figure 10. *The metal atom M is surrounded by six equivalent oxygen-coordinated dimethyl sulfoxide ligands in the $[M(dmso)_6]^{+3}$ complexes, M = Al, Ga, In, Sc and Tl. The figure displays the gallium(III) complex with 50% probability ellipsoids.*

The M-O bond distances 1.894(4), 1.974(4), 2.145(3), 2.224(3) and 2.069(3) Å at ambient temperature were obtained for the $[M(dmso)_6]^{3+}$ complexes with M = Al, Ga, In, Tl and Sc, respectively.[I-III] At low temperature (150 K) a longer Tl-O bond distance, 2.240(4) Å, was obtained.[II] This difference is larger than expected between two different temperatures for the Tl-complex. The thermal ellipsoids of the thallium, oxygen and sulfur atoms at 150 K are elongated principally along the c-axis, while at 295 K the appearance is normal. This indicates some disorder in the crystal structure of the $[Tl(dmso)_6](ClO_4)_3$ compound at low temperature (Fig. 11).

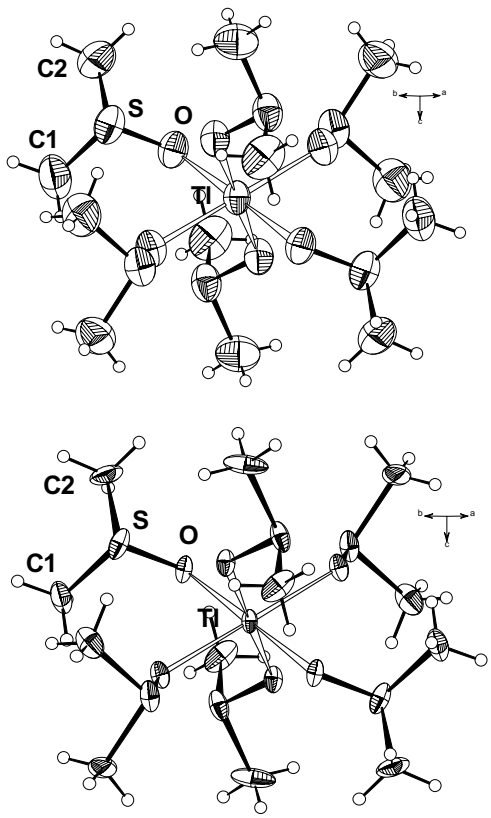

Figure 11. *The hexakis(dimethyl sulfoxide)thallium(III) complex in the crystal structure of $[Tl(dmso)_6](ClO_4)_3$ (50% probability ellipsoids); Top: at 295 K, below at 150 K.*

The M-O(dmso) bond distances for Tl and In complexes with mixed ligands of dimethyl sulfoxide and halides are found to be longer than the corresponding values in the hexakis(dimethyl sulfoxide) solvates. The In-O bond distances 2.195 and 2.199 Å in the $InX_3(dmso)_3$ compounds, where X = Cl and Br, respectively,[51] and also Tl-O bond lengths 2.469 and 2.42(2) Å

for the $TlI_3(dmso)_2$ and $[TlCl_5(dmso)](C_5H_6N)_2$ compounds, respectively,[37,52] are found to be longer than the corresponding bond distances in the compounds **3** and **4**. This indicates that these halides as ligands bind more strongly to indium(III) and thallium(III) than dimethyl sulfoxide. However, even in saturated dimethyl sulfoxide solution, the iodide ion is not able to compete with dimethyl sulfoxide molecules as ligand to indium(III).[I]

A recent report of the disordered crystal structure of $[Sc(dmso)_6](ClO_4)_3$ shows the Sc-O bond distance 2.068(6) Å for the major component (86% occupancy) close to Sc-O bond distance 2.069(3) Å in the compound **3**.[53] Also, in the crystal structure of $[Sc(H_2O)_6][Sc(OSO_2CH_3)_6]$, the Sc-O distance 2.085(6) Å,[54] is consistent with that expected for six oxygen-coordinated ligands. However, the Sc-O bond length in the hydrated scandium(III) ion in aqueous solution reported in the range 2.15-2.18 Å, supports a coordination of at least seven water molecules.[54-56]

The M-O-S angle decreases with increasing covalency of the M-O bond. This angle is found to be small, 116.4(3)°, for the hexakis(dimethyl sulfoxide)mercury(II) trifluoromethanesulfonate with high covalency of the Hg-O bonds, with a much larger value, 132.5(3)°, for the compound **5** with low Sc-O bond covalency. The smallest M-O-S angle in the $M(dmso)_6^{3+}$ complexes for the group 13 metal ions M = Al, Ga, In, and Tl, is found for thallium(III), 120.7(2)°, and the largest for aluminium, 127.1(3)° (Table 3),[I] consistent with decreasing covalency in the M-O bonds from M = Tl to Al.

Compression ratio

An octahedron can be viewed as a regular $\mathbf{D}_{3d}$ trigonal antiprism, *cf*. Fig.12. The twist angle between the triangular surfaces, θ, or the ratio of the side of the triangle to the distance between triangles, *s/h*, can be used as measures of distortions (Fig. 12).

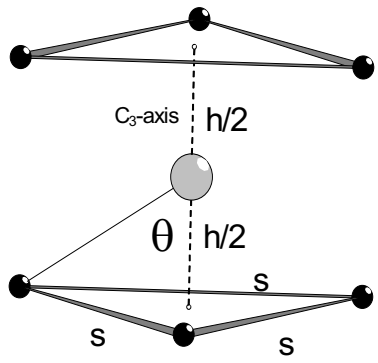

Figure 12. *The octahedral MO_6 center in the $[M(dmso)_6]^{3+}$ structures is compressed along the three-fold axis. For a perfect octahedron s/h = $\sqrt{3}/2$ = 1.225, where s is the side of the equilateral triangles, and h is the distance between the triangles.*

The increasing distances between the oxygen atoms within the MO_6 kernel in the compounds **1**-**5**, allow significant deviation from a regular octahedral symmetry. This deviation can be measured by the compression ratio *s/h* and compared to the regular octahedron (*s/h* = 1.225).[57]

The relations between the M-O bond distances in the compounds **1**-**5** and hexakis(dimethyl sulfoxide)indium(III) perchlorate, their compression ratios, *s/h*, and cell volumes are shown in Figure 13. The three smallest of these ions, aluminium(III), gallium(III) and scandium(III), obtain similar compression ratios of about 1.287 in the compounds **1**, **2** and **5**, while the compression ratio increases to 1.335 for the compound **3** (Fig. 13a). This is reflected in the cell volume, which is smallest for the compound **3** (Fig. 13b). A comparison between the isostructural hexasolvated indium(III) and thallium(III) perchlorates shows similar behavior, with compression ratios of 1.373 and 1.455, respectively.[36] The larger ion, thallium(III), has the smaller cell volume.

The M-O-S angle in the $[M(dmso)_6]^{3+}$ complexes is another factor affecting the cell volume. This angle is 3.0 degrees larger for the aluminium than gallium in the compounds **1** and **2** and can explain why cell volumes of the compounds are quite similar despite the difference in M-O bond distances.

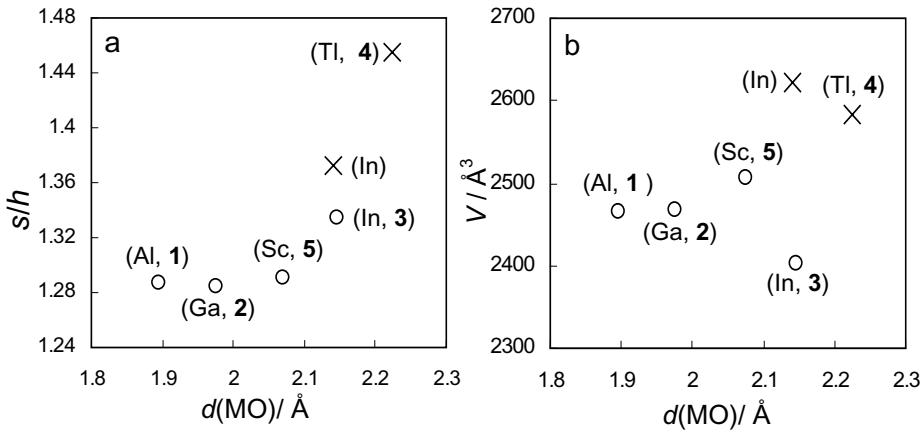

Figure 13. *Correlation between bond lengths and a) compression ratio (s/h) and b) unit cell volume (V). The symbol (o) denotes $[M(dmso)_6]I_3$ complexes (M = Al, Ga, Sc and In), and (×) $[M(dmso)_6](ClO_4)_3$ complexes (M = In and Tl).*

Table 3. *Bond Lengths (Å) and Angles (°) for $[M(dmso)_6]^{n+}$ Complexes.*

metal atom anion	Tl(III) perchlorate[a]	In(III) perchlorate[b]	In(III) iodide[c]	Ga(III) iodide[c]	Al(III) iodide[c]	Sc(III) iodide[d]	Hg(II) triflate[e]	Uncoordinated dimethylsulfoxide[f]
M-O	2.224(3)	2.140(3)	2.145(3)	1.974(4)	1.894(4)	2.069(3)	2.347(5)	
compression ratio *s/h*[g]	1.455(3)	1.373(4)	1.335(4)	1.285(6)	1.287(3)	1.291(4)	1.390(6)	
cell volume	2584.0(5)	2622.0(12)[h]	2403.5(7)	2468.1(6)	2467.2(5)	2507.7(6)	2593.8(6)[h]	
Closest O···O distance	2.948(5)	2.915(5)	2.945(4)	2.746(6)	2.636(5)	2.874(5)	3.182(7)	
O-S	1.544(4)	1.542(3)	1.541(3)	1.539(5)	1.540(5)	1.536(3)	1.543(5)	1.495(4)
S-C(1)	1.758(8)	1.763(8)	1.787(5)	1.774(8)	1.776(7)	1.754(5)	1.766(8)	1.773(4)
S-C(2)	1.770(7)	1.771(6)	1.765(5)	1.773(8)	1.776(7)	1.773(6)	1.764(9)	
O-M-O′	96.20(13)	94.2(1)	93.3(1)	91.8(2)	91.9(2)	90.0(2)	94.6(2)	
M-O-S	120.7(2)	124.0(2)	123.1(2)	124.1(3)	127.1(3)	132.6(2)	116.4(3)	
O-S-C(1)	103.2(3)	102.9(2)	104.1(2)	104.6(4)	104.0(4)	103.8(2)	104.1(3)	105.7(2)
O-S-C(2)	104.2(3)	103.6(3)	103.3(2)	102.9(3)	102.6(4)	103.9(2)	106.5(4)	
C(1)-S-C(2)	99.8(4)	99.6(3)	98.5(3)	98.3(4)	98.4(4)	99.1(3)	98.6(5)	98.0(3)

[a] Ref. II. [b] Ref. 36. [c] Ref. I. [d] Ref. III. [e] Ref. 34. [f] Ref. 30. [g] Ref. 57; *s/h* = 1.225 for a regular octahedron.
[h] With hexagonal unit cell (*Z* = 3).

EXAFS measurements

Analyses of EXAFS data collected for the dimethyl sulfoxide solvated gallium(III), indium(III), thallium(III) and scandium(III) ions in solution result in similar M-O bond distances as for the solid solvates.[I-III] The refined EXAFS parameters for the above complexes are compared in Table 4 with three different program systems used for the data treatment. The coordination number was held constant, and the amplitude reduction factor, S_0^2, obtained reasonable values for WinXAS and EXAFSPAK, Table 4.

A minor feature at about k = 3 Å^{-1} in the EXAFS oscillation of the hexakis(dimethyl sulfoxide)scandium(III) solvate (Fig. 14), is caused by double electron excitation, a phenomenon that affects the S_0^2 value. The mean square displacement parameters (σ^2) in the scandium(III) complex vary with the three program packages. This value probably contains accumulated errors from spline and background subtraction procedures, and from the modeling of multiple scattering. The fit of the model function with separate contributions from the scattering pathways is displayed in Fig. 14.[III]

Space-group determination can be a problem in crystals with twinning or disorder. The systematic absences from the diffraction data for the hexakis(dimethyl sulfoxide)thallium(III) perchlorate, **4**, at ambient temperature are consistent with either *R*3 (No. 146) or $R\bar{3}$ (No. 148) space groups. A crystallograpic data set was collected at low temperature (150 K), but did not help in deciding between these two space groups. Refining the structure in *R*3 resulted in a distribution of Tl-O bond distances, while in $R\bar{3}$ there is only a single Tl-O bond distance.

Low temperature EXAFS data (10 K) were then collected, which revealed relatively small Debye-Waller factors for the mean Tl–O and Tl···S distances and indicated no disorder in the $[Tl(dmso)_6]^{3+}$ complex. Fourier transformed EXAFS data for solid $[Tl(dmso)_6](ClO_4)_3$ at 10K display a much sharper Tl-O peak than at ambient temperature because of less vibrational movement at the lower temperature. This indicates absence of positional disorder of the Tl-O bond distances (Fig. 2 and 3, paper II), and supports the choice of the space group $R\bar{3}$ with a single metal-oxygen bond distance.[II]

Table 4. *EXAFS results for the dimethyl sulfoxide solvated group 13 ions, gallium(III), indium(III) and thallium(III) in solution and in the solid state. Bond distances, d/Å, Debye-Waller factors, σ^2/Å^2, number of distances, N, and amplitude reduction factor, S_o^2, are given with estimated standard deviation from least squares refinement within brackets (systematic error are not considered).*

State	Pathway	*r*/Å	σ^2/Å^2	*N*	S_o^2	Program
$Ga(ClO_4)_3$	Ga - O	1.955(2)	0.0065(2)	6	1.27(3)	EXAFSPAK
solution	Ga…S	3.108(4)	0.0112(6)	6		
(295±2 K)	Ga-O-S	3.194(18)	0.019(4)	12		
	MS	3.964(14)	0.0054(20)	3x6		
$[Ga(dmso)_6]$-	Ga-O	1.954(2)	0.0050(2)	6	1.19(4)	EXAFSPAK
$(CF_3SO_3)_3$	Ga…S	3.117(3)	0.0079(4)	6		
solid	Ga-O-S	3.280(23)	0.015(4)	12		
(295±2 K)	MS	3.982(25)	0.0080(40)	3x6		
$In(CF_3SO_3)_3$	In - O	2.135(2)	0.0054(2)	6	1.03(3)	EXAFSPAK
solution	In…S	3.320(6)	0.0094(5)	6		
(295±2 K)	In-O-S	3.481(9)	0.0036(9)	12		
	MS	4.19(3)	0.011(5)	3x6		
$[In(dmso)_6]$-	In - O	2.143(2)	0.0043(2)	6	0.96(3)	EXAFSPAK
$(ClO_4)_3$	In…S	3.282(3)	0.0071(3)	6		
solid	In-O-S	3.519(11)	0.012(2)	12		
(295±2 K)	MS	4.35(7)	0.034(20)	3x6		
$Tl(CF_3SO_3)_3$	Tl – O	2.22(1)	0.0066(7)	6	0.66(2)	WinXAS
solution	Tl…S	3.33(2)	0.015(3)	6		
(295±2 K)	Tl-O-S	3.53(5)	0.017(6)	12		
	MS	3.77(4)	0.007(5)	4x6		
$[Tl(dmso)_6]$-	Tl - O	2.221(4)	0.0022(3)	6	0.86(2)	WinXAS
$(ClO_4)_3$	Tl …S	3.282(6)	0.0028(3)	6		
solid	Tl-O-S	3.45(3)	0.0030(5)	12		
(10 K)	MS	4.44(4)	0.06	3x6		
$Sc(CF_3SO_3)_3$	Sc-O[b]	2.093(3)	0.0016(2)	6	1.0	GNXAS
solution	S-O	1.535(5)	0.0014(3)	6		
(295±2 K)	Sc-S[d]	3.374(10)				
	Sc-O	2.090(5)	0.0027(3)	6	0.91	EXAFSPAK
	Sc…S	3.351(9)	0.0048(8)	6		
	Sc-O-S[c]	3.501(12)	0.003(1)	12		
	Sc-O-O[c]	4.22(4)	0.008(5)	12		
	Sc-O	2.088(4)	0.0046(3)	6	0.96	WinXAS
	Sc…S	3.303(6)	0.0080(6)	6		
	Sc-O-S[c]	3.467(10)	0.0022(6)	12		
	Sc-O-Sc-O[c]	4.12(2)	0.009(2)	3×6		

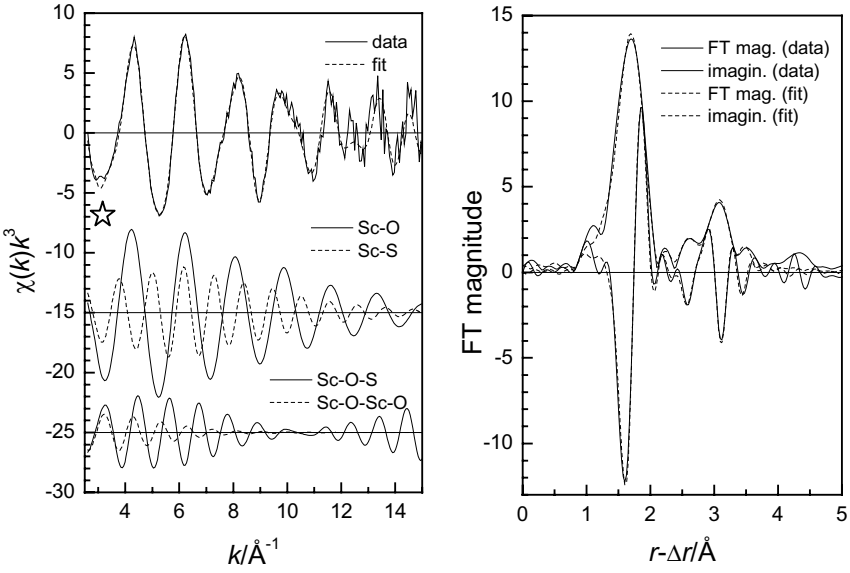

Figure 14. *(Left) k^3-weighted EXAFS data, fitted model function and individual backscattering contributions for $[Sc(OSMe_2)_6]^{3+}$ in dimethylsulfoxide solution, cf. Table 4 (WinXAS: Sc-O and Sc···S single backscattering, offset -15 and 3-leg Sc-O-S and 4-leg linear Sc-O-Sc-O multiple-scattering, offset –25); (right) Fourier transforms of experimental data and model function with magnitude and imaginary part. The star (☆) indicates a double transition (see page 28).*

Vibrational spectroscopy

Metal ion-ligand interactions generally give rise to new bands below 600 cm^{-1}, and also the internal 'group frequencies' of the ligands may shift and split. This gives rise to a characteristic pattern of vibrational frequencies, which often is used to identify solid coordination compounds by IR-spectroscopy. For complexes in solution, Raman measurements mostly are preferable, because the IR absorption of polar solvents generally is strong.

However, beyond such qualitative identifications, there is a wealth of detailed coordination and bonding information to be derived from a thorough analysis of the vibrational spectra. A normal coordinate analysis can reveal the intricate pattern of coupled vibrational modes. By evaluating the force field of the molecular vibrations, resulting in a potential energy distribution, assigments of each normal vibration to the dominating atomic movements can be made. Discussions of changes in metal-ligand bond strength and character, by comparing shifts and splitting of vibrational frequencies in a series of complexes, can safely be performed only if based on such analyses.

The $[M(dmso)_6]^{3+}$ (M = Al, Ga, Sc, In and Tl) complexes consist of 25 atoms, considering each methyl group as a point mass.[I-III] In this description, these complexes possess 69 normal vibrations. The $[M(dmso)_6]^{3+}$ complexes can be described in the S_6 point group, with the normal vibrations belonging to $11A_g + 11E_g + 12A_u + 12E_u$ symmetry species (Appendix B). The symmetry species denoted *E* represents a doubly degenerate state. For these centrosymmetric complexes, the symmetric modes should only be Raman-active, and the asymmetric ones only IR-active.

Averaged frequencies of the six stretching modes, $\bar{\nu} = \frac{\nu_{A_g} + \nu_{A_u} + 2\nu_{E_g} + 2\nu_{E_u}}{6}$, are given in Table 5 for the $[M(dmso)_6]^{3+}$ (M = Al, Ga, Sc, In and Tl) complexes. The average frequency, $\bar{\nu}$, seems to be a better indicator of the bond strength, including more efficiently the effects of the ligand-ligand interactions than the frequently used comparisons based only on the symmetric stretching frequency, ν_{A_g}. The decreasing values for the group 13 metal ions are consistent with decreasing electrostatic contribution to the bond strength when the size of the central atom increases.

The splitting between the asymmetric $\nu(E_u)$ and symmetric $\nu(A_g)$ stretching modes is caused by the ligand-ligand interactions. The splitting in relation to the bond strength, $\frac{\Delta\nu}{\bar{\nu}}$ where $\Delta\nu = \nu(E_u) - \nu(A_g)$, decreases from Al to In for both the M-O and S-O bonds. The thallium(III) complex deviates from these trends probably because of a considerable increase in covalency in the metal-oxygen bond. This change is far less for the S-O bond, which is farther from the central atom than the M-O bond. The M-O and S-O frequencies in the scandium(III) complex do not follow the trends of the group 13 metal ions (see Table 5). The reason is probably an effect of the more electrostatic M-O bond character in the scandium(III) complex and the much higher contribution of M-O asymmetric stretching (A_u and E_u) as shown by the potential energy distribution, than for the group 13 metal ions (Table 4, paper I). The $\frac{\Delta\nu}{\bar{\nu}}$ values for the C-S bond, which are still more distanced from the central atom than S-O, are less than 1%, showing that the ligand-ligand interactions are small. This explains why frequencies of the asymmetric and symmetric stretching modes, and the scissoring modes of SC_2 for the different symmetry species A_g, E_g and A_u, E_u, respectively, appear at the same positions (Table 4, paper I).

Raman spectra for the solid compounds **1**-**5** and also for liquid dimethyl sulfoxide, are displayed in Fig. 15. When compared to the spectrum of liquid DMSO, two new bands, corresponding to symmetric and asymmetric M-O bond stretching, appear below 550 cm^{-1} from the DMSO-solvated metal ions (Fig. 15). In the $Tl(dmso)_6(ClO_4)_3$ spectrum new bands (934, 625 and 455 cm^{-1}) appear from the perchlorate ion; the latter band overlapping with the Tl-O stretching vibration.

Table 5. *Average stretching frequencies for the M-O and S-O bonds in the $M(dmso)_6^{3+}$ (M = Al, Ga, Sc, In and Tl) complexes.*

	Al	Ga	Sc	In	Tl
M-O	1.89	1.97	2.07	2.15	2.22
$\bar{\nu}$ [a]	502	494	436	447	442
$\Delta\nu$ [b]	52	12	24	8	26
$\frac{\Delta\nu}{\bar{\nu}}.100\%$	10.4	2.4	5.4	1.8	5.9
S-O	1.54	1.54	1.53	1.54	1.54
$\bar{\nu}$	919	909	959	910	913
$\Delta\nu$	23	14	3	12	21
$\frac{\Delta\nu}{\bar{\nu}}.100\%$	2.5	1.5	0.3	1.3	2.3

[a] $\bar{\nu} = \frac{\nu_{A_g} + \nu_{A_u} + 2\nu_{E_g} + 2\nu_{E_u}}{6}$, [b] $\Delta\nu = \nu_{E_u} - \nu_{A_g}$

Generally O-coordination causes a decrease, and S-coordination an increase, in the S-O stretching vibration frequency.[14] Bands at about 1067 cm^{-1}, corresponding to the uncoordinated S-O stretching mode in liquid DMSO, shift to lower frequencies when the DMSO molecule coordinates through its oxygen atom to the metal ion (Figure 15).

Vibrational modes with frequencies lower than that of M-O stretching are assigned as MOS, CSO and SC_2 bendings. Asymmetric and symmetric stretching frequencies of SC_2 do not change significantly when the DMSO molecule is coordinated and appear at about 700 cm^{-1}.

The preliminary assignment of the experimental frequencies was made by comparison with similar studies of dimethyl sulfoxide complexes from the literature, including and considering shifts due to isotopic substitutions.[III] Final assignment and labeling of the experimental frequencies was made from the potential energy distribution obtained by normal coordinate analysis of the vibrational modes.

We firstly simplified the calculations of the force constants by considering the metal ion with only one DMSO ligand. The resulting force constants were used as a starting point when refining new force constants for the $M(dmso)_6^{3+}$ complex. The force field obtained for the compounds **1-5** are summarized in Table 6.[I-III]

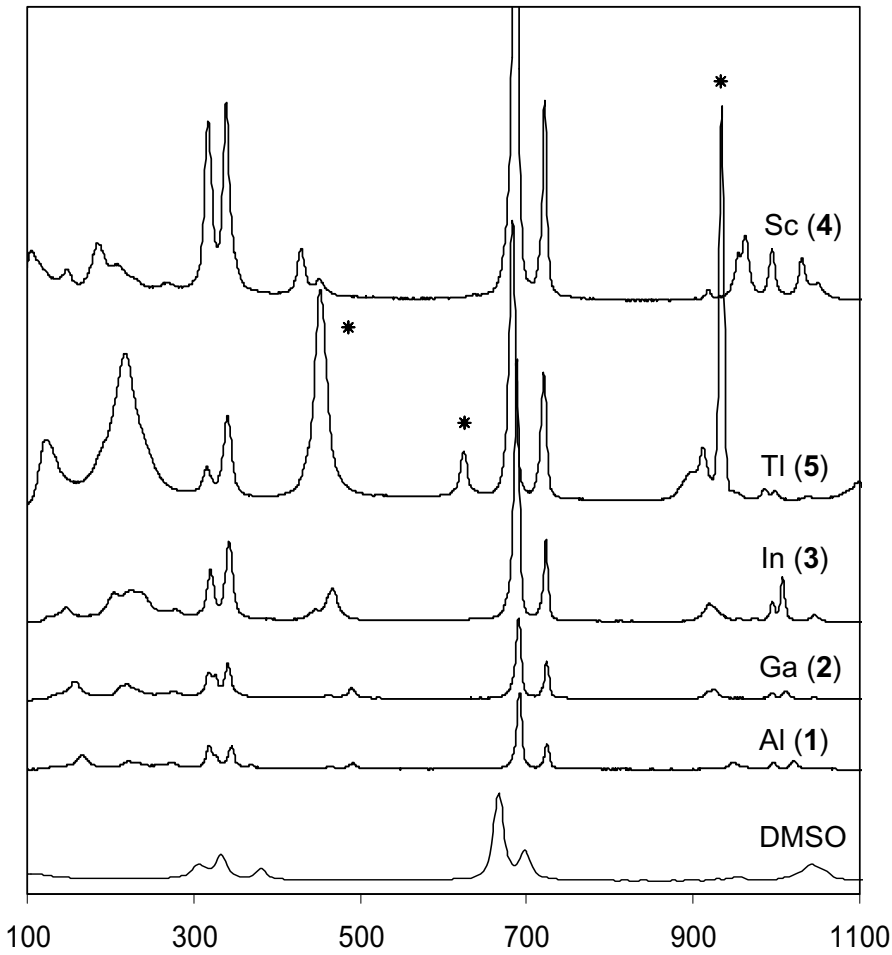

Figure 15. *Raman spectra of the hexakis(dimethyl sulfoxide) group 13 and scandium metal ions compared with liquid dimethyl sulfoxide.*
** ClO_4^- bands*

The correlation between the M-O stretching force constants and the M-O bond distance in Fig. 16 is almost linear with some deviation for the $[Tl(OSMe_2)_6]^{3+}$ solvate, which has substantial covalent bond character. The different character of the bonding in the $[Tl(OSMe_2)_6]^{3+}$ complex is also clearly shown in a comparison of the sulfur K-edge x-ray absorption spectra of the group 13 $[M(OSMe_2)_6]^{3+}$ solvates.[58]

***Table 6**. Calculated force constants for $M(dmso)_6^{3+}$ complexes (M = Al, Ga, In and Tl).*

Coordinates	dmso	Al (**1**)	Ga (**2**)	Sc (**5**)	In (**3**)	Tl (**4**)	units
stretching							
K(MO)		1.761	1.617	1.462	1.318	1.300	a
		(1.779)	(1.670)	(1.643)	(1.552)	(1.469)	a*
K(OS)	5.061	4.599	4.168	4.402	4.274	4.279	a
		(4.805)	(4.652)	(4.653)	(4.758)	(4.809)	a*
K(CS)	2.063	2.500	2.519	2.194	2.495	2.471	a
stretch-stretch							
F(MO,MO)trans		-0.171	0.448	0.451	0.184	0.071	a
F(MO,MO)cis		-0.048	0.007		0.003	0.012	a
F(OS,OS)trans		-0.124	0.012	-0.173	0.024	-0.034	a
F(OS,OS)cis		-0.031	-0.018		-0.001	-0.032	a
F(CS,CS)	0.228	-0.037	-0.019	0.119	-0.016	-0.012	a
bending							
H(SC_2)	1.522	0.968	1.057	0.862	0.953	0.874	b
H(OSC)	1.070	0.664	0.367	0.513	0.396	0.134	b
τ(MOSC)		0.134	0.145		0.148	0.134	b
bend-bend							
h(OSC,OSC)		0.201	0.227		0.026	0.022	b
stretch-bend							
f(MO,OSC)		0.070	0.070		0.071	0.070	c

Units: a. N cm^{-1} ; b. 10^{-16} $Nm.rad^{-2}$; c. 10^{-6} $N.rad^{-1}$

*The MO and OS stretching force constants within brackets were obtained using a simplified M-$OS(CH_3)_2$ monoligand model.

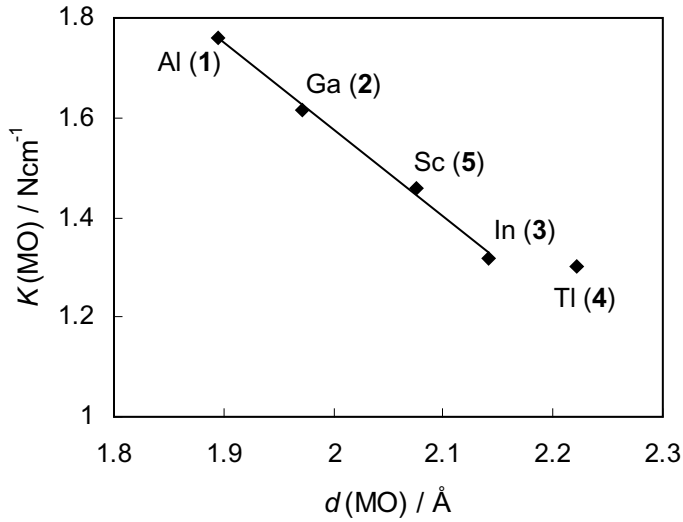

***Figure 16.** Correlation between metal-oxygen (M-O) force constants and bond lengths in the compounds **1-5**.*

The S-O stretching frequencies and the corresponding force constant decreases by oxygen-coordination to metal ions, while the C-S stretching frequencies and force constant increase as compared to free dimethyl sulfoxide (Table 6). However, the correlation between the S-O bond distances and the S-O force constants in the compounds **1**-**5** shows a complex behavior. For the aluminum and scandium complexes the S-O stretching force constants are significantly higher than expected, probably because for these d^0 ions no back-bonding is possible. In the gallium(III), indium(III) and thallium(III) ions with d^{10} electronic configuration, back-bonding can increase the M-O bond strength, resulting in a weakened S-O bond. The contribution of M-O stretching to the S-O stretching mode near 950-970 cm^{-1} decreases significantly from the solvates of the group 13 metal ions to scandium(III); this also correlates to a substantial increase in the MOS angle (from ca. 124° to 132.6°). The coordination of the dimethyl sulfoxide molecule leads to significant decrease in the SC_2 scissoring vibrational frequencies and the corresponding bending force constants, while the S-C stretching frequencies and stretching force constants increase.[I-III]

3.2.1.2 Bisaquamercury(II) trifluoromethanesulfonate (**6**) and trisaquathallium(III) trifluoromethanesulfonate (**7**)

Crystal structures

The crystal structure of $[Hg(OH_2)_2(CF_3SO_3)_2]_\infty$ was described in the triclinic space group $P\bar{1}$ (No. 2).[VII] The structure consists of almost linear $Hg(OH_2)_2^{2+}$ ions linked together by two trifluoromethanesulfonate ions in infinite $Hg(OH_2)_2^{2+}<(CF_3SO_3^-)_2>Hg(OH_2)_2^{2+}$ chains. The mercury(II) ion binds strongly to the two water molecules at a mean Hg-O bond distance of 2.11 Å. The $Hg(OH_2)_2^{2+}$ ion interacts with four oxygen atoms from four different trifluoromethanesulfonate ions with Hg-O bond distances between 2.46 and 2.66Å, Fig. 17. The trifluoromethanesulfonate ions bridge two $Hg(OH_2)_2^{2+}$ ions with two oxygen atoms, while the third oxygen atom is hydrogen bonded to a water molecule in a $Hg(OH_2)_2^{2+}$ ion in a neighboring chain, Fig.17.

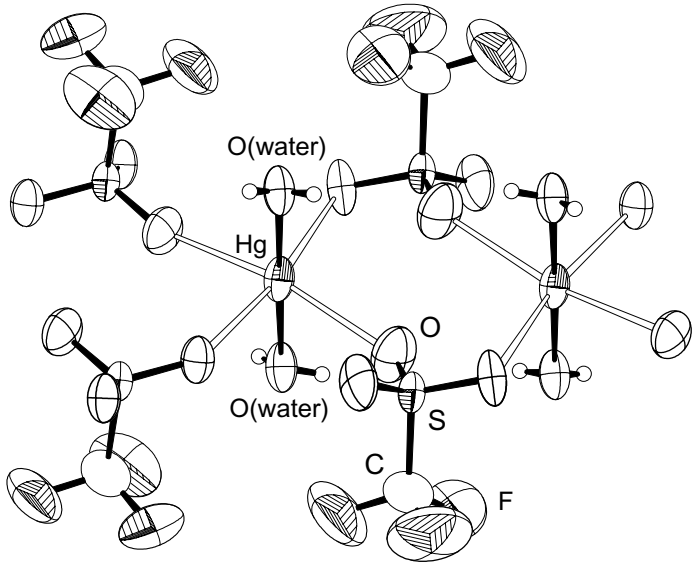

Figure 17. *The strongly bonded $Hg(OH_2)_2^{2+}$ entities joined by double bridges (unfilled bonds) of Hg-O bonds to oxygen atoms of trifluoromethanesulfonate ions into $[Hg(OH_2)_2(O_3SCF_3)_2]_\infty$ chains.*

These fairly strong hydrogen bonds hold the chains together in sheets, from which the $-CF_3$ groups emerge (Fig. 18). The average O-(H)···O hydrogen bond distance between the water molecules and the trifluoromethanesulfonate ions is 2.71 Å.[VII] The hydrogen-bonded sheets are held together merely by van der Waals interactions between the fluorine atoms. This layer structure explains why the crystals are very fragile and easily split into thin plates.

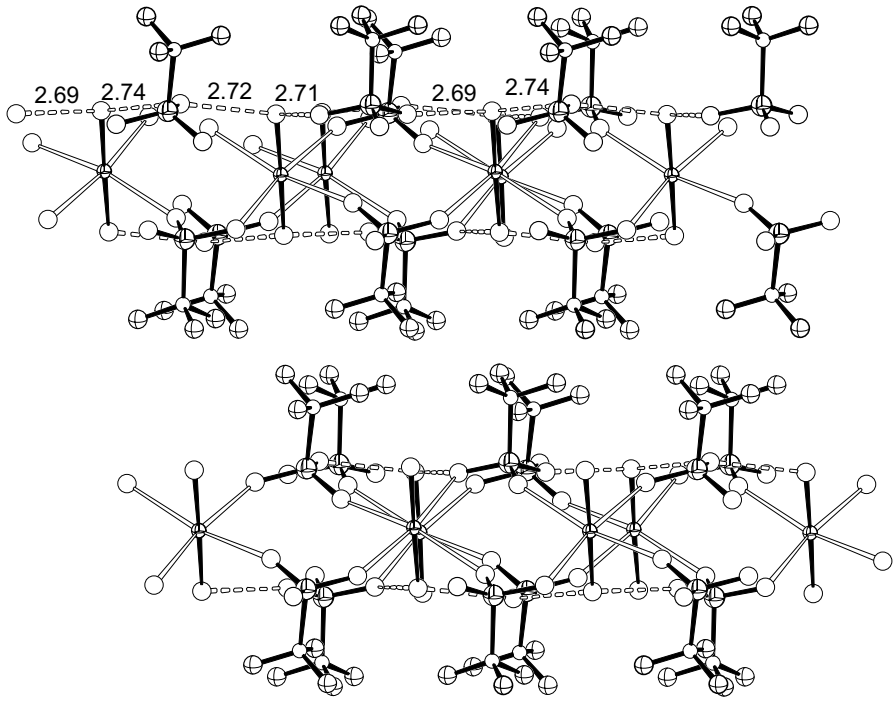

Figure 18. *In the bisaquamercury(II) trifluoromethanesulfonate compound, layers are formed by hydrogen bonding between* $[Hg(OH_2)_2(O_3SCF_3)_2]_\infty$ *chains. The layers are held together merely by van der Waals interactions between the* $-CF_3$ *groups.*

The crystal structure of **7**, $Tl(OH_2)_3(CF_3SO_3)_3$, was described in the monoclinic space group *C*2/*c* (No. 15).[VII] The structure is built up of discrete trisaquatris(trifluoromethanesulfonate)thallium(III) molecules where the thallium(III) ion coordinates to three water molecules and three oxygen atoms from three trifluoromethanesulfonate ligands in approximately octahedral geometry (Fig. 19). The Tl-O bond distance 2.205(2) Å, obtained from the EXAFS data, is consistent with the crystallographic mean value, 2.21 Å, and also close to previous determinations of the hexahydrated thallium(III) ion in aqueous solution and the solid state, ca. 2.21 Å.[II] The average O-(H)···O hydrogen bond distance between the coordinated water molecules and the trifluoromethanesulfonate ions in **7**, 2.70 Å, is similar to that in **6**, 2.71 Å. This indicates that mercury(II) ion polarizes its aqua ligands in this compound as much as thallium(III) in the $[Tl(OH_2)_3(CF_3SO_3)_3]$ complexes, despite the higher formal charge for thallium(III), see Hydrogen bonds (p. 41).

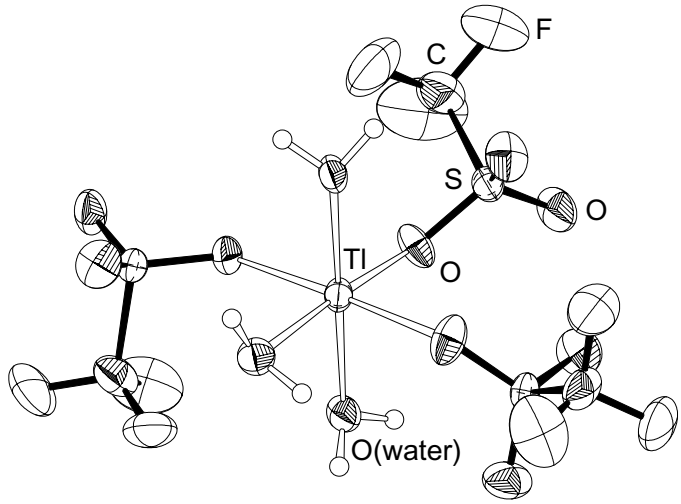

***Figure 19**. The molecular structure of **7**. The mean Tl-O bond distances to the aqua ligands are: 2.196(10) Å, and to trifluoromethanesulfonate oxygen atoms: 2.217(9) Å (thermal ellipsoids at 50 % probability level).*

EXAFS data

One example of how EXAFS methods can be useful complements to crystallography was discussed in section 3.2.1.1, where EXAFS results were useful in distinguishing between two different possible space groups for describing the crystal structure of the hexakis(dimethyl sulfoxide)-thallium(III) perchlorate. The structure determination of bisaquamercury(II) trifluoromethanesulfonate with its poor crystal quality, provides another example. EXAFS data indicated an unusual structure of the hydrated mercury(II) ion with two tightly bonded oxygen atoms, but the crystals were very fragile forming thin flakes, and single crystals for a complete structural determination by x-ray diffraction (XRD) were difficult to obtain. Eventually, a single crystal of sufficient quality was found and a linear $Hg(OH_2)_2^{2+}$ entity could be confirmed by XRD. However, the thermal ellipsoids were in the model description elongated along the Hg–O bond direction (Fig. 17); an indication of disorder or deficient crystal quality. An absorption correction for the thin crystal substantially changed the value obtained for the Hg-O distance (Chapter 2.1.1). In such a case the EXAFS determination probably provides a more accurate value for the Hg–O mean bond distance than the crystallographic value.[VII]

The reason is that bond distances from XRD are obtained as calculated interatomic distances between the individually determined mean positions of atoms in a crystal lattice, while in EXAFS an average of the instantaneous separations between atoms is obtained. However, the interpretation of the EXAFS data suffers some difficulties; especially for compounds with a distribution of interatomic distances, since the oscillations from different scattering pathways are partially out-of-phase and become reduced due to destructive interference. The EXAFS data for the compounds **6** and **7** are given in the Table 7.

***Table** 7. EXAFS studies of the solids **6** and **7**, Mean bond distances, d/Å, Debye-Waller factors, $\sigma^2/Å^2$, number of distances, N, and amplitude reduction factor, S_o^2.*

Sample	Interaction	*d*	σ^2	*N*	S_o^2
6	Hg-O	2.111(3)	0.0041(4)	2	0.76(5)
	Hg-O	2.47(1)	0.018(1)	4	
	MS[a]	4.21(3)	0.02(1)	2x2	
7	Tl-O	2.205(2)	0.0039(3)	6	0.48(1)
	Tl-O-O	3.76(3)	0.01(1)	24	
	MS[b]	4.41(3)	0.02(1)	3x6	
	Tl…S	3.40(2)	0.02(1)	3	

[a] The multiple scattering pathways along the linear HgO_2 entities, Hg-O-O and Hg-O-Hg-O, have the same values for the structural parameters (*d*, σ and *N*).
[b] The Tl-O-O and two different Tl-O-Tl-O multiple scattering pathways, have been refined with the same values for the structural parameters (*d*, σ and *N*).

Vibrational spectroscopy

A force field study was undertaken of vibrational spectra of the compounds **6** and **7** to gain insight in the metal-oxygen bonding, and also to study how the coordination affects the trifluoromethanesulfonate ions. The Hg-entity used for the calculations, $Hg(OH_2)_2(O_3SCF_3)_4$, has 51 vibrational degrees of freedom, and the Tl-complex, $Tl(OH_2)_3(O_3SCF_3)_3$, 78, considering the water molecules as point masses.[VII]

In order to simplify the initial calculations, we firstly considered only a single O_3S-CF_3 ligand coordinated to the metal ions. The symmetry of the SO_3 group in the trifluoromethanesulfonate ion changes due to the coordination. In the Hg-compound, two oxygen atoms of the $O_3SCF_3^-$ ion forms a bridge between two mercury atoms, while the third oxygen is hydrogen bonded to the water molecule in a neighboring chain (Fig. 17). In the Tl-complex, the $CF_3SO_3^-$ ion coordinates as a monodentate ligand to the Tl(III) ion.

In both cases, the S-O bonds in the $-SO_3$ group become non-equivalent and the local symmetry for the $O_3S\text{-}CF_3$ ligand reduces from $\mathbf{C}_{3v}$ to be close to $\mathbf{C}_s$ point group symmetry, which would give $11A'$ and $7A''$ internal vibrational modes.

When the free $O_3SCF_3^-$ ion coordinates to the mercury atom, its asymmetric S-O stretching frequency shifts from 1285 cm^{-1} (Table 2) to 1037 cm^{-1} (Table 8, calculated value), while the symmetric stretching 1038 cm^{-1} (Table 2) shifts to 950 cm^{-1} (Table 8, calculated value). The oxygen-coordination causes the SO_2*♦ stretching force constant (5.64 $N\cdot cm^{-1}$) to decrease as compared to that of the non-coordinated SO_3 ligand (8.35 $N\cdot cm^{-1}$). However, the force constant of the non-coordinated SO bond increases (9.73 $N\cdot cm^{-1}$), due to the additional increase in the donor-acceptor interaction between oxygen and sulfur atoms.

In the thallium complex the $O_3SCF_3^-$ ligand coordinates with only one oxygen atom (O*) to thallium. Therefore, the $-SO_3$ group frequency splits into two SO_2 bands (asymmetric stretching at 1304 cm^{-1} and symmetric at 1273 cm^{-1}, IR-data), and one SO* stretching band at 829 cm^{-1}, Table 9.

A second type of calculation has been made for the coordination sphere of the metal ions with oxygen or water ligands in a distorted octahedral configuration. Around the Hg-atom four SO_3 oxygen atoms form an equatorial plane with two *trans*-water molecules in axial positions (see Fig. 17). The mercury coordination can be described as an $HgO^*_4O_2$♦ entity in approximately D_{4h} point group symmetry. The 7 atoms would give rise to 15 normal vibrations belonging to the $2A_{1g} + B_{1g} + B_{2g} + E_g + 2A_{2u} + B_{1u} + 3E_u$ symmetry species.

The coordination sphere of the $Tl(OH_2)_3(O_3SCF_3)_3$ complex can be simplified as TlO_3*O_3♦, described in the C_{2V} point group with the symmetry species $6A_1 + A_2 + 4B_1 + 4B_2$ of the 15 normal vibrational modes (*cf.* Fig. 19). The water molecules in the coordination sphere were considered as point masses in all the normal coordinate calculations.

The vibrational spectra of the hexaaqua mercury(II) and hexaaqua thallium(III) complexes were also examined by normal coordinate methods to provide a comparison with the M-O bond strength in the present aqua complexes (Table 4, paper V). The correlation between the M–O force constants and corresponding reciprocal bond lengths is presented in Fig. 20, showing that the force constant decreases substantially with an increase in the M-O bond length.

♦ O* denotes a coordinated SO_3 oxygen atom.

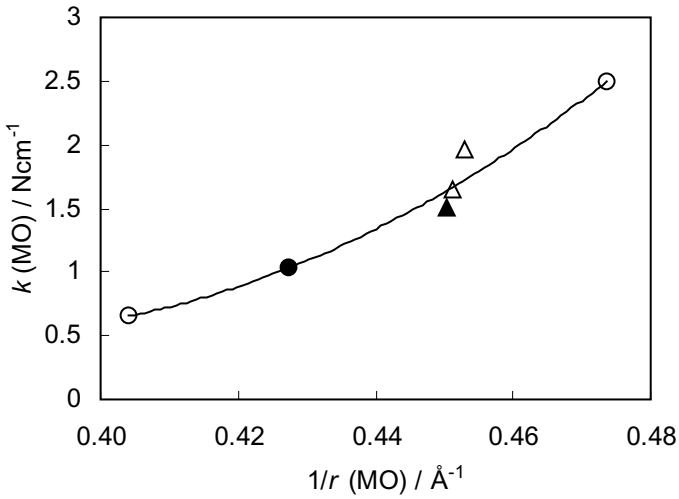

Figure 20. *Correlation between metal-oxygen (MO) force constants and inverse bond lengths in* ***6*** *(○),* ***7*** *(△) , $[Hg(OH_2)_6]^{2+}$ (●) and $[Tl(OH_2)_6]^{3+}$ (▲) complexes. The Tl-O bonds in* ***7*** *were treated as two groups (see text).*

The experimental and calculated fundamental frequencies of compound **7** are summarized in Table 9. The Tl-O bonds were treated as two groups, Tl-$3O_{aq}$, and Tl-$3O^*$, in $\mathbf{C}_{2v}$ symmetry. The mean metal-oxygen bond lengths in these two TlO_3 entities are slightly shorter than in the $[Tl(OH_2)_6]^{3+}$ complex, which corresponds to their higher force constants (Fig. 20).

Hydrogen bonding

The symmetric and asymmetric HgO_2 stretching vibrations in the almost linear $Hg(OH_2)_2^{2+}$ entity in **6** occur at higher frequency than the averaged Hg-O stretching mode of the $[Hg(OH_2)_6]^{2+}$ complex. The reason is the much shorter and stronger Hg-O bonds, 2.11 Å, in the two-coordinated $Hg(OH_2)_2^{2+}$ entity, than those of the hexa-coordinated $[Hg(OH_2)_6]^{2+}$ complex, 2.34 Å.

In order to investigate how the strong Hg-O bonding affects the hydrogen bonding around the $Hg(OH_2)_2^{2+}$ entity, an IR spectroscopic study was undertaken. Partial isotopic substitution was made by recrystallizing the salt from an aqueous solution with about 5% D_2O. After background subtraction, the spectrum shows a broad O-D stretching band centered at about 2400 cm^{-1} (ca. 170 cm^{-1} bandwidth) of the O-D stretching frequency. At such low deuterium concentration the O-D oscillators do not couple and the band is still well defined.

This frequency is much lower than that for the O-D stretching of the hexahydrated Hg^{2+} ion in partially deuterated $[Hg((H,D)_2O)_6](ClO_4)_2(s)$, which occurs at 2567 cm^{-1} (width 106 cm^{-1}), and it is slightly lower than that of the broad O-D band of the $[Hg((H,D)_2O)_6]^{2+}$ ion in aqueous solution, 2416 cm^{-1} (width 193 cm^{-1}).[59]

A lower O-D stretching frequency of the water molecules indicates a stronger hydrogen bond, and is consistent with a shorter O···O bond distance. The frequency 2400 cm^{-1} corresponds to a mean O(-H)···O distance of about 2.74 ± 0.07 Å, according to a solid state correlation between hydrogen bonded O···O distances and ν_{OD} wavenumbers.[60] This is in fair agreement with the crystallographic values, with the mean O-(H)···O distance 2.71 Å. The comparison with the hexahydrated mercury(II) ions, shows that these hydrogen bonds are significantly stronger. Hence, the strong Hg-O bond in the almost linear $Hg(OH_2)_2^{2+}$ entity polarizes the coordinated water molecules and considerably enhances the hydrogen bond strength to the trifluoromethanesulfonate oxygen atoms.

In bulk water with added D_2O, the O-D stretching occurs at 2506 cm^{-1}.[61] Thus, the hydrogen bonds from the $Hg(OH_2)_2^{2+}$ entity are also stronger than those formed between water molecules in aqueous solution, even though the oxygen atoms of the $–SO_3$ group are less efficient hydrogen-bond acceptors. These hydrogen bonds become equally strong as those formed by the aqua ligands of the trivalent thallium(III) ion in the $[Tl(OH_2)_3(CF_3SO_3)_3]$ complexes, see 3.2.1.2.[VII]

Table 8. *Observed and calculated frequencies (cm^{-1}), potential energy distribution (PED) and assignments for* ***6****, according to the model calculations.*

Observed		Calcul-ated	PED (%)	Assignment	Point group (symmetry species)[a]	
Raman	Infrared				$\mathbf{C}_s$	$\mathbf{D}_{4h}$
1289 m	1284 sh	1280	85 ν(SO), 15 $\nu_S(SO_2^*)$	SO str		
					A'	
1273 m						
	1247 vvs	1235	62 $\nu_s CF_3$), 17 $\delta_s(CF_3)$, 17ν(CS)	CF_3 sym str	*A'*	
1230 s	1230 sh					
1199 sh	1204 m	1190	47 $\nu_a(CF_3)$, 27 $\delta_a(CF_3)$	CF_3 asym str	*A''*	
1187 m						
1178 sh	1178 vs	1157	48 ν_a (CF_3), 27 $\delta_a(CF_3)$	CF_3 asym str	*A'*	
1104[b] vw						
1043 vvs	1033 vs	1037	83 $\nu_a(SO_2^*)$, 11 ν_a(HgO*), 6$\delta_s(SO_3)$	SO_2* asym str	*A"*	
1039 sh						
	988 sh	950	76 $\nu_s(SO_2^*)$, 12 ν(SO), 11 ν_s(HgO*)	SO_2* sym str	*A'*	
	907 vw					
	847 vw					
773 vs	769 s	774	45 $\delta_s(CF_3)$, 34 ν(CS), 16 $\nu_s(CF_3)$	CF_3, sym. Deform	*A'*	
	641 vs					
593 m		595	33 $\delta_s(SO_3)$, 24 $\delta_a(SO_3)$, 10 $\delta_s(CF_3)$, 8ν(CS), 5 ν_s(HgO*)	SO_3 sym deform	*A'*	
	580 s	574	68 $\delta_a(SO_3)$, 26 $\nu_a(HgO_4^*)$	SO_3 asym deform	*A''*	
574 m		572	46 $\delta_a(SO_3)$, 19 $\delta_s(SO_3)$, 8 ν_s(HgO*)	SO_3 asym deform	*A'*	
574 m		573	96 $\nu_s(HgO_2)$, 4 $\nu_s(HgO_4^*)$	HgO_2 sym str		A_{1g}
	(519 vs)	511	74 $\delta_a(CF_3)$, 17 $\nu_a(CF_3)$, 6 $\delta_a(CF_3)$	CF_3, asym. deform	*A'*	

	(519 vs)	511	68 $\delta_a(CF_3)$, 19 $\nu_a(CF_3)$	CF_3, asym. deform	*A''*	
410 w	410 vw	411	94 $\nu_a(HgO_2)$, 6 $\delta(HgO_4^*)$	HgO asym. str		A_{2u}
	352 s	353	57 $\rho(SO_3)$, 11 $\rho(CF_3)$, 9 $\nu_a(CF_3)$, 6$\nu_s(HgO_4^*)$	SO_3 rocking	*A'*	
349 s		347	66 $\rho(SO_3)$, 16 $\rho(CF_3)$	SO_3 rocking	*A''*	
323 vs	322 s	317	34 ν(CS), 27 $\delta_s(CF_3)$, 26 $\delta_s(SO_3)$, 6$\nu_s(HgO_4^*)$	CS stretch	*A'*	
318 sh	318 sh					
	285 w,b	281	100 $\nu(HgO_4^*)$	HgO_4^* asym str		E_u
	272 w,b					
256 vw,b		254	100 $\nu_s(HgO_4^*)$	HgO_4^* sym str		A_{1g}
	234 vw	227	70 $\rho(CF_3)$, 9 $\nu_s(HgO_4^*)$, 8 $\nu_a(CF_3)$	CF_3 rocking	*A'*	
214 vw	218 vw,b	211	72 $\rho(CF_3)$, 6 $\nu_a(HgO_2)$, 6 $\nu_a(CF_3)$	CF_3 rocking	*A''*	
185 m,b		189	100 $\nu_a(HgO_4^*)$	HgO_4^*, (trans) sym str		B_{2g}
144 m	148 w					
125 sh	124 w					
		82	100 $\delta(HgO_2O_2^*)$	OHgO* deform		E_u
		78	86 $\delta(HgO_2O_2^*)$, 14 $\delta'(HgO_2O_2^*)$	OHgO* deform		E_u
75 m		75	100 $\delta(HgO_2)$	HgO_2 deform		B_{1g}
		72	78 $\delta(HgO_2O_2^*)$, 22 $\nu_a(HgO_2)$	OHgO* deform		A_{2u}
65 sh		56	50 δ (HgO_4^*), 50 $\delta(HgO_2O_2^*)$	HgO_4^* deform		E_g
		53	100 $\delta(HgO_2O_2^*)$	OHgO* deform		B_{1u}

[a] $\mathbf{C}_s$ point group refers to the local symmetry of the coordinated $O_3SCF_3^-$ anion and the $\mathbf{D}_{4h}$ point group represents the approximate symmetry of the octahedrally coordinated Hg entity. O* denotes the coordinated oxygen atom of the SO_3 groups in the square planar HgO_4^* equatorial plane of the octahedra, and O the oxygen atom of the coordinated water molecule.

Table 9. *Observed and calculated frequencies (cm^{-1}) and potential energy distribution (PED) for* ***7***.

Observed		Calc.	PED[a] (%)	Assignment	Point group[b]	
Raman	Infrared				C_s	C_{2v}
1334 w						
1312 w	1304m	1304	$79\nu_a(SO_2)$, $6\nu_a(CF_3)$	SO_2 asym str	*A"*	
1293 vw	1282sh					
1264 vw	1273w	1268	$71\nu_s(SO_2)$, $5\nu_a(CF_3)$, $5\nu_s(CF_3)$	SO_2 sym str	*A'*	
1246 m	1245vw	1235	$64\nu_s(CF_3)$, $14\delta_s(CF_3)$, 13ν(CS)	CF_3 sym str	*A'*	
1230 s	1227vw,sh			free triflate		
1180 s	1184vw,sh	1183	$49\nu_a(CF_3)$, $18\delta_a(CF_3)$, $17\nu a(SO_2)$, $6\rho(CF_3)$	CF_3 asym str	*A'*	
1176 sh	1171w,m					
1154 w	1156m,sh	1149	$44\nu_a(CF_3)$, $23\nu_a(SO_2)$, $17\delta_a(CF_3)$, $5\rho(CF_3)$	CF_3 asym str	A"	
1036 vs	1030s	1010		Free triflate	*A'*	
829w,m		821	71ν(SO*),$1324\nu_s(SO_2)$,$7\delta_s(SO_3)$	SO* str	*A'*	
774 vs	770m	768	$40\delta_s(CF_3)$, 35ν(CS), $12\nu_s(CF_3)$	CF_3 sym def	*A'*	
	734sh					
	720vs					
	707s,sh					
596 m		598	$43\delta_s(SO_3)$, $21\delta_s(CF_3)$, 13δ(TlOS), 11ν(TlO*)		*A'*	
581 m,s	575s	580	$78\delta_a(SO_3)$,5ν(TlO*)	SO_3 asym def	*A'*	
581 m,s	575s	580	$85\delta_a(SO_3)$, $5\nu_a(SO_2)$	SO_3 asym def	*A"*	
532 w	536m	534	$53\delta_a'(CF_3)$, $34\delta_a(CF_3)$, $8\nu_a'(CF_3)$	CF_3 asym def	*A'*	
519 w,sh	519s	517	$52\delta_a(CF_3)$, $33\delta_a'(CF_3)$, $10\nu_a(CF_3)$	CF_3 asym def	*A"*	
	493m					
519 w,sh	519 s	513	$100\nu_s(TlO_2)$, 33ν(TlO)	TlO_3 sym str		A_1
432 s	430 vvw	428	$98\nu_s(TlO_2*)$	TlO_3* sym str		A_1
397 w		409	82ν(TlO*), $18\nu_a(TlO_2)$	TlO_2* (trans) asym str		B_2

375 w		381	76ν_a (TlO_2), 24ν_s(TlO_3*)	TlO_2 (trans) asym str		B_1
358 s	353 s	356	89ν(TlO*), 11ν_s(TlO_2*)	TlO_2* (trans) sym str		A_1
347 s		354	98ν_s(TlO_2)	TlO_2 (trans) sym str		A_1
327 vs	319 w	316	30ν(CS), 26δ_s (SO_3), 20ν(TlO*), 17δ_s(CF_3)	CS str	*A'*	
318 sh						
261 w						
241 w	214 m	217	69ρ(CF_3), 21ν_a(CF_3), 9ρ(SO_3),	CF_3 rocking	*A"*	
224 sh						
192 m		187	48ρ(CF_3), 22ν(TlO*), 15ν_a(CF_3), 9ρ (SO_3),	CF_3 rocking	*A'*	
186 m,w	177 vw					
157 vw	150 m					
137vw	140 w					
109vw	103 w	96	100 δ(OTlO*)	OTlO* def		B_1
109 vw	103 w	99	100 δ(TlO_2)	TlO_2 def		B_2
109 vw	103 w	98	65 δ(TlO_2*), 35 δ(TlO_2)	O*TlO* def		A_2
80 sh	84 vw	84	100 δ(OTlO)	OTlO def		A_1
80 sh		84	70 δ(OTlO*), 30 δ(TlO_2*)	OTlO* def		B_1
80 sh		82	86 δ(OTlO*), 16 δ(TlO_2*)	OTlO* def		B_2
		78	100 δ(O*TlO*)	OTlO def		A_1
		77	62 δ(OTlO*), 38 δ(O*TlO*)	O*TlO* def		B_1
		76	100 δ(O*TlO*)	O*TlO* def		B_2

a. Notation of the vibrational modes: ν- stretching, δ- deformation, ρ- rocking, s- symmetric, a- asymmetric.

b. $\mathbf{C}_s$ point group refers to local symmetry of coordinated $O_3SCF_3^-$ anion. $\mathbf{C}_{2v}$ point group represents the approximate symmetry of the Tl complex O* means the coordinated oxygen atom of the SO_3 group; means the oxygen atoms of the coordinated water molecules.

3.2.1.3 Distorted octahedral coordination

Hexakis(dimethyl sulfoxide)thallium(III) perchlorate

The relatively small Tl-O and Tl···S disorder parameters, σ in the EXAFS Debye-Waller factor $\exp(-2\sigma^2k^2)$, for the solid compound at low temperature, *cf.* Table 4, are consistent with the expected thermal movements of the atoms, indicating no static disorder of the ligands in the complex.[II] However, the octahedral MO_6 centra in the $M(dmso)_6^{3+}$ complexes are compressed along the 3-fold axis as described by the compression ratio, see Figures 12 and 13 and Table 3. For the thallium(III) complex in dimethyl sulfoxide solution, the disorder parameter $\sigma = 0.081(4)$ Å is about twice as large as that for the solid (Table 4). The relatively large σ–value indicates an anomalously large spread in the Tl-O bond distances in solution. This is possibly caused by a dynamic disorder due to vibronic mixing of electronic states with close energy levels, a weak PJTE (see section 1.3.1), adding to the thermal disorder, i.e. the vibrational movement.[12]

Bisaquamercury(II) trifluoromethanesulfonate

Symmetry lowering by the PJTE requires pseudo-degeneracy of electronic states. With sufficiently strong mixing of the ground state with one or more excited states, the nuclei may displace from the equilibrium positions of the highest symmetry configuration.[12] This mechanism may favor the coordination of ligand atoms with different donor properties, by creating stronger and more covalent bonds in certain directions. The crystal structures of the $[Hg(OS(CH_3)_2)_6](ClO_4)_2$ and $[Hg(NC_5H_5)_6](CF_3SO_3)_2$ solvates display centrosymmetric hexasolvated mercury(II) complexes with the four equatorial Hg-O/N bonds significantly shorter, ca. 0.05 Å, than the axial ones.[33,61]

For the $Hg(H_2O)_6^{2+}$ complex a PJTE coupling to the excited state was revealed using theoretical *ab initio* calculations,[13] resulting in a large spread in the Hg-O distances, also manifested experimentally in large disorder parameters in aqueous solution. The $Hg(H_2O)_2(CF_3SO_3)_2$ compound has quite large differences in the Hg-O bond distances in the equatorial and axial positions. It seems that mercury(II) in all octahedral complexes studied so far has some distortion of the coordination figure, probably due to a PJTE (Fig. 4).[12]

3.2.2 Coordination number seven

When twisting the triangular sides of an octahedron 180°, a trigonal prism in $\mathbf{D}_{3h}$ symmetry will form. However, when the central atom is large enough to accommodate one additional ligand, the seventh donor atom can approach most closely to the central atom from the rectangular side of the trigonal prism, giving rise to a monocapped trigonal prismatic coordination geometry. In the crystal structure of $[Sc(H_2O)_7][C(SO_2SCF_3)_3]_3.H_2O$ seven water molecules coordinate to the scandium ion in a distorted monocapped trigonal prism.[63] In acidic aqueous solution, a distinct Sc-O bond distance of 2.17(1) Å and weak interactions in the range 2.3-2.5 Å obtained by means of EXAFS and large angle x-ray scattering (LAXS) methods also indicate a monocapped trigonal prismatic configuration around the scandium(III) ion.[54]

In the low temperature phase of the hydrated trifluoromethane-sulfonate salt the scandium(III) ion is at 150 K surrounded by seven water molecules, mean Sc-O length of 2.187 Å, in a distorted monocapped trigonal prism. Two more distant water molecules with less than half occupation, mean Sc-O value 2.559 Å, are also capping the rectangular faces (see section 3.2.4).

3.2.3 Coordination number eight

3.2.3.1 Octakis(dimethyl sulfoxide)lanthanum(III) (**8**), praseodymium(III) (**9**), samarium(III) (**10**), gadolinium(III) (**11**), erbium(III) (**12**) and lutetium(III) (**13**) iodide.

Crystalline solvates

The crystal structures of **8** and **9** were satisfactorily described in the orthorhombic space group *Pbca* (No. 61), while the structures of **10**-**13** were characterized in the monoclinic space group $P2_1/n$ (No. 14) with the monoclinic angle close to 100° (Table 1, paper IV). Two unit cell edges are rather similar for all compounds **8-13,** while the third is almost doubled in the orthorhombic cells of compounds **8** and **9**. The volume 1018 $Å^3$ per praseodymium(III) metal ion in **9**, is less than that for **10, 11,** and **12**, 1053 $Å^3$, 1044 $Å^3$ and 1030 $Å^3$, respectively, despite the larger ionic radius, indicating a more efficient packing in the orthorhombic structures.

All crystal structures **8 - 13** comprise discrete octakis(dimethyl sulfoxide)lanthanoid(III) complexes (Fig. 21) surrounded by iodide ions. The trivalent lanthanoid ions coordinate the oxygen atoms of the eight dimethyl sulfoxide ligands in a distorted square antiprism. The mean M-O bond distances decrease, 2.456(11), 2.431(7), 2.400(7), 2.383(7), 2.337(9)

and 2.302(6) Å, as also the M-O-S bond angles, 139.2(7), 138.1(5), 137.5(5), 135.1(5), 132.9(6) and 132.5(3)°, for M = La, Pr, Sm, Gd, Er and Lu, respectively. Plots of ionic radius and MOS angles versus the M-O bond length (Fig. 22), indicate a break in the trends between the praseodymium(III) and samarium(III) solvates, which probably is due to the change of unit cell symmetry.

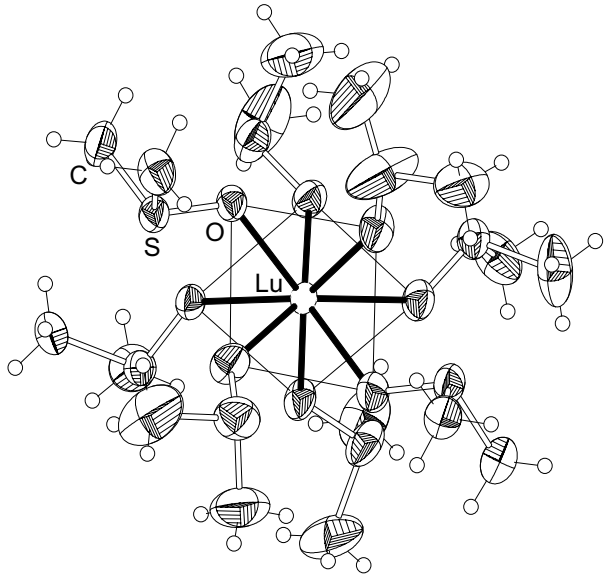

Figure 21. *The metal atom M is surrounded by eight oxygen-coordinated dimethylsulfoxide ligands in the compounds* ***6-11****. The figure shows the lutetium complex with 40% probability ellipsoids.*

Positional disorder, due to alternative orientations of the dimethyl sulfoxide ligands, was found for one ligand for the $[La(dmso)_8]^{3+}$ and $[Gd(dmso)_8]^{3+}$, and two for the $[Sm(dmso)_8]^{3+}$ complexes.[IV] Two positions for the sulfur atoms, corresponding to an inversion of the pyramidal ligand, were refined and their site occupancy factors are given in Table 10.

Table 10*. Occupancy factors of sulfur atoms (Occu. S) in the* $[M(dmso)_8]^{3+}$*, M = La, Sm and Gd complexes.*

M	Occu. S (%)	
	1	2
La	64 / 36	
Sm	52 / 48	62 /38
Gd	56 / 44	

The average La-O(dmso) bond lengths, 2.492(9) and 2.485(10) Å, found for 8-coordination in the $[La(dmso)_8][(\mu\text{-}WSe_4)_3Ag_3]$ and for 9-coordination in the $La(dmso)_6(H_2O)PW_{12}O_{40}$ compounds are similar to that for **8**, 2.485(4) Å.[64,65] The mean Pr-O bond distance, 2.454(6) Å of the discrete $[Pr(dmso)_8]^{3+}$ complexes in the $[Pr(dmso)_8]_2PMo_{10}V_2O_{40}(NO_3)\cdot$dmso compound, is longer than for **9.**[66] For the polymeric structure of $Pr(dmso)_6(H_2O)](PMo_{12}O_{40})$ with coordination number 9, a very similar value as for **9**, 2.429(11) Å, is reported.[67] Octakis(dimethyl sulfoxide)gadolinium(III) hexacyanoferrate (III) has a mean Gd-O bond distance of 2.393(5) Å, which is close to the value for **11**.[68]

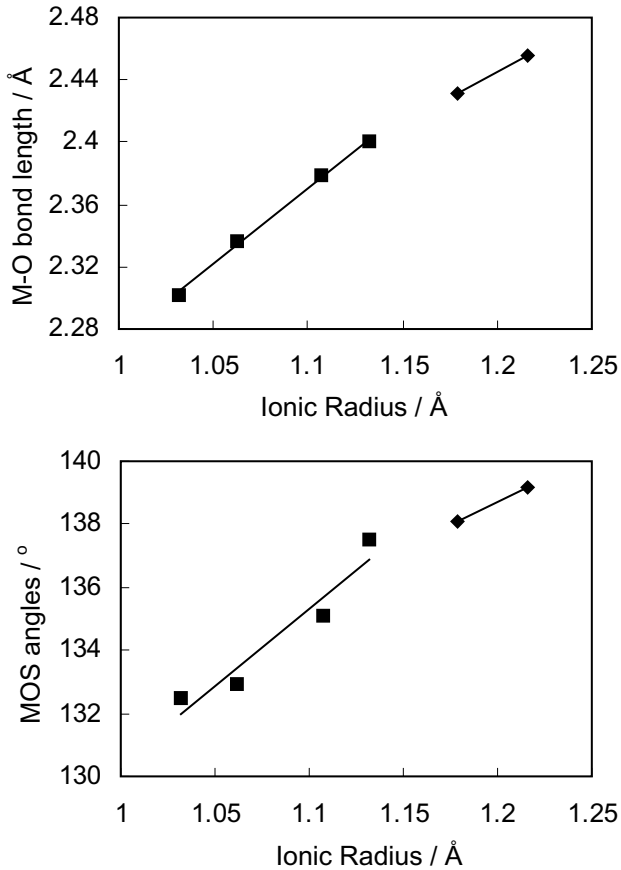

***Figure 22**. Ionic radius versus M-O bond length (top) and MOS angles (down) of the $[M(dmso)_8]^{3+}$, M = La, Pr, Sm, Gd, Er and Lu, complexes.*

Vibrational spectroscopy

The $\mathbf{D}_{4d}$ point group symmetry is the highest possible for describing the $[M(OS(CH_3)_2)_8]^{3+}$ complexes, considering the methyl groups as point masses, with 93 normal vibrations belonging to the symmetry species $7A_1 + 4A_2 + 5B_1 + 7B_2 + 12E_1 + 12E_2 + 11E_3$.[IV] The modes belonging to the A_1, E_2 and E_3 symmetry species should only be Raman-active in ideal $\mathbf{D}_{4d}$ symmetry, whereas B_2 and E_1-modes should only be IR-active, and the A_2 and B_1 modes inactive in the vibrational spectra. However, the allowed IR and Raman bands can coincide, and distortions of the complexes may cause symmetry-forbidden modes to appear as weak bands in the spectra.

Averaged Ln-O stretching frequencies were obtained for the Ln-O bonds as given in Table 11.

Table 11. *Average stretching frequencies for the M-O bonds in the $[M(dmso)_8]^{3+}$, M = La, Pr Nd, Gd, Tb, Dy, Er and Lu complexes.*

	La	Pr	Nd	Gd
M-O	2.456	2.431		2.383
$\bar{\nu}$ [a]	401	414	420	425

	Tb	Dy	Er	Lu
M-O			2.337	2.302
$\bar{\nu}$ [a]	425	427	433	432

[a] $\bar{\nu} = \dfrac{\nu_{A_1} + \nu_{B_2} + 2\nu_{E_1} + 2\nu_{E_2} + 2\nu_{E_3}}{8}$

The results showed that the decrease in ionic radius in the series of lanthanoid(III) ions, which shortens the metal-oxygen bond distance, increases the averaged stretching frequencies. Correlations between the force constants versus the inverse of the bond distances squared, and also the frequency $\bar{\nu}$ against reciprocal bond distances, are shown in Figure 23, with trends clearly reflecting the effect of the lanthanoid contraction.[IV]

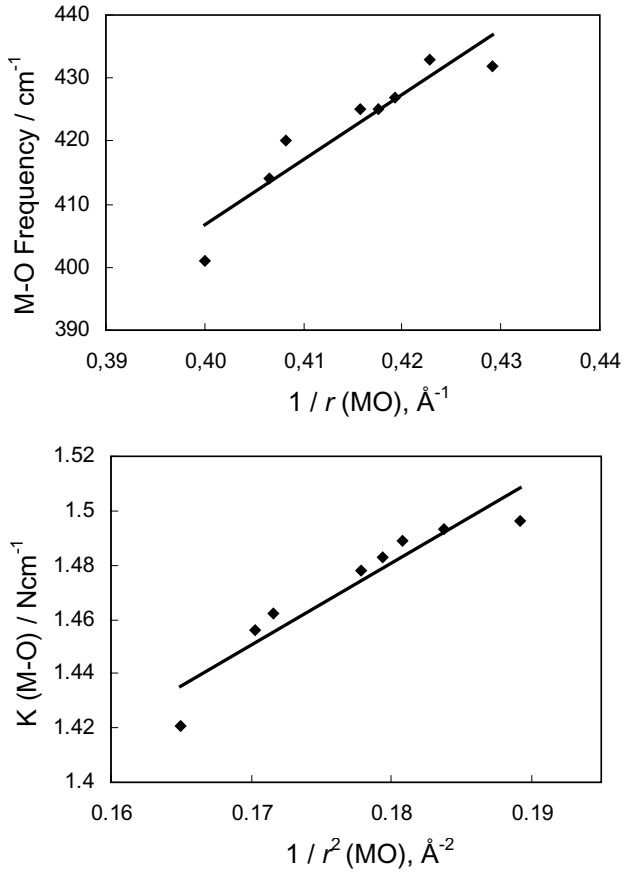

***Figure 23**. M-O frequency versus inverse bond distances (top) and force constant against inverse squared bond distances (bottom), according to eqn 4 & 5 (Section 1.4) in the $M(dmso)_8^{3+}$ complexes, M = La, Pr, Nd, Gd, Tb, Dy, Er and Lu.*

The correlation of Ln-O(dmso) stretching force constants versus Ln-O(dmso) bond lengths is compared in Figure 24 with the corresponding values in the nonaaqua complexes of lanthanoid(III) ions, and also with octahedral hexa-coordinated group 13 metal ions with dimethyl sulfoxide as ligand.[I,III] The Ln-O(dmso), bond lengths decrease by 7% from lanthanum to lutetium, while force constants increase by 5%. This change is significantly larger in the hydrated lanthanoid(III) ions, and the Ln-O force constants increase by 43%, while the corresponding Ln-O (prism) bond length decreases from lanthanum to lutetium by 9%. Similar effects are found for the capping Ln-O bonds, for which 33% increase in the force constants leads to 4% bond shortening. This indicates that the ligand-ligand repulsion in the capping position is higher than that in the prism.

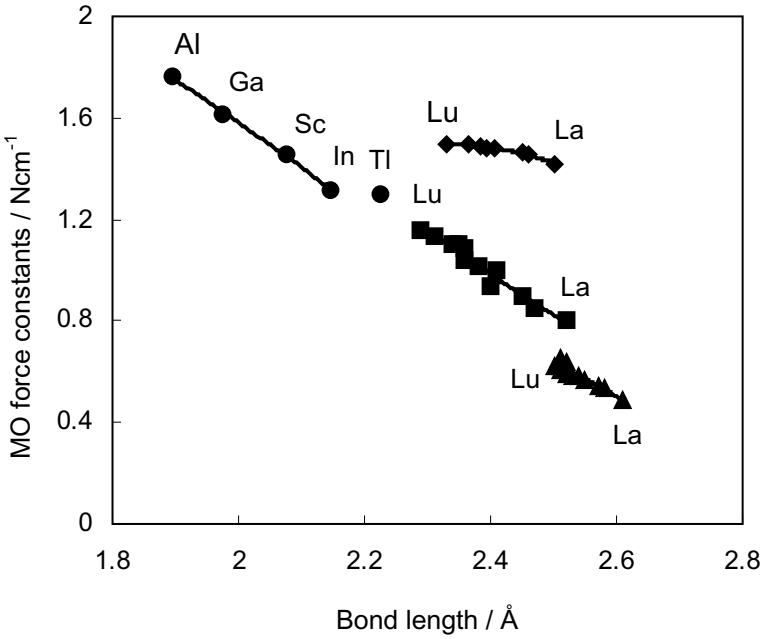

Figure 24. *Correlation between MO bond distances versus MO force constants for the $M(dmso)_6^{3+}$, M = Al, Ga ,Sc, In and Tl (●), $M(dmso)_8^{3+}$, M = La, Pr, Nd, Gd, Tb, Dy, Er and Lu (♦), Prism (■) and Capping (▲) MO in the $M(H_2O)_9^{3+}$, M = La, Pr, Nd, Sm, Gd, Tb, Dy, Ho, Er, Tm, Yb and Lu complexes.*

There is strong coupling between the MO stretching and some SC_2 wagging modes, which therefore also show frequency changes. However, the force constants of the S-O and the C-S stretching modes are rather insensitive to the size of the central atom. Their variations are within 3.2% for S-O, and within 1.7% for the C-S stretching. The relatively higher sensitivity of SO stretching force constants is due to the coupling of this mode with the MO stretching mode. The S-O stretching force constant of thallium(III) with high covalency in the Tl-O bonds, 4.28 N cm^{-1},[I] is less than the corresponding value for the isostructural scandium(III) compound, 4.40 Ncm^{-1},[III] and also much lower than the mean value, 4.64 Ncm^{-1}, obtained for the lanthanoid(III) series (Table 6). The S-O bond has partial double bond character, and is evidently influenced more by M-O bond covalency for thallium(III) than the increase in electrostatic character with decreasing size in the series of lanthanoid(III) ions. The M-O stretching force constants do not increase much for the smallest lanthanoid(III) ions, probably due to the steric repulsion between the bulky dimethyl sulfoxide ligands.

3.2.4 Coordination number nine

3.2.4.1 Hydrated scandium(III) (**14**), lutetium(III) (**15**), ytterbium(III) (**16**), thulium(III) (**17**), erbium(III) (**18**) and terbium(III) (**19**) trifluoromethanesulfonates

Crystalline hydrates

The crystal structures of **14-19** were described in the space group $P6_3/m$ (No. 176) with the trivalent metal ions located in a site of $\bar{6}$ symmetry. For the relatively large lanthanoid(III) ions three water oxygen atoms can approach the metal ion closest at the three rectangular sides of a trigonal prism formed by six aqua ligands in the primary coordination sphere. Thus, the water oxygen atoms surround the metal ions at the vertices of a tricapped trigonal prism (Fig. 25). The TTP coordination geometry comprises two groups of M-O bond distances, where the six within the prism are shorter than those to the capping positions. The coordinated water molecules and the surrounding trifluoromethanesulfonate ions are linked *via* hydrogen bonds. The structures of the isomorphous yttrium(III) and lanthanoid(III) $[M(H_2O)_9](CF_3SO_3)_3$ compounds, M = La to Lu, have been discussed in detail elsewhere.[47,69]

The lanthanoid(III) ions lighter than erbium(III) are sufficiently large to accommodate nine water molecules in TTP configuration, while for the heavier ones with smaller ionic radius, water deficiency starts to occur in the capping positions due to steric ligand-ligand repulsion. Refinements of the occupancy factors for the hydrated lutetium(III) trifluoromethanesulfonate indicate no deficiency of water in the prismatic positions, but 0.5(1) water molecules are found missing from the three capping positions.[V]

Even though scandium(III) has smaller ionic radius than lutetium(III), it is in many respects lanthanide-like, and in the isomorphous hydrated scandium(III) trifluoromethanesulfonate, 1.0(1) water molecules are missing from the capping positions. The relatively strong hydrogen bonding to the anions is evidently responsible for stabilizing the TTP cage around the trivalent metal ions, even when capping water molecules are missing.[V] Empty accessible capping positions probably can play an important role when these ions act as Lewis acids, catalyzing many types of organic syntheses.[2,3]

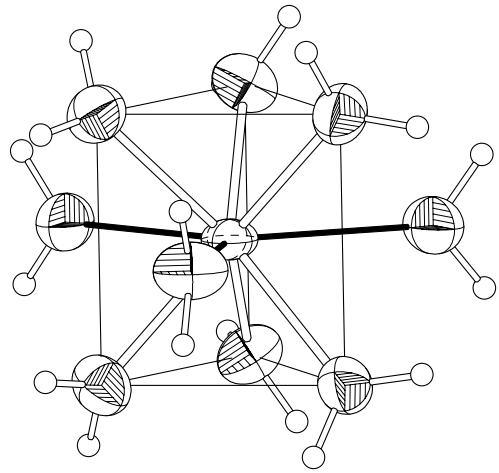

Figure 25. *The metal atom M is surrounded by nine oxygen atoms of water molecules forming a tricapped trigonal prism in the nonahydrated lanthanoid(III) complexes.*

Crystallographic refinement of the oxygen occupancy parameters, and density measurements by means of flotation in CCl_4 + CBr_4 mixtures were performed in all cases (Table 12).[70] For the scandium and lutetium salts also thermogravimetric analysis (TGA) was used. The weight loss was recorded when heating 5-10 mg samples at a rate of 5 K min^{-1} from 293 to 573 K, under constant flow of dry air (Figure 26). The analyses showed the water/metal molar ratio to vary from about 8.0 up to 9.0 for the crystalline compounds **14** to **19**. Refinement of the site occupancy factors in all cases resulted in full occupancy of the prism positions, 6.0 oxygen atoms (O_p), while for the capping (O_c) positions they vary between 2.0 to 3.0 (Table 12).

Table 12. The average number of water molecules in the TTP hydrates $[M(H_2O)_{9-x}](CF_3SO_3)_3$ from XRD site occupancy factors, TGA analysis, and crystal density.

M	XRD	TGA	Density
Sc (**14**)	8.02(4)	8.1(1)	8.0(1)
Lu (**15**)	8.46(9)	8.4(1)	8.4(1)
Yb (**16**)	8.72(3)	_[a]	8.7(1)
Tm (**17**)	8.84(5)	_[a]	8.7(1)
Er (**18**)	8.96(5)	_[a]	8.8(1)
Tb (**19**)	9.00	_[a]	9.0(1)

[a] Further decomposition prevented accurate analysis.

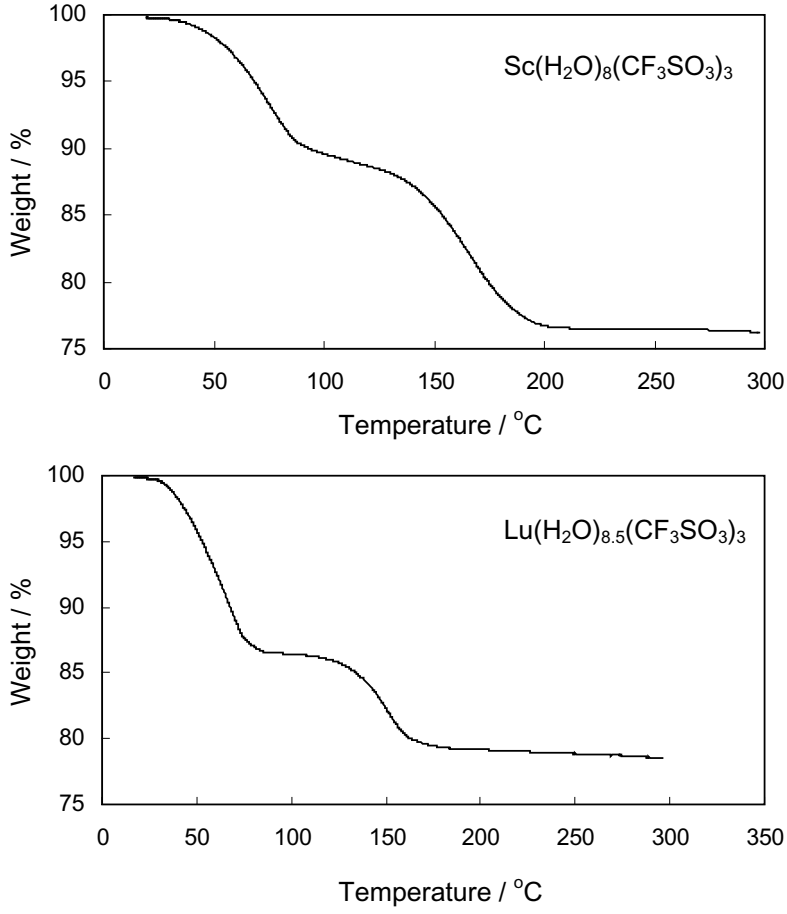

Figure 26. *Thermal gravimetric analysis of $[M(H_2O)_{9-x}](CF_3SO_3)_3$ where M, x = Sc, 1.0; and Lu, 0.5, respectively. The figures show the weight loss by heating 5-10 mg sample at a rate of 5 K min^{-1}, under constant flow of dry air.*

The low temperature phase **14***

The thermal parameters of the scandium atom in **14** were remarkably high in the refinements, as also for the capping oxygen atoms.[V] To find the reason, single crystal data were collected while reducing the temperature stepwise (293, 250, 200, 150 and 100 K). The thermal parameters decreased relatively uniformly for all atoms in the structure, except for scandium, until 188 K when a phase transition occurred. The unit cell dimensions increased 3 times in the *c*-direction and by a factor $\sqrt{3}$ in the *a* and *b* directions, and the space group changed from $P6_3/m$ to $R\bar{3}$, see Fig. 27.

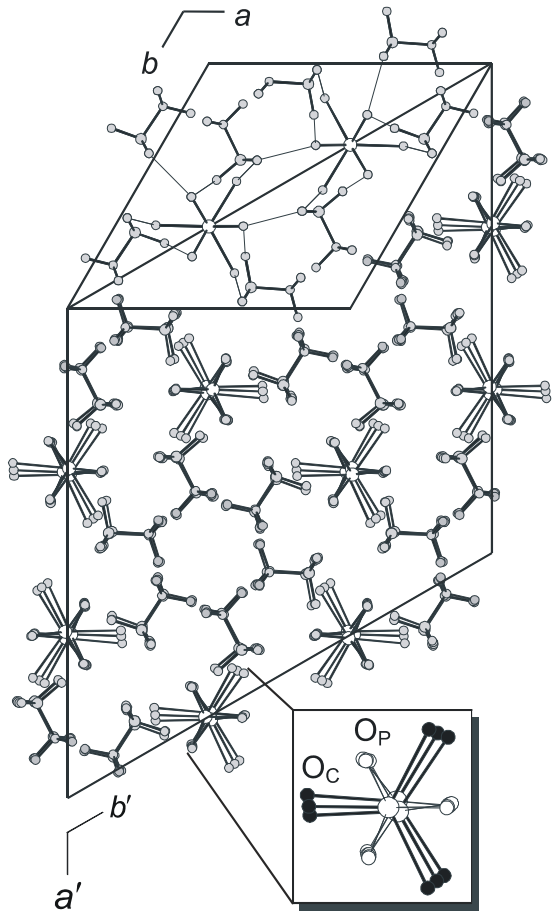

Figure 27. *Relation between the unit cells of* ***14*** *at 293 K (smaller cell) and the low-temperature phase* ***14**** *at 150 K (larger cell), projected along the c axis. The cell edges increase about 3 times in the c direction and by √3 in the a and b directions at the phase transition at 188 K.*

For the low temperature phase of the hydrated scandium(III) trifluoromethanesulfonate **14***, one rectangular surface (Table 13, edges in **bold**) of the distorted trigonal prism has become wider, allowing one capping water oxygen to approach closer, Sc-O_c(7) 2.291(3) Å at 150 K. and the seven fully occupied oxygen atom positions form a distorted monocapped trigonal prism around the scandium(III) ion. The two other capping sites are then pushed out, Sc-O_c(8) 2.536(5) Å and Sc-O_c(9) 2.582(5) Å (Figure 28).

The mean contact distance between the capping oxygen for the fully occupied site and the four atoms of the rectangular surface, $O_c(7)\cdots O_p$ 2.68 Å, is actually equal to the $O_c\cdots O_p$ distance estimated for a stable TTP cage,[V] while the mean $O_c\cdots O_p$ distance, 2.61 Å, is shorter for both the half-occupied sites $O_c(8)$ and $O_c(9)$ (*cf.* Table 13).

Table 13. *Sc-O bond distances to prism (O_p) and capping (O_c) water ligands, their hydrogen bond distances to trifluoromethanesulfonate oxygen atoms (O_t), and closest oxygen-oxygen contact distances $O_p\cdots O_p$ and $O_c\cdots O_p$ in the distorted capped trigonal prism of* ***14****, $[Sc(H_2O)_{8.0}](CF_3SO_3)_3$, at 150 K (cf. Figure 28).*

Water O(*x*)	Sc-O/ Å	O-(H)$\cdots$O$_t$ (Å)	O(x)$\cdots$O(*y*) within triangular surfaces	O(x)$\cdots$O(*y*) between triangles
$O_p(1)$	2.169(2)	2.757(5), 2.769(4)	*3*: 2.675(4), *5*: 2.703(5)	*2:* 2.729
$O_p(2)$	2.171(2)	2.790(4), 2.804(5)	*4:* 2.688(5), *6:* 2.704(5)	*1:* 2.729
$O_p(3)$	2.193(3)	2.727(4), 2.784(3)	*1:* 2.675(4), *5:* **2.796(3)**	*4*: **3.092(4)**
$O_p(4)$	2.176(3)	2.717(4), 2.738(4)	*2:* 2.688(5), *6:* **2.790(4)**	*3:* 3.092(4)
$O_p(5)$	2.146(3)	2.722(4), 2.728(4)	*1:* 2.703(5), *3:* 2.796(3)	*6:* **3.089(4)**
$O_p(6)$	2.165(3)	2.729(4), 2.776(4)	*2:* 2.704(5), *4:* 2.790(4)	*5:* 3.089(4)
$O_c(7)$	2.291(3)	2.892(4), 2.893(4)	*5:* 2.603(5), *3:* 2.746(4) *6:* 2.627(5), *4:* 2.735(4)	
$O_c(8)$[a]	2.536(5)	3.028(5), 3.055(5)	*5:* 2.530(6), *1:* 2.675(4) *6:* 2.566(6), *2:* 2.679(4)	
$O_c(9)$[b]	2.582(5)	2.954(6), 2.963(5)	*3:* 2.472(7), *1:* 2.754(5) *4:* 2.450(7), *2:* 2.753(5)	

[a] Occupancy factor refined to 0.50(1); [b] Occupancy factor 0.43(1);

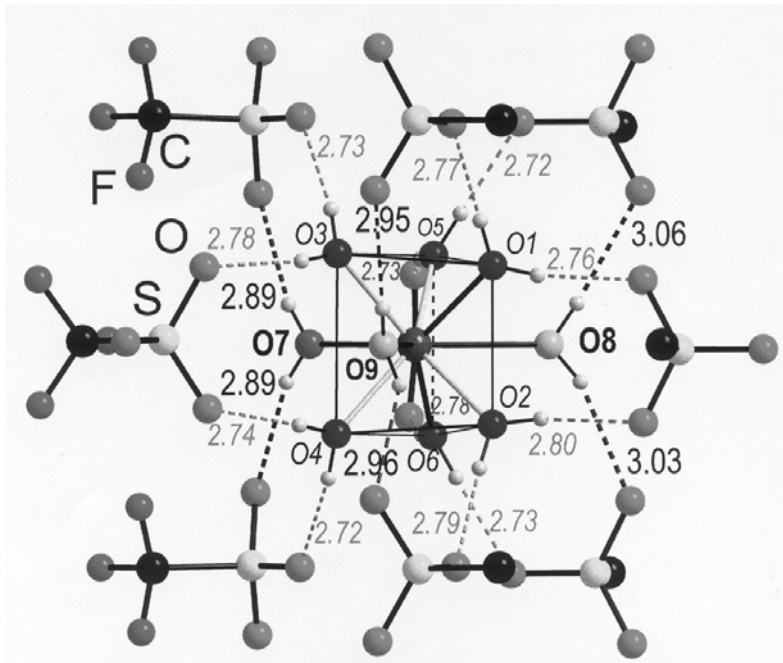

Figure 28. *The low-temperature phase* ***14**** *of* $[Sc(OH_2)_{8.0}](CF_3SO_3)_3$. *The enlarged rectangular side of water oxygen atoms, O1, O2, O3, O4, allows the capping* $O_c(7)$ *atom of the TTP polyhedron to approach the scandium(III) ion, Sc-*$O_c(7)$ *2.291(3) Å. This is reflected in the stronger hydrogen bonds (dashed black) from* $O_c(7)$ *to the trifluoromethanesulfonate anions,* $O_c(7)$-$(H)\cdots O_t$: 2×2.89 *Å, than those from the more distant capping* $O_c(8)$ *and* $O_c(9)$ *water oxygen atoms in half occupied sites,* $O_c(8)$-$(H)\cdots O_t$: *3.03, 3.06 and* $O_c(9)$-$(H)\cdots O_t$: *2.95, 2.96 Å. The 12 hydrogen bonds (dashed) from the prism water oxygen atoms, O1 – O6, are within 2.72 to 2.80 Å. The fluorine atoms of most trifluoromethanesulfonate ions are omitted for clarity.*

Differential scanning calorimetry (DSC)

The Perkin-Elmer DSC Pyris 1 instrument is equipped with two pans connected to a flow path. The sample is placed in one pan and the difference in cooling flow between the two pans against temperature is monitored. Phase transitions were detected by measuring the energy absorbed or released when small amounts of the crystalline samples (≈10-20 mg) were cooled from 293 to 133 K at a rate of 10 $K\cdot min^{-1}$, followed by a temperature increase to 293 K.[V] DSC measurements revealed reversible phase transitions at 185-190 K for all the water deficient compounds. For the lanthanoids the sharp feature, which decreased up to erbium(III), was hardly discernible for holmium(III), and absent for the fully hydrated dysprosium(III), terbium(III), yttrium(III) and lanthanum(III) salts (Fig. 29).

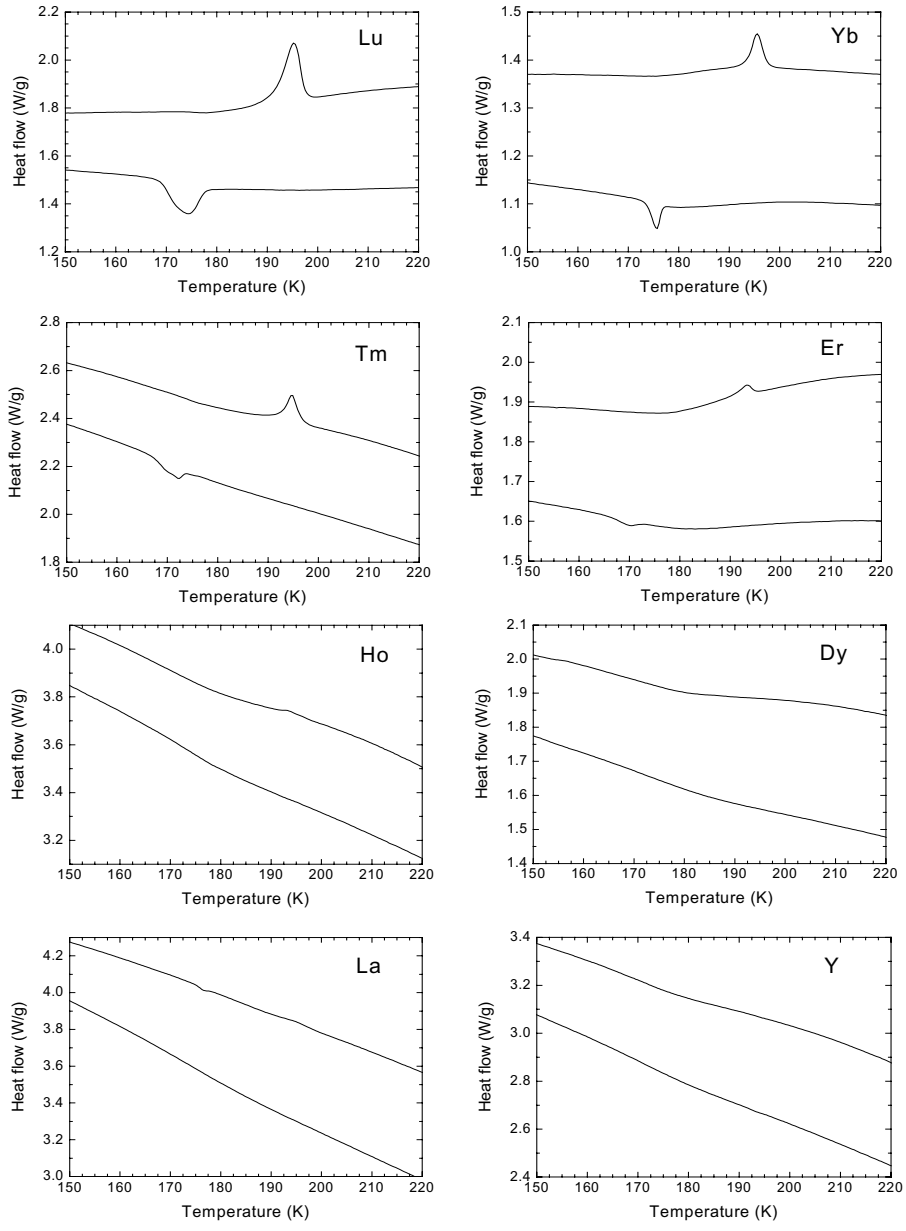

Figure 29. *Differential scanning calorimetry (DSC) measurements for hydrated $[M(H_2O)_n](CF_3SO_3)_3$ compounds, M = Sc, Lu, Yb, Tm, Er, Ho, Dy, Tb, La and Y, showing reversible phase transitions at about 185-190 K for the water deficient compounds, see text.*

Residual electron density maps

The refinement of the crystal structures showed water deficiency in the capping TTP water sites of the scandium(III), lutetium(III), ytterbium(III), thulium(III) and erbium(III) hydrates (**14 - 18**).[V] A random distribution of the vacancies is required for the space group $P6_3/m$. The U_{11} component of the thermal ellipsoid, which describes displacement in the plane of the capping oxygen atoms, is abnormally high for the metal ions in the water deficient compounds **14 – 18**, with the highest value for scandium (Fig. 30). The U_{11} value of scandium remains high also at lower temperatures (293, 250 and 200 K) revealing positional disorder of the metal atoms in the equatorial plane containing the capping oxygen atoms, rather than high thermal motion.

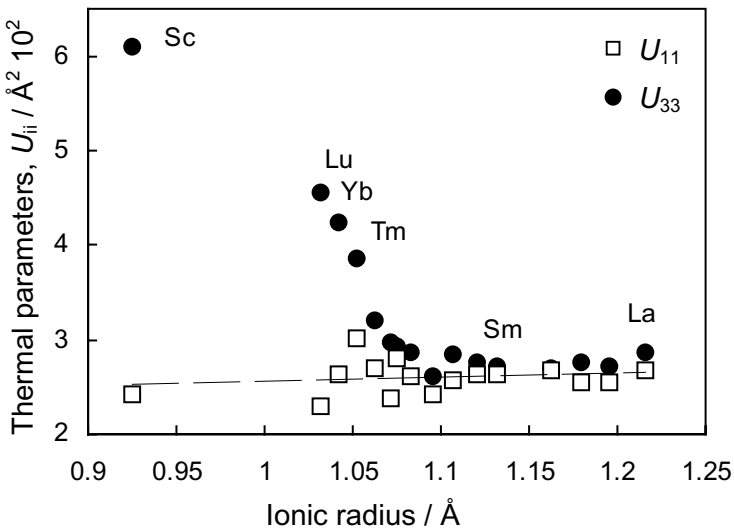

Figure 30. *Anisotoipic displacement parameters for the trivalent metal atom in the TTP hydrates.*

A difference electron density map of this region (Fig. 31) illustrates this disorder. Three domains of residual electron density are symmetrically located at about 0.7 Å from the crystallographic position (1/3, 2/3, 1/4) of scandium, opposite the Sc-O_c bond directions. The three maxima, evidently correspond to the direction of displacement of the scandium ion, attracted by the two remaining oxygen when the opposite capping (O_c) position is empty. Similar electron density features are also observed around the lutetium, ytterbium, thulium and erbium ions, but are absent for the fully hydrated terbium ion (Fig. 31).

Similar electron density difference maps have previously been reported for the two smallest ions, lutetium(III) and ytterbium(III), in a study of a series of $[M(H_2O)_9](CF_3SO_3)_3$ lanthanoid(III) compounds, and was then proposed to be a 4*f*-5*d* contribution to the electron density.[69] However, for scandium(III) without *f* or *d*-electrons the electron density features are clearly caused by disorder and also for all the other water deficient $[M(H_2O)_{9-x}](CF_3SO_3)_3$ hydrates, M = Sc, Lu, Yb, Tm and Er.

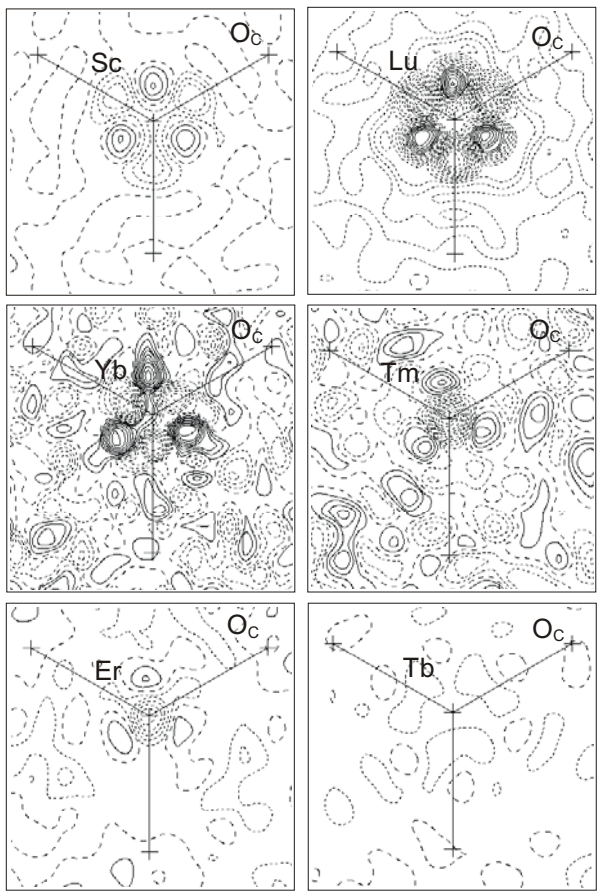

Figure 31. *Residual electron density maps in the plane of the capping oxygen atoms O_c for $[M(H_2O)_{9-x}](CF_3SO_3)_3$, M = Sc, Lu, Yb, Tm, Er and Tb. Positive contours are shown with solid lines and negative with dotted. Contour levels (min, max, interval) are Sc: –0.60, 1.00, 0.20 e Å^{-3}; Lu: -3.20, 1.40, 0.20 e Å^{-3}; Yb: -2.00, 1.80, 0.20 e Å^{-3}; Tm: -2.40, 1.20, 0.20 e Å^{-3}; Er: -1.00, 1.00, 0.20 e Å^{-3}; and Tb: –0.40, 1.00, 0.20 e Å^{-3}.*

Hydrogen bonds

The TTP geometry of the hydrated ions is surprisingly stable in the present isomorphous compounds.[V] An important factor must be the hydrogen bonds bridging the aqua ligands. Two different oxygen atoms (O_t) of each trifluoromethanesulfonate group accept hydrogen bonds from two TTP water molecules, and form symmetric bridges between two O_p atoms along the threefold axis, or asymmetric bridges between one O_p and one O_c atom, as shown in Fig. 32.

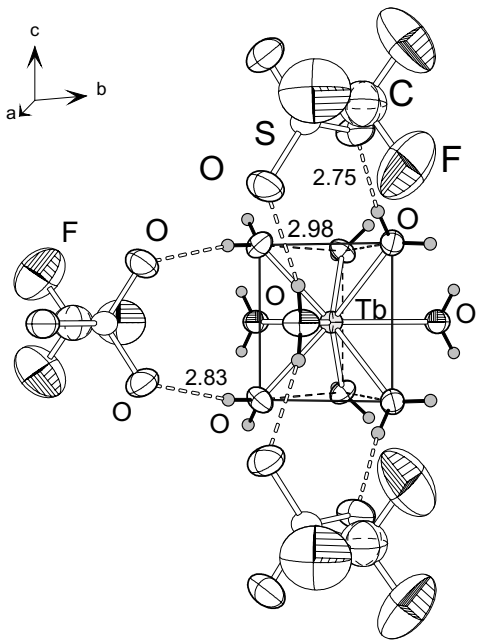

Figure 32. *The nonahydrated terbium(III) ion with six water oxygen atoms (O_p) forming a trigonal prism, three water oxygen atoms capping (O_c) the rectangular surfaces, and the bridging hydrogen bonds(O-(H)…O_t distances in Å) formed to the oxygen atoms (O_t) of the trifluoromethanesulfonate ions (50% probability ellipsoids). For clarity, only three of the nine symmetry-equivalent $CF_3SO_3^-$ anions surrounding the Tb(III) ion, are shown.*

With shrinking radius in the series of lanthanoid(III) ions, the size of the trigonal prism decreases until the $O_p \cdots O_p$ ligand-ligand repulsion in the triangular surfaces becomes too severe. The rectangular surfaces of the trigonal prism also shrinks (Table 14), and the $O_c \cdots O_p$ repulsion of the capping water molecules (O_c) increases so much that the M-O_c distance starts to increase for the smallest lanthanoid(III) ions. Eventually, the release of one capping water can become more favorable than keeping all sites in the TTP fully occupied. For the hydrated scandium(III)

trifluoromethanesulfonate a reversible transition to an ordered structure occurs at about 188 K, with the scandium atom displaced toward one capping oxygen atom. The distance to the closest capping oxygen is Sc-O_c(7) 2.291(3) Å, while the Sc-O_c distances to two other, half occupied sites, have increased Sc-O_c(8) 2.536(5) Å, and Sc-O_c(9) 2.582(5) Å (Table 13).

The hydrogen bonding in **14*** also reflects the distortion in the coordination geometry. The 12 hydrogen bonds, O_p-(H)···O_t, from the prism water molecules to the surrounding trifluoromethanesulfonate oxygen atoms, remain short in the range 2.72 to 2.80 Å (Table 13, Figure 28). However, the hydrogen bonds from the fully occupied capping water site, O_c(7)-(H)···O_t 2×2.89 Å, are shorter than those from the more distant sites, O_c(8)-(H)···O_t 2.95, 2.96 Å and O_c(9)-(H)···O_t 3.03, 3.06 Å. This is consistent with the shorter Sc- O_c(7) bond, increasing the polarisation of the O_c(7) water molecule and thereby the hydrogen bond strength.

The reversible phase transitions shown by DSC measurements to occur at low temperature (~185 K) for all the water deficient hydrates probably reflect a similar structural change from a regular TTP prism to a distorted capped configuration, as for the scandium compound.

Table 14. *Metal-oxygen bond distances, hydrogen bond distances from water molecules to trifluoromethanesulfonate ions, and closest oxygen-oxygen contact distances in the trigonal prism.*[a]

	M-O_p	M-O_c	O_p-(H)···O_t	O_c-(H)···O_t	O_p···O_p[d], O_p···O_p[e]	O_c···O_p
Sc[b]	2.169(3)	2.439(6)	2.781(4), 2.796(4)	2×2.989(4)	2×2.748(4), 2.959(6)	2×2.561(6), 2×2.649(6)
Lu[b]	2.287(4)	2.499(8)	2.734(6), 2.796(6)	2×2.993(6)	2×2.846(7), 3.182(9)	2×2.641(8), 2×2.788(8)
Yb[b]	2.304(2)	2.523(4)	2.756(3), 2.802(3)	2×3.011(3)	2×2.842(4), 3.234(5)	2×2.663(4), 2×2.827(4)
Tm[b]	2.322(3)	2.522(5)	2.745(4), 2.812(4)	2×3.006(3)	2×2.844(6), 3.283(6)	2×2.663(5), 2×2.855(5)
Er[b]	2.340(2)	2.518(4)	2.740(4), 2.814(4)	2×2.999(3)	2×2.865(4), 3.309(5)	2×2.677(4), 2×2.855(4)
Y[c]	2.344(3)	2.525(6)	2.750(6), 2.830(3)	2×3.004(5)	2×2.862(4), 3.324(5)	2×2.688(4), 2×2.861(6)
Tb[b]	2.383(2)	2.530(3)	2.750(3), 2.829(3)	2×2.979(3)	2×2.904(3), 3.387(4)	2×2.699(3), 2×2.901(3)
La[c]	2.519(2)	2.619(5)	2.755(5), 2.840(2)	2×2.932(4)	2×3.082(4), 3.551(3)	2×2.793(3), 2×3.041(5)

[a] p = prism, c = capping, t = trifluoromethanesulfonate,
[b]This work, [c] Ref. 47. [d] side of triangular surfaces, [e] between triangles.

^{2}H NMR studies of water mobility

The low temperature phase **14*** (= $[Sc(H_2O)_{8.0}](CF_3SO_3)_3$), has one fully occupied capping water position, $O_c(7)$ and two about half-occupied, $O_c(8)$ and $O_c(9)$.[V] However, the reversible phase transition, reverting back to a high-temperature phase with all capping water molecules in an equivalent site, indicated that the coordinated water molecules could exchange positions in the TTP hydrates, even in the solid state.

In order to study the water mobility, ^{2}H solid-state NMR studies on $[M(^2H_2O)_n](CF_3SO_3)_3$ salts were performed in the temperature range -5 to 85 ^oC. Only diamagnetic compounds, containing metal ions without unpaired electrons, gave useful results, and the isomorphous fully hydrated yttrium(III) and lanthanum(III) hydrates of group 3 were investigated for comparison with the water deficient scandium(III) and lutetium(III) compounds.

The ^{2}H NMR spectra of the four hydrates display three types of spectral features (Figure 6 paper V): I. A sharp peak at zero frequency from free or surface water. II. A broad feature occurring at low temperatures for the yttrium(III) and lanthanum(III) hydrates, which is characteristic of a rapid flip rotation of the water molecule.[71] III. A narrow, so called powder pattern with a peak width of about 40 Hz appears for all scandium and most lutetium spectra, and also high temperature yttrium and lanthanum spectra, which corresponds to a new dynamical process with a rate of $\sim 10^5$ s^{-1}.

For the yttrium and lanthanum compounds, the broad line shape appears at low temperature when the coordinated water molecules start performing flipping motion, *i.e.* twisting 180^o around their C_2-axis, in their lattice position, see Fig. 6, paper V. When the temperature is increased, the broad feature is replaced by an intense pattern of relatively sharp lines. In previous investigations of hydrated solids,[72] this feature is ascribed to positional exchange of the water molecules that is fast ($>>10^5$ s^{-1}) on the ^{2}H NMR time scale.[73] This occurs at about 70 and 85 ^oC for the yttrium and lanthanum hydrates, respectively.

Because only one such single exchange-averaged ^{2}H spectrum is observed at high temperatures, the water molecules in all TTP sites, prism and capping must be equally mobile around the metal ions. The water dynamics observed for the scandium and lutetium hydrates is similar, even though the onset temperatures for the fast exchange of water molecules between the TTP sites are considerably lower. In fact, for scandium the fast exchange starts already at temperatures below the lowest measuring temperature -5 ^oC, and for lutetium at about 10 ^oC. Thus, it seems that a higher number of vacant capping positions around the metal ion correspond to higher water mobility at a given temperature.

In order to check the reversibility of this process, ^{2}H solid-state NMR was performed for the hydrated yttrium(III) ion starting from 85 °C, cooling down to –5 °C and again heating up to 85 °C (Figure 33). As evident from the figure, there is no specific difference between the two spectra at 85 °C before and after cooling.

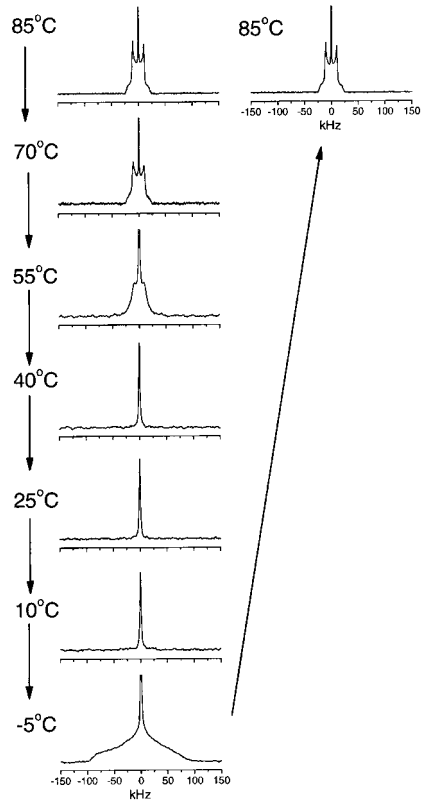

***Figure 33**. Solid-state ^{2}H NMR spectra of $[Y(^2H_2O)_9](CF_3SO_3)_3$ cycling the temperature from 85 to -5 °C followed by heating to 85 °C.*

The results from the ^{2}H NMR studies in all of the investigated solid hydrates indicate rapid positional exchange of water molecules between the prism and capping oxygen atom positions in the TTP configuration. The prism positions always appear fully occupied in the crystal structure, while vacant water oxygen positions are equivalently distributed in the capping sites due to the mobility. The rapid water exchange for the fully nonahydrated lanthanum(III) and yttrium(III) ions shows that vacancies in the TTP structure are not needed for exchanging the positions of the coordinated water molecules.

A possible mechanism, allowing the coordinated water molecules to exchange positions, is illustrated in Figure 34. Regarding the TTP as a mono-capped square antiprism, and twisting the lower square plane 90° can scramble all prism and capping water molecules. Theoretical calculations by Kowall *et al.* shows that the energy difference between the lowest energies for mono-capped square antiprism and the regular TTP configuration is small, only about 1.2 kJ/mol.[74]

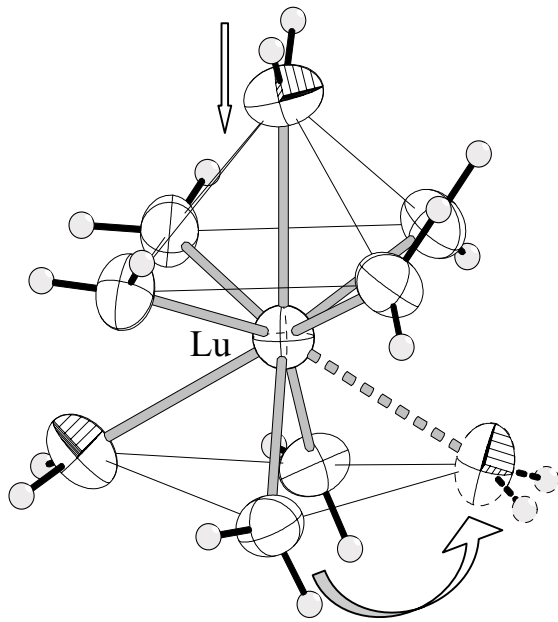

Figure 34. *Proposed mechanism for exchange of the prism (crosses) and capping (octands) water molecules in TTP hydrated metal ions, displayed for the hydrated* $Lu(H_2O)_9^{3+}$ *ion with some water deficiency. The ellipsoids enclose 50% of the electron density.*

Vibrational spectroscopy

Infrared, far-infrared and Raman spectra have been recorded for the hydrated lanthanoid(III) trifluoromethanesulfonates, $[Ln(OH_2)_9](CF_3SO_3)_3$, (Ln = La, Pr, Nd, Sm, Gd, Tb, Dy, Ho, Er, Tm, Yb and Lu), and also for the deuterated $[La(OD_2)_9](CF_3SO_3)_3$ compounds.[VI] The $Ln(H_2O)_9^{3+}$ complexes can be described with 10 atoms, considering the water molecules as point masses. Thus, the LnO_9^{3+} entity will have 24 normal vibrations, and can with a regular TTP arrangement be described in $\mathbf{D}_{3h}$ point group symmetry, with the normal vibrations belonging to $3A_1' + A_2' + A_1'' + 3A_2'' + 5E' + 3E''$ symmetry species. With a total of 16 fundamental skeletal normal modes, 11 Raman active vibrations belong to the $3A_1' + 5E' + 3E''$ symmetry species and 8 infrared active belong to $3A_2'' + 5E'$ species, while $A_2' + A_1''$ are inactive modes.

The assignment of the IR and Raman frequencies in the spectra of the $Ln(OH_2)_9^{3+}$ complexes is not straightforward. The co-existence of six water ligands belonging to the prism with three capping water molecules with slightly weaker Ln-O bonding, together with very strong bands of the trifluoromethanesulfonate anion in the Ln-O stretching region make the assignment difficult (Fig. 2, paper VI). In order to characterize the bands of trifluoromethanesulfonate anion, the IR and Raman spectra of the $NaCF_3SO_3$ salt have been used. The isotope sensitive modes of the $La(OD_2)_9^{3+}$ complex give further information to help distinguish the metal-water vibrations.

Few experimental data are available for the skeletal deformational modes and in the cases when we did not obtain additional frequencies of the deuterated complexes, only the primary diagonal force constants of the stretching modes could be calculated and refined, while constraining the bending force constants. From seven experimental stretching frequencies, six force constants were obtained. The calculated stretching force constants are given in the Table 2; paper VI. The measured fundamental Ln-O stretching frequencies, used for calculations, are listed in Table 4, paper VI, and together with Ln-O bond lengths from crystal structures.

Averaged Ln-O stretching frequencies were obtained for the Ln-O bonds in the prism as $\nu_{prism} = 1/6(\nu_1 + \nu_6 + 2\nu_9 + 2\nu_{14})$, and for the equatorial bonds, $\nu_{cap} = 1/3\ (\nu_2 + 2\nu_{10})$. The averaged stretching frequencies and the Ln-O force constants increase by decreasing the M-O bond distances. The correlations between the M-O bond distances against corresponding stretching frequencies in the prism and capping positions of the hydrated ions (Fig. 3 and 4, paper VI), clearly show the effect of the contraction in the series of lanthanoid(III) ions with increasing atomic number. The absence of significant deviation from the linear correlations suggests that no abrupt change in structure or bonding takes place in this series of hydrated species.

4. CONCLUSIONS

The important factors determining the arrangement of monodentate neutral solvent molecules as ligands around solvated ions in solution are found to be the ionic size, ligand-ligand interactions, and to some extent electronic effects such as covalency and PJTE, in the case studies described below. For coordination studies, comparisons with especially the three-dimensional atomic arrangements from crystal structures can provide much more comprehensive information than merely structure studies of solutions. Detailed vibrational spectra are also easier to obtain from solid compounds, allowing in-depth bonding analyses by means of normal coordinate methods.

Single-crystal x-ray diffraction, x-ray absorption fine structure (EXAFS) and vibrational spectroscopy have been used to study coordination compounds containing solvated metal ions. However, in the solid state columbic forces and effects of the packing arrangement of the ionic species, and also directed forces such as hydrogen bonding, may influence not only the structure but also the coordination number even of discrete solvated metal ions, and will certainly hide the influence of weak PJTE. Care must be taken when making comparisons with solutions, and especially if replacement of solvent molecules with "non-coordinating" anions occurs in the metal ion coordination sphere, profound changes will take place. In addition, the crystal structure determination of structures with polyatomic non-interacting anions often suffers from disorder effects that may make it difficult to extract reliable structural information. In such cases, the lattice-independent EXAFS method is useful in providing accurate bond lengths or in choosing between space groups.

The crystal and solution structure of the six-coordinated dimethyl sulfoxide solvates of aluminium(III), gallium(III), indium(III), thallium(III) and scandium(III), has been studied. All the crystal structures belonged to the space group $R\bar{3}$, with the octahedral MO_6 entities increasingly compressed along one threefold axis with increasing size of the trivalent ions. EXAFS measurements on the solvated gallium(III), indium(III), thallium(III) and scandium(III) ions display similar M-O bond distances in dimethyl sulfoxide solution as in the solid solvates. For thallium(III) the disorder parameter is about twice as large in dimethyl sulfoxide solution as for the solid, indicating a distribution of the Tl-O distances that is larger than expected from the thermal disorder. This can be interpreted as an additional dynamic configurational disorder due to a symmetry-allowed vibronic mixing of electronic states with close energy levels, a weak PJTE.

Distortions from regular octahedral six coordination have also been discussed in terms of PJTE for the hydrated isoelectronic soft mercury(II) and thallium(III) ions in the solid bisaquamercury(II) and trisaquatallium(III) trifluoromethanesulfonate compounds. The trifluoromethanesulfonate ion

can, in contrast to perchlorate, replace water ligands in the hexaaqua ions of mercury(II) and thallium(III) when the hydrated salts crystallize from aqueous solution. The thallium(III) ion retains an almost regular octahedral coordination of oxygen atoms in discrete neutral $[Tl(OH_2)_3(CF_3SO_3)_3]$ complexes. Mercury(II), which is generally much more strongly influenced by PJTE, displays a 2 + 4 configuration in the bisaquamercury(II)-trifluoromethanesulfonate. The connectivity is unusual with $Hg(OH_2)_2^{2+}$ entities (Hg-O 2.11 Å) joined in $[Hg(OH_2)_2(CF_3SO_3)_2]_\infty$ chains by four bridging trifluoromethanesulfonate ions with Hg-O bond distances from 2.46 to 2.66 Å. The chains are held together in sheets by hydrogen bonds, while the sheets interact via van der Waals forces, explaining the fragile layer structure of the crystals. Force constants evaluated for the M-O bonds of these compounds have been compared with those of the hexaaqua ions, and the effect of the coordination on the trifluoromethanesulfonate ions and the hydrogen bonding from the strongly bonded aqua ligands has been evaluated.

The crystal structure of the octakis(dimethyl sulfoxide)lanthanoid(III) iodides comprises discrete complexes of the metal ions ligated to eight dimethyl sulfoxide molecules, surrounded by iodide ions. The lanthanum(III) and praseodymium(III) solvates crystallize in the orthorhombic space group *Pbca*, and the heavier ions in the lanthanoid series in the monoclinic $P2_1/n$. The mean M-O bond distances decrease from lanthanum to lutetium consistent with the decreasing ionic radii from light to heavy rare earth ions. Normal coordinate analyses of the vibrational spectra of the octakis(dimethyl sulfoxide)lanthanoid(III) complexes showed substantial changes in the vibrational frequencies of the coordinated dimethyl sulfoxide molecules, as compared to neat dimethyl sulfoxide. The averaged M-O stretching frequencies and the M-O stretching force constants increase smoothly with decreasing M-O distances. However, the increase is less for the smallest lanthanoid(III) ions, which probably reflects the effect of steric repulsion between the bulky dimethyl sulfoxide ligands.

For the coordination compounds with discrete complexes of dimethyl sulfoxide solvated metal ions the strength and nature of the metal-oxygen bond has been evaluated by normal coordinate analysis of vibrational spectra, and correlated with the S-O stretching mode. Generally, the S-O stretching frequency and the corresponding force constant decreases when the dimethyl sulfoxide molecule ligates via the oxygen atom to the metal ion, while the C-S stretching frequency and force constant increases. The correlation between the S-O bond distances and force constants reveals for the aluminium and scandium complexes high S-O stretching force constants, probably because for these d^0 ions no back-bonding is possible. In the gallium(III), indium(III) and thallium(III) ions with d^{10} electronic configuration, back-bonding can increase the M-O bond strength, resulting in a weakened S-O bond.

The higher covalency in the thallium(III)-oxygen bonds than e.g. in the scandium(III) solvates is for the hydrated ions evident from the higher number of water molecules around the smaller scandium(III) ion, and for the six-coordinated dimethyl sulfoxide solvates, $[M(dmso)_6]^{3+}$, from the much smaller M-O-S bond angle (for M = Tl^{III} 120.7°, and for M = Sc^{III} 132.5°).

The hydrated trivalent scandium(III) and lanthanoid(III) ions, La to Lu, form tricapped trigonal prisms in the isomorphous series of nonahydrated trifluoromethanesulfonates, $[M(H_2O)_n](CF_3O_3)_3$. With decreasing size of the metal ion for M = Er, Tm, Yb, Lu, Sc, the hydration numbers decrease below nine, and the values n = 8.96(5), 8.8(1), 8.7(1), 8.5(1), 8.0(1), respectively, were obtained. The crystal structure showed water deficiency in the capping positions, and the residual electron density indicated randomly distributed vacancies. Relatively strong hydrogen bonds from the trifluoromethane-sulfonate ions hold the water molecules together pair-wise along the threefold axis, stabilizing the trigonal prism around the trivalent metal ions.

DSC measurements showed for all the water deficient trifluoromethanesulfonate compounds, $[M(H_2O)_{9-x}](CF_3O_3)_3$, M = Sc, Lu, Yb, Tm and Er, reversible and exothermic (when cooled) phase transitions at 190 to 185 K. Single crystal data at 150 and 100 K showed that the $[Sc(H_2O)_{8.0}](CF_3SO_3)_3$ compound transformed to an almost 9 times larger trigonal cell with the scandium ion surrounded by seven fully occupied oxygen atom positions, and another two distant positions approximately half occupied. The phase transitions are probably triggered by the instability when the three capping oxygen atoms are strongly repelled by the prism oxygen atoms for the shrinking trigonal prism around the small metal ions. By distorting the prism, expanding one side to allow one capping oxygen atom to approach closer, a more stable configuration can be achieved.

The averaged stretching Ln-O frequencies and the Ln-O stretching force constants of the aqua complexes of the lanthanoid(III) ions in the hydrated trifluoromethanesulfonate showed a satisfactory correlation with the M-O bond distances. The Ln-O stretching force constants, increasing from 0.81 to 1.16 Ncm^{-1} for the Ln-O prism, showed a smooth correlation with the Ln-O bond distances to the prism oxygen atoms, while the correlation to the Ln-O capping oxygen atoms, with force constants between 0.49 and 0.65 N cm^{-1}, has a different shape, reflecting the increased ligand-ligand repulsion with decreasing lanthanoid(III) ion size.

^2H solid-state NMR was used to show the mobility of the water molecules in the coordination sphere of the diamagnetic compounds $[M(H_2O)_n](CF_3SO_3)_3$, M = Sc, Lu, Y and La. Also for the fully nonahydrated yttrium(III) and lanthanum(III) ions positional exchange between coordinated water molecules was found to occur. Fast positional exchange on the ^2H NMR time scale ($>>10^5$ s^{-1}) started at a lower onset temperature for the water deficient scandium(III) and lutetium(III) hydrated ions.

REFERENCES

1. K. Burger, *Solvation, Ionic and Complex Formation Reactions in Non-aqueous Solvents,* Elsevier, Amsterdam, **1983**.
2. S. Kobayashi, *Eur. J. Org. Chem.* **1999**, 15; S. Kobayashi, Y. Mori, Y. Yamashita, *Comp. Coord. Chem. II* **2004**, *9*, 399.
3. S. A. Cotton, *Polyhedron* **1999**, *18*, 1691.
4. R. G. Pearson, *Chem. Brit.* **1967**, *3*, 103.
5. R. G. Pearson, *J. Am. Chem. Soc.* **1963,** *85,* 3533.
6. M. Sandström, I. Persson and P. Persson, *Acta Chem. Scand.* **1990**, *44*, 653.
7. D. F. Shriver and P. W. Atkins, *Inorganic Chemistry*, 3rd ed., Oxford University Press, **1999**.
8. D. Putzas, H. W. Rotter, G. Thiele, K. Broderson and G. Pezzei, *Z. Anorg. Allg. Chem.* **1991**, *595,* 193.
9. I. Persson, M. Sandström, H. Yokohama and M. Chaudhry, *Z. Naturforsch. A: Phys. Sci.* **1995,** *50,* 21.
10. J. E. Huheey, E. A. Keiter and R. L. Keiter, *Inorganic Chemistry,* 4th ed., HarperCollins College Publisher, **1993**.
11. I. Persson, P. Persson, M. Sandström and A.-S. Ullström, *J. Chem. Soc., Dalton Trans*. **2002***,* 1256.
12. I. B. Bersuker, *Chem. Rev.* **2001**, *101,* 1067.
13. D. Strömberg, M. Sandström and U. Wahlgren, *Chem. Phys. Lett.* **1990,** *172,* 49.
14. K. Nakamoto, *Infrared and Raman Spectra of Inorganic and Coordination Compounds,* 5th ed., John Wiley & Sons, New York, **1997**.
15. J. Israelachvili, *Intermolecular and Surface Forces,* 2nd ed., Academic Press, London, **1994**.
16. W. Massa, *Crystal Structure Determination,* Springer-Verlag, Berlin Heidelberg, **2000**.
17. (a) X-SHAPE version 1.02, (b) X-RED version 1.09, STOE & Cie GmbH, Darmstadt, Germany, **1997**.
18. G. M. Sheldrick, *Acta Crystallogr., Sect. A* **1990**, *46***,** 467.
19. G. M. Sheldrick, SHELXL97, *A Program for Crystal Structure Solution and Refinement*; University of Göttingen: Germany, **1997**; http://shelx.uni-ac.gwdg.de/SHELX/.
20. G. E. Brown Jr., G. Galas, G. A. Waychunas and J. Petiau, *Spectroscopic Methods in Mineralogy and Geology*, Reviews in mineralogy 18, Mineralogical Society of America, Chapter 11, **1988**.
21. D. E. Sayers and B. A. Bunker, In *X-ray absorption: Principles, Applications, Techniques of EXAFS. SEXAFS and XANES*; D. C.

Koningsberger, R. Prins, Eds.: Wiley-Interscience: New York, **1988**, Chapter 6.
22. F. Jalilehvand, *Structure of Hydrated Ions and Cyano Complexes by X-Ray Absorption Spectroscopy*, Doctoral Thesis, Department of Chemistry, Royal Institute of Technology, Stockholm, May **2000**; http://media.lib.kth.se:8080/dissengrefhit.asp?dissnr=2963.
23. J. W. Robinson, *Handbook of Spectroscopy*; CRC Press: Boca Raton: Florida, **1991**.
24. E. I. Solomon and A. B. P. Lever, *Inorganic Electronic Structure and Spectroscopy,* Volume I: Methodology, John Wiley & Sons, Inc., **1999**.
25. G. N. George and I. J. Pickering, *EXAFSPAK; A Suite of Computer Programs for Analysis of X-ray Absorption Spectra*, SSRL, Stanford University, CA., USA, **1993**.
26. B. K. Teo, *EXAFS-Basic Principles and Data Analysis*, Springer-Verlag: Berlin, Chapter 6, **1986**.
27. (a) S. I. Zabinsky, J. J. Rehr, A. Ankudinov, R. C. Albers and M. J. Eller, *J. Phys. Rev. B* **1995**, *52*, 2995; (b) J. J. Rehr, A. Ankudinov and S. I. Zabinsky, *Catal. Today* **1998**, *39*, 263; http://Feff.phys.washington.edu/feff.
28. B. Schrader, *Infrared and Raman Spectroscopy,* VCH, Weinheim, **1994**.
29. J. Mink and L. M. Mink, *Computer Program System for Vibrational Analyses of Polyatomic Molecules* (in Lahey-Fujitsu Fortran Win32), Stockholm **2004**; available from Prof. J. Mink, Institute of Isotopes and Surface Chemistry, Chemical Research Center of the Hungarian Academy of Sciences, P. O. Box 77, H-1525 Budapest and Analytical Chemistry Department, University of Veszprém, P. O. 158, Hungary.
30. M. Calligaris and O. Carugo, *Coord. Chem. Rev*. **1996**, *153*, 83.
31. S. Myneni, Y. Luo, L. Å. Näslund, M. Cavalleri, L. Ojamäe, H. Ogasawara, A. Pelmenschikov, P. Wernet, P. Väterlein, C. Heske, Z. Hussain, L. G. M. Pettersson and A. Nilsson, *J. Phys.: Condens. Matter* **2002**, *14*, L213.
32. D. Martin and H. G. Hauthal, *Dimethyl sulfoxide*, Van Nostrand Reinhold, Wokingham, Berkshire, England, **1975**.
33. M. Sandström and I. Persson, *Acta Chem. Scand. Ser. A* **1978**, *32*, 95.
34. J. M. Hook, P. A. W. Dean and D. C. R. Hockless, *Acta Crystallogr. Sect. C* **1995**, *51*, 1547.
35. M. Calligaris, *Coord. Chem. Rev.* **2004**, *248,* 351.
36. M. J. Harrowfield, B. W. Skelton and A. H. White, *Aust. J. Chem.* **1990,** *43*, 759.

37. G. Ma, A. Fischer and J. Glaser, *Acta Crystallogr. Sect. C* **2002**, *58,* 177.
38. G. Shridjar, K. Hermansson and J. Lindgren, *J. Phys. Chem.* **1993**, *97*, 3712.
39. M. A. Marques and M. I. DeBarros Marques, *Proc. K. Ned. Akad. Wet., Ser. B: Phys. Sci.* **1974**, *77*, 286.
40. W. Bol and T. Welzen, *Chem. Phys. Lett.* **1977**, *49*, 189.
41. R. Caminiti, G. Licheri, G. Piccaluga, G. Pinna and T. Radnai, *J. Chem. Phys.* **1979**, *71*, 2473.
42. R. Caminiti and T. Radnai, *Z. Naturforsch., A: Astroph. Phys., Phys. Chem.* **1980**, *35*, 1368.
43. P. Lindqvist-Reis, A. Muñoz-Páez, S. Diaz-Moreno, S. Pattanaik, I. Persson and M. Sandström, *Inorg. Chem.* **1998**, *37*, 6675.
44. J. Blixt, J. Glaser, J. Mink, I. Persson, P. Persson and M. Sandström, *J. Am. Chem. Soc.* **1995**, *117*, 5089, and references therein.
45. P. Lindqvist-Reis, S. Pattanaik, M. Sandström and I. Persson, unpublished results.
46. P. Lindqvist-Reis, K. Lamble, S. Pattanaik, M. Sandström and I. Persson, *J. Phys. Chem., Sect. B* **2000**, *104*, 402.
47. J. M. Harrowfield, D. L. Kepert, J. M. Patrick and A. H. White, *Aust. J. Chem*. **1983**, *36*, 483.
48. J. Näslund, P. Lindqvist-Reis, M. Sandström and I. Persson, *Inorg. Chem.* **2000**, *39*, 4006.
49. P. Lindqvist-Reis, J. Näslund, M. Sandström and I. Persson, *J. Chem. Soc., Dalton Trans.* **2000**, *16*, 2703.
50. R. D. Shannon, *Acta Crystallogr., Sect. A* **1976**, *32*, 751.
51. W. T. Robinson, C. J. Wilkins and Z. Zeying, *J. Chem. Soc., Dalton Trans.* **1990**, 219.
52. B. D. James, M. B. Millikan and M. F. Mackay, *Inorg. Chim. Acta* **1983***, 77,* L251.
53. E. J. Chan, B. G. Cox, J. M. Harrowfield, M. I. Ogden, B. W. Skelton and A. H. White, *Inorg. Chim. Acta* **2004**, *357*, 2365.
54. P. Lindqvist-Reis, *Structure of Solvated Metal Ions*, Doctoral Thesis, Royal Institute of Technology (KTH), Stockholm, Sweden, **2000**, Available at http://www.lib.kth.se/Sammanfattningar/reis000614.pdf.
55. T. Yamaguchi, M. Niihara, T. Takamuku, H. Wakita and G. Kanno, *J. Chem. Phys. Lett.* **1997**, *274*, 485.
56. P. Smirnov, H. Wakita and T. Yamaguchi, *J. Phys. Chem., B* **1998**, *102*, 4802.
57. E. I. Steifel and G. F. Brown, *Inorg. Chem*. **1972**, *11*, 434.
58. E. Damian, F. Jalilehvand, A. Abbasi, L. G. M. Pettersson and M. Sandström, *Phys. Scr.*, **2004**, in press.
59. P.-Å. Bergström, J. Lindgren, M. Sandström and Y. Zhou, *Inorg. Chem*. **1992,** *31*, 150.

60. B. Berglund, J. Lindgren and J. Tegenfeldt, *J. Mol. Struct*. **1978**, *43*, 179.
61. O. Kristiansson, A. Eriksson and J. Lindgren, *Acta Chem. Scand. A* **1984**, *38,* 609.
62. R. Åkesson, M. Sandström, C. Stålhandske and I. Persson, *Acta Chem. Scand.* **1991**, *45*, 165.
63. F. J. Waller, A. G. M. Barrett, D. C. Braddock, D. Ramprasad, R. M. McKinnell, A. J. P. White, D. J. Williams and R. Ducray, *J. Org. Chem.* **1999**, *64,* 2910.
64. Q. F. Zhang, W. H. Leung, X. Q. Xin and H. K. Fun, *Inorg. Chem.* **2000**, *39*, 417.
65. M. S. Grigoriev, I. B. Shirokova, A. M. Fedoseev and C. Den Auwer, *Cryst. Reports* **2002**, *47*, 970.
66. T. E. Plotnikova, M. S. Grigor'ev, A. M. Fedoseev and M. Yu. Antipin, *Russ. J. Coord. Chem.* **2004**, *30*, 60.
67. J. Y. Niu, M. L. Wei and J. P. Wang, *J. Mol. Struc.* **2004**, *689*, 147.
68. M. Klinga, R. Cuesta, J. M. Moreno, J. M. Dominguez-Vera, E. Colacio and R. Kivekäs, *Acta Crystallogr. Sect. C* **1998**, *54*, 1275.
69. A. Chatterjee, E. N. Maslen and K. J. Watson, *Acta Crystallogr. Ser. B* **1988**, *44*, 381.
70. *International Tables for Crystallography,* Kluwer Academic Publisher, Norwell, MA, **1995**, *C,* p. 142.
71. S. Ketudat and R. V. Pound, *J. Chem. Phys.* **1957**, *26*, 708.
72. M. G. Usha and R. J. Witterbort, *J. Am. Chem. Soc.* **1992**, *114,* 1541.
73. H. W. Spiess, *Adv. Polym. Sci.* **1985**, *66*, 23.
74. T. Kowall, F. Foglia, L. Helm and A. E. Merbach, *J. Am. Chem. Soc.* **1995**, *117*, 3790.

ACKNOWLEDGEMENT

I would like to express my deepest gratitude to my supervisor *Prof. Magnus Sandström* who invited and introduced me to a wonderful world of '*Solvation of Metal Ions*'. I also wish to thank for friendly discussions whenever I need, that I never had before like this, and of course for your great help with this thesis, without your help I would probably still be writing. **Tack så hemskt mycket.**

I also would like to thank *Prof. Ingmar Persson* who inspired several of these studies and for helping me to solve my problems on EXAFSPAK. Thank you very much.

I am also grateful to *Dr. Farideh Jalilehvand* who supervised me when I was at Sharif University of Technology (Tehran) and made it possible for me to come to Sweden.

Many thanks to *Prof. János Mink* for teaching me so much about spectroscopy and for all help with normal coordinate calculations.

I also would like to express my gratitude to *Dr. Lars Eriksson* and *Dr. Mikael Kritikos* for helping me to solve the crystal structures. I am most grateful for the collaborations that I have had with them. Many thanks to *Dr. Dick Sandström* for expert help with solid state NMR, as well as *Sahar* for NMR discussions, also to *Prof. Sven Lidin* for his far from disordered mind that ordered the low temperature structure of the scandium(III) hydrate.

Special thanks to *Prof. Rolf Norrestam* for giving the structural chemistry course and also to *Prof. Osamu Terasaki* for encouragement.

A grateful acknowledgement is made to *Dr. Mikhail Skripkin,* who comes every summer and has helped me a lot. Many thanks to *Yura* and *Ljuba* for the skilful syntheses.

I wish to thank *Dr Kjell Jansson* who showed me how to run the TGA and DSC instruments, and *Pelle Jansson* and *Hans-Erik Ekström* for the technical support, *Roffe Eriksson* and *Per-Erik Persson* for solving my computer problems and also *Lars Göthe* for all powder films.

Thank you *Annbritt Rönnell*, *Eva Petterson*, and *Hillevi Isaksson* for always being helpful with all paper work and so many practical things.

I wish to thank *Prof. Julius Glaser* from KTH, *Dr. Vadim Kessler*, *Ann-Sofi Ullström* from SLU for their collaborations. I also wish to thank *Dr. Guibin Ma*, *Dr. Mikhail Maliarik* and especially *Dr. Patric Lindqvist-Reis* for his friendly collaboration and a never-ending stream of new references.

In particular, I would like to thank the members in our own group; *Elena*, *Emiliana*, *Yvonne* and my roommate *Karin*. *Yvonne*, *Pardis* calls you aunt and she always very thankful for your nice presents. *Emiliana*, thanks a lot for all discussions; I think more than with anyone else in our department.

I would like to add my personal thanks to my close Iranian friend *Dr. Shahrad Amerioun* and his family for all help that I got when I came to

Stockholm University. *Hamid*, your help was great for preparing my seminar, thank you.

I also would like to thank all who have contributed to this thesis in some way, and to all kind people at the department: *Prof. Jozef Kowalewski, Prof. Gunnar Svensson, Prof. Ingeborg Csöregh, Dr. Lars-Johan Norrby, Andreas Flemström, Kristina Lund, Dr. Hanna Lind, Fredrik Lindberg, Tomas Olsson, Liqui Tang, Dr. Hong Peng, Andreas Tengå, Tomas Björling, Prof. Dag Noréus, Dr. Tadahiro Yokosava, Johanna Nylén, Richard Becker, Jeppe and Kirsten Christensen, Prof. Sven Hovmöller, Dr. Ulrich Häussermann, Dr. Karim Kadir, Prof. Arnold Maliniak, Zuzana Mayerová, Dr. Fujita Nobuhisa, Peter Oleynikov, Åsa Borin, Arne Sjödin, Sigita Urbonaite, Prof. Xiaodong Zou* and *Leila*.

I would also like to acknowledge here my gratitude to *Dr. Mostafa Ghaffari* and his wife for great opinions and friendly talks. I always can rely on this friendship.

Last but not least, from my deepest heart I would like to thank my wife, *Elaheh* for her love, support and encouragement, who always stands beside me. Now to my little girl *Pardis*, you don't know how blessed we feel every time we look at your cheerful and lovely face. It's my pleasure to play with you jumping around (*hoppa, heja*!!!) even during writing my thesis. I love you two so much. You, your mom and I, we are a team, who always support each other, no matter what. I am also indebted to my parents for their support and encouragement during this period.

وقتی فکر می کنم از چه کسی باید تشکر کنم اسامی زیادی به ذهنم خطور میکند
که قطعا قادر به سپاسگذاری از تک تک آنها نمی باشم .
مامان و بابای عزیزم بدون ایثار و فداکاری شما و زحمات زیادی که برای من
متحمل شده اید من هرگز به این مرحله دست پیدا نمی کردم. از صمیم قلب ازتون
تشکر کرده و دستان مهربانتان را میبوسم .
خواهران عزیزم شما همیشه در کنار م و پشتیبان من بوده اید متشکرم.
همچنین از خانواده محترم همسرم که همیشه مدیون لطف و مهربانی آنها هستم
سپاسگذارم . دوستتان دارم و دستتان را می فشارم.
از تمام فامیل و دوستان گرامی که همیشه حامی من بودند و هستند تشکر می کنم.

بهار ۱۳۸۴
علیرضا عباسی

APPENDIX A. Crystal Data

	1	**2**	**3**	**4**	**4** (150 K)
Formula	$C_{12}H_{36}S_6O_6I_3Al$	$C_{12}H_{36}S_6O_6I_3Ga$	$C_{12}H_{36}S_6O_6I_3In$	$C_{12}H_{36}Cl_3O_{18}S_6Tl$	$C_{12}H_{36}Cl_3O_{18}S_6Tl$
M ($g \cdot mol^{-1}$)	876.45	919.19	964.62	971.49	971.49
Crystal system	hexagonal	hexagonal	hexagonal	hexagonal	hexagonal
Space group	$R\bar{3}$ (No. 148)	$R\bar{3}$ (No. 148)	$R\bar{3}$ (No. 148)	$R\bar{3}$ (No. 148)	$R\bar{3}$ (No. 148)
a/ Å	10.7617(11)	10.9272(13)	11.3584(17)	11.9764(13)	11.8995(9)
c/ Å	24.599(3)	23.868(4)	21.512(4)	20.802(2)	20.467(2)
α/ ^{o}	90	90	90	90	90
β/ ^{o}	90	90	90	90	90
γ/ ^{o}	120	120	120	120	120
V/ $Å^3$	2467.2(5)	2468.1(6)	2403.5(7)	2584.0(5)	2509.9(4)
Z	3	3	3	3	3
T/ K	295 ± 2	295 ± 2	295 ± 2	295 ± 2	150 ± 2
μ(Mo–Kα)/mm^{-1}	3.279	4.052	4.040	5.349	5.507
D_{calcd} / $g \cdot cm^{-3}$	1.770	1.855	1.999	1.873	1.928
Measured reflections	7819	6431	6285	5314	8126
Unique reflections	1342(R_{int} = 0.125)	1085(R_{int} = 0.046)	1059(R_{int} = 0.065)	1345(R_{int} = 0.061)	1357(R_{int} = 0.0104)
Observed reflections	885	651	579	1292	1322
R_1, wR_2 [$I > 2\sigma(I)$][a]	0.068, 0.118	0.029, 0.081	0.024, 0.051	0.032, 0.079	0.030, 0.068
(all data)	0.100, 0.131	0.062, 0.126	0.065, 0.060	0.033, 0.079	0.034, 0.085

	5	6	7	8	9
Formula	$C_{12}H_{36}S_6O_6I_3Sc$	$C_2H_4F_6O_8S_2Hg$	$C_{12}H_{36}Cl_3O_{18}S_6Tl$	$C_{16}H_{48}S_8O_8I_3La$	$C_{16}H_{48}S_8O_8I_3Pr$
M ($g \cdot mol^{-1}$)	894.43	534.76	705.63	1144.63	1146.63
Crystal system	hexagonal	Triclinic	Monoclinic	orthorhombic	orthorhombic
Space group	$R\bar{3}$ (No. 148)	P-1 (No.2)	C 2/c (No.15)	Pbca (No. 61)	Pbca (No. 61)
a/ Å	11.1244(13)	7.878(3)	26.990(9)	19.336(5)	19.015(9)
b/ Å	11.1244(13)	7.977(3)	13.376(4)	19.081(5)	19.363(10)
c/ Å	23.399(4)	9.831(4)	19.133(6)	22.064(6)	22.122(10)
α/ °	90	98.339(7)	90	90	90
β/ °	90	98.779(7)	149.737(18)	90	90
γ/ °	120	96.104(7)	90	90	90
V/ $Å^3$	2507.7(6)	598.9(4)	3481(2)	8141(4)	8145(6)
Z	3	2	8	8	8
T/ K	295 ± 2	295 ± 2	293 ± 2	295 ± 2	295 ± 2
μ(Mo–Kα)/mm^{-1}	3.385	13.31	9.79	1.868	1.870
D_{calcd} / $g \cdot cm^{-3}$	1.777	2.966	2.693	3.766	3.911
Measured reflections	4720	3726	7288	23818	36008
Unique reflections	1318(R_{int} = 0.107)	2572 (R_{int} = 0.092)	1822 (R_{int} = 0.080)	3795(R_{int} = 0.152)	6367(R_{int} = 0.082)
Observed reflections	565	2373	1350	2204	3979
R_1, wR_2 [$I > 2\sigma(I)$][a]	0.040, 0.081	0.044, 0.128	0.036, 0.077	0.063, 0.157	0.057, 0.144
(all data)	0.115, 0.095	0.048, 0.131	0.054, 0.080	0.107, 0.179	0.095, 0.157

	10	**11**	**12**	**13**	**14**
Formula	$C_{16}H_{48}S_8O_8I_3Sm$	$C_{16}H_{48}S_8O_8I_3Gd$	$C_{16}H_{48}S_8O_8I_3Er$	$C_{16}H_{48}S_8O_8I_3Lu$	$C_3H_{16.0}F_9O_{17}S_3Sc$
M ($g \cdot mol^{-1}$)	1156.07	1156.93	1172.98	1180.69	636.30
Crystal system	monoclinic	monoclinic	monoclinic	monoclinic	Hexagonal
Space group	$P2_1/n$ (No. 14)	$P2_1/n$ (No. 14)	$P2_1/n$ (No. 14)	$P2_1/n$ (No. 14)	$P6_3/m$
a/ Å	12.475(5)	12.4233(17)	12.3374(14)	12.257(3)	12.999(2)
b/ Å	18.922(3)	18.929(3)	18.853(2)	18.747(4)	12.999(2)
c/ Å	18.131(6)	18.045(2)	17.992(2)	17.933(4)	7.7680(10)
α/ °	90	90	90	90	90
β/ °	100.33	100.12	100.02	99.92	90
γ/ °	90	90	90	90	120
V/ $Å^3$	4210(2)	4177.4(10)	4121.1(8)	4059.4(15)	1136.7(3)
Z	4	4	4	4	2
T/ K	295 ± 2	295 ± 2	295 ± 2	295 ± 2	295 ± 2
μ(Mo–Kα)/mm^{-1}	1.824	1.840	1.891	1.932	0.742
D_{calcd} / $g \cdot cm^{-3}$	4.021	4.234	4.719	5.155	1.859
Measured reflections	32110	16913	12525	17226	8734
Unique reflections	7813(R_{int} = 0.087)	5457(R_{int} = 0.033)	3843(R_{int} = 0.038)	5648(R_{int} = 0.036)	786(R_{int} = 0.046)
Observed reflections	5191	4347	3178	4336	525
R_1, wR_2 [$I > 2\sigma(I)$][a]	0.061, 0.156	0.051, 0.147	0.053, 0.155	0.041, 0.102	0.047, 0.118
(all data)	0.094, 0.173	0.067, 0.156	0.065, 0.166	0.060, 0.108	0.073, 0.130

	14*	15	16	17	18
Formula	$C_3H_{16.0}F_9O_{17}S_3Sc$	$C_3H_{16.92}F_9O_{17.46}S_3Lu$	$C_3H_{17.4}F_9O_{17.7}S_3Yb$	$C_3H_{17.7}F_9O_{17.83}S_3Tm$	$C_3H_{18}F_9O_{18}S_3Er$
M ($g \cdot mol^{-1}$)	636.30	774.60	776.99	775.34	776.61
Crystal system	trigonal	hexagonal	hexagonal	hexagonal	hexagonal
Space group	$R\bar{3}$	$P6_3/m$	$P6_3/m$	$P6_3/m$	$P6_3/m$
a/ Å	22.411(2)	13.217(2)	13.290(3)	13.3984(10)	13.4622(16)
b/ Å	22.411(2)	13.217(2)	13.290(3)	13.3984(10)	13.4622(16)
c/ Å	23.070(2)	7.7440(10)	7.7810(10)	7.6955(5)	7.6672(10)
α/ °	90	90	90	90	90
β/ °	90	90	90	90	90
γ/ °	120	120	120	120	120
V/ $Å^3$	10034.6(15)	1171.6(3)	1190.2(4)	1196.38(15)	1203.4(3)
Z	18	2	2	2	2
T/ K	150	295 ± 2	295 ± 2	295 ± 2	295 ± 2
μ(Mo–Kα)/mm^{-1}	0.756	4.622	4.332	4.110	3.887
D_{calcd} / $g \cdot cm^{-3}$	1.895	2.196	2.168	2.152	2.143
Measured reflections	12202	7717	14789	8955	9310
Unique reflections	4353(R_{int} = 0.029)	819(R_{int} = 0.044)	1848(R_{int} = 0.135)	1196(R_{int} = 0.065)	853(R_{int} = 0.062)
Observed reflections	2663	746	860	792	780
R_1, wR_2 [$I > 2\sigma(I)$][a]	0.053, 0.124[b]	0.033, 0.064	0.026, 0.047	0.032, 0.055	0.024, 0.054
(all data)	0.088, 0.137[b]	0.039, 0.066	0.094, 0.052	0.068, 0.060	0.028, 0.056

	19
Formula	$C_3H_{18}F_9O_{18}S_3Tb$
M ($g \cdot mol^{-1}$)	768.27
Crystal system	hexagonal
Space group	$P6_3/m$
a/ Å	13.6599(11)
b/ Å	13.6599(11)
c/ Å	7.5589(5)
α/ °	90
β/ °	90
γ/ °	120
V/ $Å^3$	1221.47(16)
Z	2
T/ K	295 ± 2
μ(Mo–Kα)/mm^{-1}	3.290
D_{calcd} / $g \cdot cm^{-3}$	2.089
Measured reflections	9541
Unique reflections	852(R_{int} = 0.041)
Observed reflections	797
R_1, wR_2 [$I > 2\sigma(I)$][a]	0.018, 0.044
(all data)	0.020, 0.045

[a] $R_1 = \Sigma||F_o|-|F_c|| / \Sigma|F_o|$; $wR_2 = [\Sigma[w(F_o^2-F_c^2)^2] / \Sigma[w(F_o^2)^2]]^{1/2}$

[b] Modelling in space group $P6_3/m$ at 150 K resulted in R_1 0.073, wR_2 0.200 for $I > 2\sigma(I)$, and R_1 0.245, wR_2 0.260 for all data

APPENDIX B

Symmetry of Normal Vibrational Modes

Description of how to deduce symmetry species of the normal vibrations by means of group theory for the $[M(Me_2SO)_6]^{3+}$ entity (the Me or CH_3 group is described as a point mass).

1. Find the point group, symmetry elements and symmetry species for a regular $M(dmso)_6^{3+}$ species belonging to the $\mathbf{S}_6$ point group with **E**, $\mathbf{C}_3$, $\mathbf{C}_3^2$, **i**, $\mathbf{S}_6^5$ and $\mathbf{S}_6$ symmetry elements, and A_g, E_g, A_u and E_u symmetry species.

2. Form the reducible matrix representation $\Gamma_{xyz}(\chi_R)$ of the atomic movements.

Point group S_6	**E**	**C_3**	**C_3^2**	**i**	**S_6^5**	**S_6**
Unshifted atoms N:	25	1	1	1	1	1
Atomic contribution f(r):[♣]	3	0	0	-3	0	0
χ_R = N. f(r)	75	0	0	-3	0	0

Reduction formula: $a_i = \frac{1}{h}\sum \chi_R \chi_i N_i$

h: order of group: $h = \sum N_i = 1 + 1 + 1 + 1 + 1 + 1 = 6$

Point group S_6	**①.E**	**①.C_3**	**①.C_3^2**	**①.i**	**①.S_6^5**	**①.S_6**
$\Gamma_{xyz}(\chi_R)$	75	0	0	-3	0	0
$A_g(\chi_i)$[♣]	1	1	1	1	1	1
χ_R .χi .Ni	75	0	0	-3	0	0

Number of $A_g = \frac{1}{h}\sum \chi_R \chi_i N_i$ = 1/6 (75-3) = 12

Continue in the same way for the remaining symmetry species:

No. of E_g = 1/6 (73-3) = 12; No. of A_u = 1/6 (75+3) = 13; No. of E_u = 1/6 (75+3) = 13

Reducible representation $\Gamma_{xyz}(\chi_R) = 12A_g + 12E_g + 13\ A_u + 13E_u$, *i.e.* 75 symmetry species. There are 3N = 3·25 = 75 degrees of freedom.

[♣] Vincent A. *Molecular symmetry and group theory*, John Wiley and Sons, **1998**, P.140 and 144.

3. Remove representations of translations and rotations.
From the character table

Symmetry species	Rotation	Translation
A_g	R_z	
E_g	R_x, R_y	
A_u		T_z
E_u		T_x, T_y

Representations of the normal vibrations (after removal of rotations and translations):

$$\Gamma_{vib} = 11A_g + 11E_g + 12A_u + 12E_u$$

In this centrosymmetric species, all symmetric vibrations (A_g and E_g) are only Raman-active and asymmetric vibrations (A_u, E_u) only IR-active.